論文 / 著書情報
Article / Book Information

題目(和文)	Radio-over-Fiber伝送技術を活用した光無線融合ネットワークに関する研究
Title(English)	Study of Optical and Radio Integrated Network Utilizing Radio-over-Fiber Transmission Technique
著者(和文)	大石将之
Author(English)	Masayuki Oishi
出典(和文)	学位:博士（工学）, 学位授与機関:東京工業大学, 報告番号:甲第10317号, 授与年月日:2016年9月20日, 学位の種別:課程博士, 審査員:安藤 真,廣川 二郎,阪口 啓,西山 伸彦,庄司 雄哉,渡辺 文夫
Citation(English)	Degree:, Conferring organization: Tokyo Institute of Technology, Report number:甲第10317号, Conferred date:2016/9/20, Degree Type:Course doctor, Examiner:,,,,,
学位種別(和文)	博士論文
Type(English)	Doctoral Thesis

Doctoral Dissertation

Study of Optical and Radio Integrated Network Utilizing Radio-over-Fiber Transmission Technique

Masayuki OISHI

September 2016

Department of Electrical and Electronic Engineering

Graduate School of Engineering

Tokyo Institute of Technology

Preface

The work presented in this thesis treats optical and radio integrated network utilizing radio-over-fiber (RoF) transmission technique based on the researches that were carried out during the author's Ph.D. studies in the Department of Electrical and Electronic Engineering, Graduate School of Engineering, Tokyo Institute of Technology. The dissertation is organized as follows.

Chapter 1 is the introduction of the thesis where the background and purpose of this study are presented. The organization of the thesis is also described with the main topics of each chapter.

Chapter 2 describes the overview of RoF transmission technique. The advantageous points of RoF transmission compared to other transmission techniques are summarized and a technical problem for practically designing optical and radio integrated network is discussed.

Chapter 3 studies RoF-based seamless optical and radio communication systems with the capability of rapid disaster recovery, and proposes an autonomous self-healing technique for optical fiber failures utilizing a self-injection-locked Fabry-Perot laser. It is experimentally confirmed that the switching operation from a failed fiber link to a backup radio link can be completed within the required restoration time for network lifelines. In addition, the degradation of signal quality due to the switching operation is quantitatively evaluated by RoF transmission experiments employing the proposed technique. Finally, the required parameters for designing the RoF-based seamless optical and radio communication system with plural backup radio links are discussed.

Chapter 4 studies beam forming of phased array-antennas using RoF transmission technique, and proposes a simple and practical scheme to decide the direction of antenna beam. The feasibility of the proposed scheme is confirmed by bidirectional

RoF transmission experiments in 2-GHz band. Moreover, two-dimensional beam forming in 37-GHz band is experimentally demonstrated for targeting future high-speed radio communication systems. The required system parameters for practical use are finally provided by investigating the induced transmission penalty.

Chapter 5 studies beam forming of an integrated photonic array-antenna (IPA), where the photodiodes are integrated with 60-GHz patch array-antenna elements into a single board, for targeting further simplification of the antenna site. The beam forming operation for the fabricated IPA is experimentally demonstrated by using a QPSK signal, and the signal quality during beam forming operation for the IPA is quantitatively evaluated. The system parameters for practical 60 GHz-band RoF-based array-antenna system are also discussed.

Chapter 6 summarizes the obtained results of this study.

This thesis summarizes the studies that have been reported by the author in *IEICE Transactions on Communications*, *IEICE Transactions on Electronics*, *IEICE Electronics Express*, and *IEEE/OSA Journal of Lightwave Technology*. The research presented in Chapter 3 was partially supported by the National Institute of Information and Communication Technology of Japan (NiCT).

Masayuki OISHI

Contents

Chapter 1

Introduction

1.1 Background

The emergence of intelligent and high-speed mobile terminals, such as smart phones and tablet PCs, has been accelerating the rapid growth of mobile data traffic. The dissemination ratio of the smart phone in Japan becomes more than 54.7% in 2014, and it is predicted that the amount of mobile data traffic beyond 2020 will become 1,000 times larger than today's data traffic [1]. To handle the explosively increasing mobile data traffic, it is required to build mobile base stations (BSs) more rapidly than ever, such as pico/femto-cells covering the area of 50 to 100 m in diameter, especially in urban and densely populated areas. In those areas, however, the room and space for installing BSs such as rooftops of buildings and telephone poles are strictly limited, and as a result, downsizing and simplification of BS equipment are strongly demanded from a telecom carriers' viewpoint. In addition, future BSs will require more advanced

functionalities, such as beam forming to alleviate the inter-cell interference (ICI) among densely distributed plural BSs [2], [3]. Therefore, a new access network architecture for accommodating a lot of BSs should be adopted in order to simplify the configuration of BSs with upgrading the functionalities of them.

Figure 1-1 shows the schematic illustration of the access network architecture for accommodating mobile BSs. The conventional BS architecture, which is known as the distributed radio access network (D-RAN) architecture, is shown in Fig. 1-1(a) where the BS consists of a set of the baseband unit (BBU) and the remote radio head (RRH), and each BS is accommodated in the central office (CO) via each Ethernet-based optical access link. The BBU plays the role of signal processing of digital baseband signals as well as operating and controlling the whole BS. The RRH is the transceiver equipment that converts the digital baseband signal to the radio-wave signal. In the conventional BS architecture, both BBU and RRH are located in the antenna site, and as a consequence, the size of BSs becomes large and the configuration of them becomes complicated.

In order to simplify the BS configuration and to realize the central control of distributed BSs, the centralized RAN (C-RAN) architecture has been proposed as depicted in Fig. 1-1(b) [4], [5]. In the C-RAN architecture, the BBU, which is required for each BS in the conventional BS architecture, is centralized in the CO, and thus the BS architecture can be simplified. Moreover, the C-RAN has a capability of central control among plural RRHs, which is utilized for the alleviation of ICI for example. The common public radio interface (CPRI)-based optical access link is utilized between the one BBU and plural RRHs in C-RAN architecture [6]. On the other hand, the optical access link in C-RAN needs the 16-fold larger transmission capacity than the D-RAN because the waveform of in-phase and quadrature-phase (I/Q) data signal is directly converted to the digital baseband signal. Considering the future multi-band BS systems, the required transmission capacity in the optical access link will

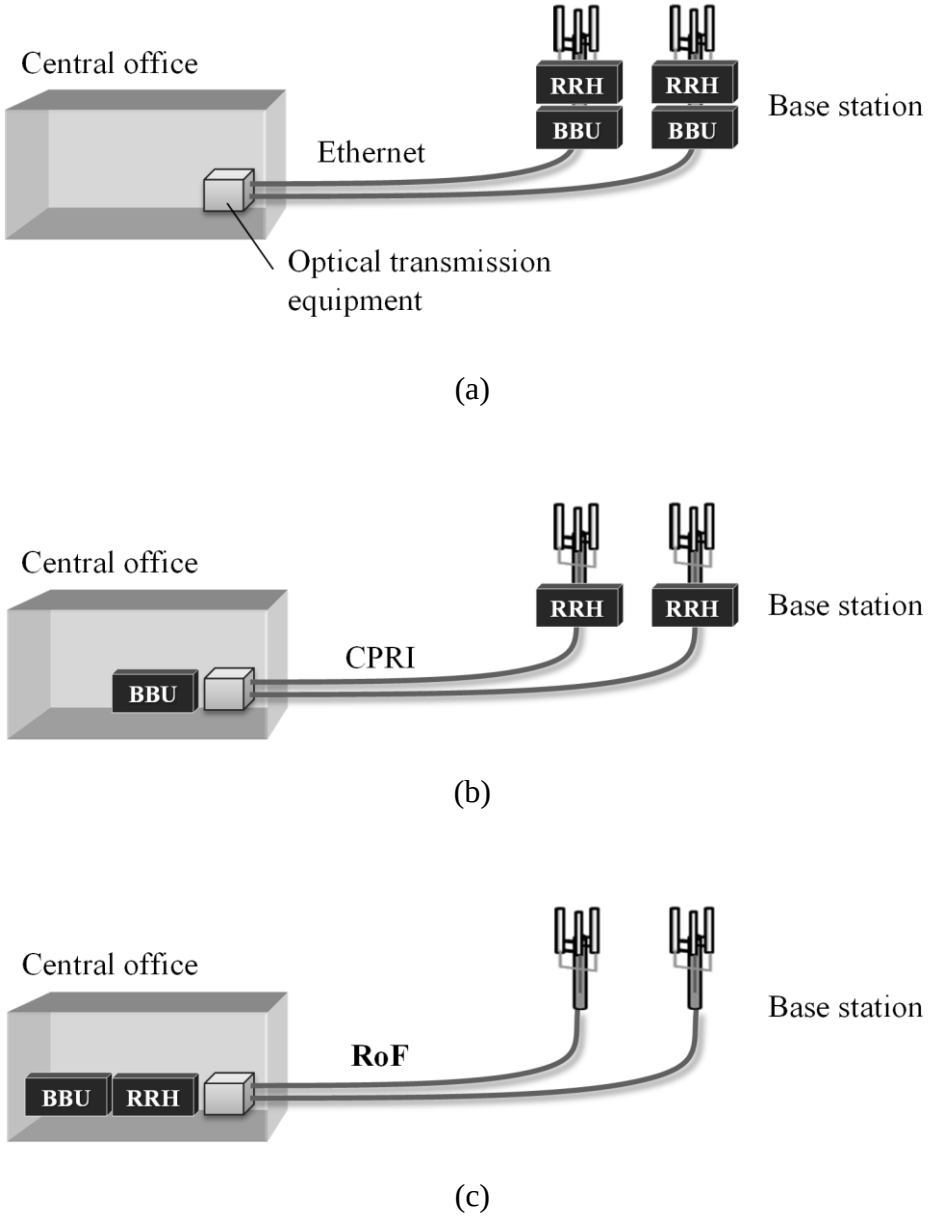

Fig. 1-1. Schematic illustration of access network architecture for mobile BSs; (a) conventional D-RAN, (b) C-RAN, and (c) RoF-based new architecture.

become several-ten Gbit/s. In addition, for the centralized control among plural BSs in C-RAN, the low-latency performance less than 100 μs (not including optical

propagation delay) is required for the optical transmission equipment, which may result in total cost increase of radio access network [7].

Radio-over-fiber (RoF) transmission, which is utilized for television signal broadcasting in practical use or in-building radio networks, has been considered as a candidate technique for simplification of the BS equipment, because it has capabilities of remote radio frequency (RF) signal feeding through optical fiber to antennas, seamless optical and radio transmission without changing the signal format, and centralized control of plural BSs at the CO [8]–[12]. Figure 1-1(c) shows the proposed architecture of the BS access network utilizing RoF transmission technique. As the RoF-based access link can convey RF-modulated optical signal, both BBU and RRH can be centralized in the CO, and therefore the BS needs only antenna as shown in Fig. 1-1(c) which enables us to drastically simplify the BS architecture [13]–[15]. Thus, the RoF transmission has a capability of seamless integration between optical and radio links. Form this feature, the RoF transmission is expected to be utilized for various systems and applications.

1.2 Purpose of This Study

The purpose of this study is to realize “optical and radio integrated network” utilizing the advantageous features of RoF transmission technique as schematically illustrated in Fig. 1-2. Chapter 3 studies a new application of the RoF transmission to rapid disaster recovery. Chapters 4 and 5 study a RoF-based remote beam forming scheme for phased array-antenna. The more detailed purpose of this study is described below.

As optical fiber transmission systems convey large capacity data for providing broadband applications and services, optical fiber failures caused by disasters have a significant impact on social telecommunication networks [16]. While a technique for

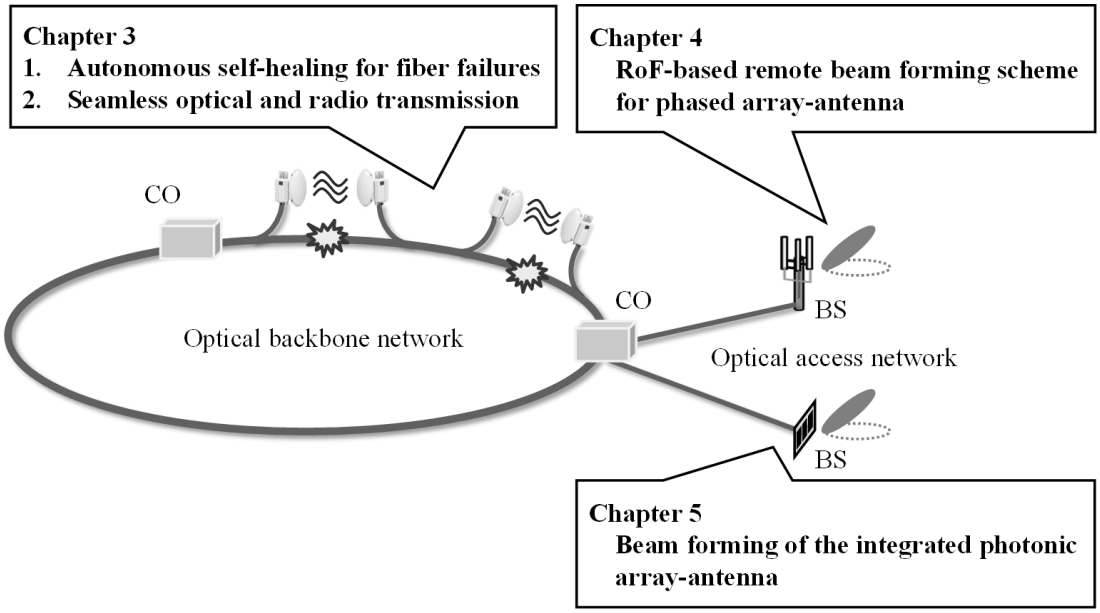

Fig. 1-2. Schematic illustration of optical and radio integrated network based on RoF transmission technique.

recovering failed links by redundant fibers has been reported [17], [18], there is a possibility that the redundant links are simultaneously damaged in the case of large-scale disasters. Optical fiber failures are likely to occur at specific sections such as paths along bridges, embankments and cliffs, and therefore, backup radio links preliminarily installed at the specific sections can rapidly recover the failed links. RoF transmission is one of the promising technologies owing to its capability of seamless integration of optical and radio links [19], [20]. From this perspective, RoF-based optical and radio communication system with rapid recovery capability against disasters is studied in this thesis. In this system, a self-healing functionality is required for detecting optical fiber failures and autonomously switching to the backup links. In addition, optical and radio switching nodes, which are pre-installed at hazardous sections, are needed to be as simple as possible for ensuring high reliability. This

thesis proposes an autonomous self-healing technique for optical fiber failures, and the feasibility of seamless optical and radio communication system employing the proposed technique is confirmed by the RoF transmission experiment. The system parameters considering the signal quality degradation caused by the switching operation is also designed. These proposal and experimental demonstration are described in Chapter 3.

RoF transmission technique also has a capability of remote power feeding to antenna and remote control of antenna beam. Therefore, several schemes for optically controlling the antenna beam have been reported [21]–[25]. The basic concept of the optically beam-controlled array-antenna was proposed by Frankel et al., where the tunable laser sources (TLSs) and the effect of fiber chromatic dispersion (CD) were used for generating an RF phase shift [21], and this concept was experimentally demonstrated in Refs. [26], [27]. However, the scheme to detect mobile terminals and decide the direction of the antenna beam has not been reported yet, whereas this functionality is indispensable for practical systems using phased array-antenna. By establishing entire techniques from the detection of the targets to the antenna beam forming, a significant advance should be achieved for enhancing the practicality of the RoF-based BS systems. The techniques are primarily of importance from an industrial viewpoint, because capital and operating expenditures of the systems would be drastically reduced. This thesis proposes a new scheme to detect the direction of mobile terminals that are expected to be employable in a practical system, and experimentally demonstrates the fundamental operation. In addition, a two-dimensional beam forming in the millimeter-wave band is demonstrated for targeting a future high-speed radio communication. The required system parameters for the practical beam forming system based on RoF technique is also provided. These proposal and experimental demonstration are described in Chapter 4.

The beam forming operation has been experimentally demonstrated in previous studies, while the array-antenna elements and photodiodes (PDs) were separated

discretely in these demonstrations. The recent progress in photonic integration technologies on tunable lasers and high-power and/or high-speed PDs [28], [29], such as uni-travelling carrier PDs (UTC-PDs) [30], will accelerate the development of more compact, light-weight, and cost-effective antennas than ever. For further simplification of BS equipment and flexibly increasing the number of array-antenna elements, an integrated photonic array-antenna (IPA), where 60 GHz-band array-antennas and UTC-PDs were fully integrated into a single board, was proposed and fabricated [31]. While the beam forming operation for the IPA has been experimentally demonstrated by using an RF tone without any signal modulation, the data signal assuming real mobile traffic should be used for the demonstration in actual situations. The signal quality during the RoF-based beam forming operation for 60-GHz array-antennas has not been clarified yet, whereas it would be one of the indispensable points from a practical point of view. This thesis studies the performance of RoF signal transmission with beam forming of the IPA. The beam forming operation for the IPA is experimentally demonstrated by using a 3.5-Gbit/s quadrature phase shift keying (QPSK) signal assuming real mobile data traffic, and the quality of the QPSK signal during beam forming operation is quantitatively evaluated. In addition, the required parameters for practical use are provided by investigating the induced transmission penalty. These experimental study and the numerical analysis are described in Chapter 5.

1.3 Organization of the Thesis

Figure 1-3 shows the organization of this thesis. Following the introduction of RoF transmission technique in this chapter, the RoF-based seamless optical and radio communication system with the autonomous self-healing functionality for optical fiber

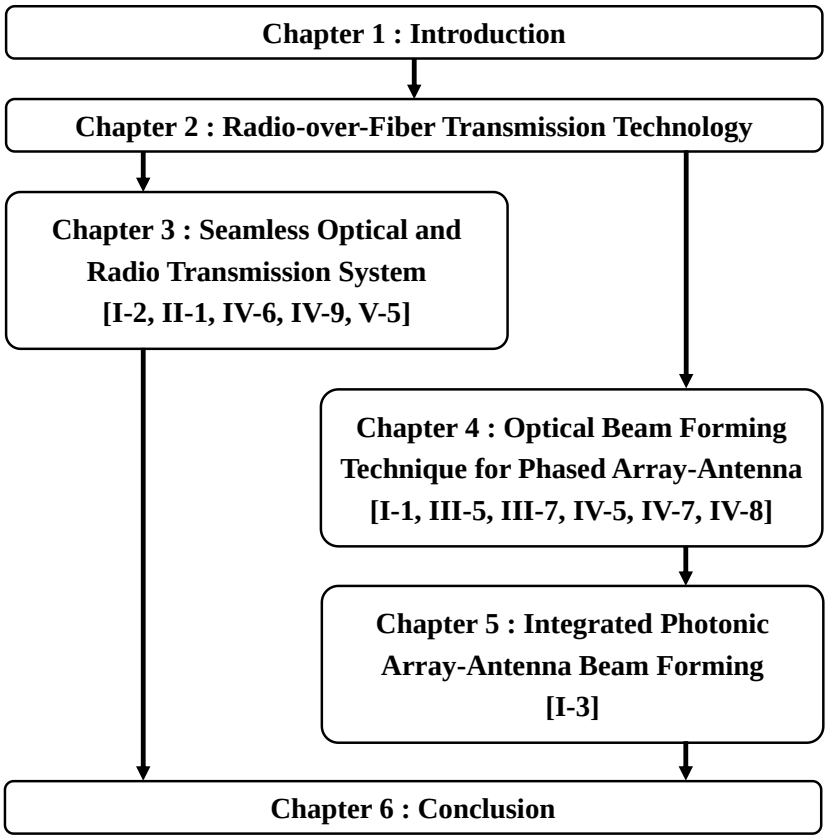

Fig. 1-3. Organization of the thesis.

failures is described in Chapter 3. The RoF-based beam forming scheme for phased array-antennas and the beam forming operation for the IPA are described in Chapters 4 and 5, respectively. The contents of each chapter are summarized as follows.

Chapter 2 describes the details of RoF transmission technique. The advantageous point of RoF technique compared to the digital baseband transmission is explained. In addition, a technical problem for practically designing optical and radio integrated network is discussed by investigating the transmission penalty.

Chapter 3 proposes an autonomous self-healing technique for optical fiber failures in the case of disasters. The proposed technique utilizes a self-injection-locked Fabry-Perot laser, which is feasible to be adopted in practical system because of its high

reliability and simple configuration. It is experimentally confirmed that the switching operation from a failed fiber link to a backup radio link can be completed within the required restoration time for network lifelines. The degradation of signal quality caused by switching operation is evaluated by RoF transmission experiments employing the proposed technique. The required parameters for designing the RoF-based seamless optical and radio communication system with plural backup radio links are also shown. The results described in Chapter 3 have been published in I-2, II-1, IV-6, IV-9, and V-5 that are shown in the list of publications by the author.

Chapter 4 proposes a simple and practical scheme to decide the direction of antenna beam. The feasibility of the proposed scheme is confirmed by bidirectional RoF transmission experiments in 2-GHz band. Moreover, two-dimensional beam forming in 37-GHz band is experimentally demonstrated for targeting future high-speed radio communication systems. The required system parameters for practical use are also provided by investigating the induced transmission penalty. The results described in Chapter 4 have been published in I-1, III-5, III-7, IV-5, IV-7, and IV-8 that are shown in the list of publications by the author.

Chapter 5 experimentally studies the beam forming operation for the fabricated IPA by using a QPSK signal assuming the real mobile data traffic, and the QPSK signal quality during beam forming for the IPA is quantitatively evaluated. The expandability for more advanced quadrature amplitude modulation (QAM) formats is also studied. Finally, the system parameters for practical 60 GHz-band RoF-based array-antenna system are discussed. The results described in Chapter 5 have been published in I-3 that is shown in the list of publications by the author.

Chapter 6 concludes the thesis with a summary of the whole results.

Chapter 2

Radio-over-Fiber Transmission Technique

2.1 Introduction

In this chapter, the transmission technologies for optical access links used in the mobile BS architecture are introduced, and the advantageous point of RoF transmission technique compared to the other techniques is explained. In addition, the technical problem for designing RoF-based optical and radio integrated network is discussed considering transmission penalty induced by the nonlinear optical fiber effects.

2.2 Overview of the Technique

Figures 2-1(a) and (b) show schematic diagrams for digital baseband transmission and RoF transmission, respectively. In the digital baseband transmission as depicted in Fig. 2-1(a), the digital data signal is transmitted from an electrical-to-optical converter (E/O) as a baseband signal, and the baseband signal propagating an optical fiber link is received by an optical-to-electrical converter (O/E). After passing through the O/E, the baseband signal is converted to a radio-wave signal in the RF signal converter and then radiated from an antenna. The digital baseband transmission technique is conventionally utilized for D-RAN and C-RAN architectures.

In the RoF transmission as shown in Fig. 2-1(b), the digital data signal is firstly converted to an RF signal in the CO, and the RF signal is converted to an optical RF signal (RoF signal) in the E/O. The RoF signal, of which signal format is same as the original RF signal, propagates an optical fiber link and can be directly converted to a radio-wave signal in the O/E without any modification of the signal format. As the RoF transmission can create RF signals by just receiving the RoF signal in the O/E, it is not required to implement complicated signal processing functions for converting the optical signal to radio-wave signal. Therefore, the RoF transmission technique can simplify the configuration of the BS, and it will be effective especially in high frequency such as millimeter-wave because the RF components in the millimeter-wave band are much more expensive than microwave band in general.

Table 2-I summarizes the pros. and cons. among three network architectures for BSs that are introduced in Chapter 1. The conventional D-RAN architecture based on the digital baseband transmission has a problem on the footprint of BSs because both BBU and RRH are required at the antenna site. The C-RAN architecture has an advantage for centralized control of plural BSs in the CO, while there is a technical

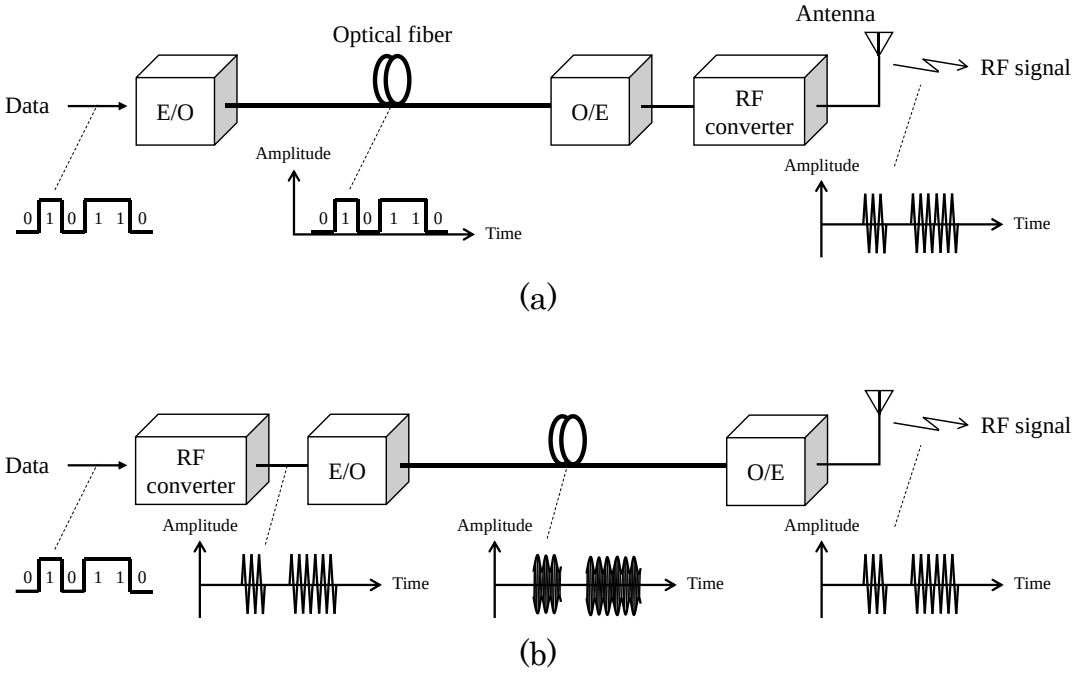

Fig. 2-1. Schematic diagrams for (a) digital baseband transmission and (b) RoF transmission.

Table 2-I. Pros. and cons. among three network architectures for base stations.

	D-RAN	C-RAN	Proposed
Transmission scheme	Digital baseband	Digital baseband	RoF
BS footprint	Bad	Good	**Very good**
Central control of BSs	Bad	**Very good**	Good
Gbit/s RF transmission	Good	Good	**Very good**
Latency	Good	Bad	Good
Signal quality	Good	Good	Bad

issue on Gbit/s-class RF transmission because the digital I/Q waveform must be directly transmitted as a baseband signal, and the strict requirement for the latency between the BBU and RRH is also a critical issue. The issue on Gbit/s-class RF transmission can

be resolved by using some I/Q data compression techniques as reported in Refs. [32], [33]. The proposed architecture based on RoF transmission will resolve these issues in the C-RAN architecture. The RoF-based architecture can simply support Gbit/s-class RF transmission because the transmission speed of RF signal is independent of the transmission technique itself. The RoF transmission also has an advantage in terms of the latency owing to its seamless signal conversion capability without changing signal format [13]. Figures 2-2(a) and (b) show the schematic diagrams of RF signal conversion with plural radio sections in digital baseband transmission and RoF transmission, respectively. In the digital baseband transmission, the RF converters are required in both radio transmitter and receiver sides of each radio section, which would complicate the whole optical and radio transmission system. In the RoF transmission, the RF converter is necessary just at the first RoF transmitter side and the other sections for RF transmission does not require any RF converters, which enables us to seamlessly connect plural optical and radio sections [34]. From this feature, the RoF transmission will be utilized for new applications, such as backup radio links in the case of optical fiber failures at the plural sections, or for rapid installation of communication links where it is difficult to newly establish optical fiber links. The technical issues to be solved for the application of rapid recovery in the case of disasters are investigated in Chapter 3.

On the other hand, the RoF transmission technique has a technical issue on signal quality that is induced by nonlinear optical fiber effects. The analog signal transmission through fiber such as RoF technique is generally susceptible to these effects, for example, the fiber chromatic dispersion (CD) effect that will be one of the critical issues to design the parameters of practical systems. In the next section, an undesired effect of the CD on RoF transmission is numerically investigated in detail.

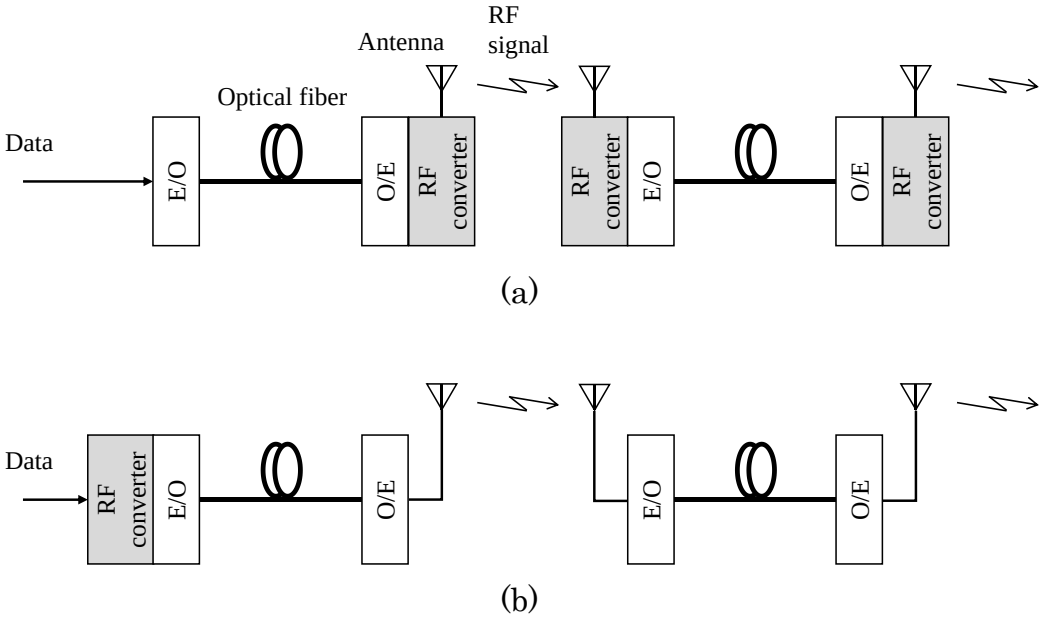

Fig. 2-2. Schematic diagrams of RF signal conversion with plural radio sections in (a) digital baseband transmission and (b) RoF transmission.

2.3 Effect of Fiber Chromatic Dispersion on RoF Transmission

In the typical RoF transmission scheme, an optical carrier is amplitude-modulated by an RF signal, which is known as the sub-carrier multiplexing (SCM) technique [35]. At the E/O side, the optical carrier is modulated by an RF signal in the optical intensity modulator (IM). After propagating an optical fiber link, the amplitude-modulated optical signal is directly detected by a PD at the O/E side, and thus the RF signal waveform can be reproduced. The phase term of the amplitude-modulated optical

signal can be expressed as the following equation;

$$\cos(2\pi f_0 t)\{1+m\cdot\cos(2\pi f_{RF} t)\} = \cos(2\pi f_0 t)+\frac{1}{2}m\cdot\cos\{2\pi(f_0+f_{RF})t\}+\frac{1}{2}m\cdot\cos\{2\pi(f_0-f_{RF})t\}, \quad (2.1)$$

where f_0 is an optical carrier frequency, m is an optical modulation index (OMI) that means the depth of the amplitude modulation, and f_{RF} is an RF carrier frequency. The first term of Eq. (2.1) indicates the optical carrier component, and the second and third terms of Eq. (2.1) indicate the upper and lower sideband components generated by amplitude-modulation of the optical carrier. Thus, the amplitude-modulated optical signal consists of the optical carrier and the double sidebands (DSB) that are separated by f_{RF} from the optical carrier frequency of f_0.

Figure 2-3 shows the mechanism of dispersion-induced RF transmission penalty in RoF link. As shown in Fig. 2-3, the RF signal waveform output from the O/E can be expressed as the summation of the beat signals among the optical carrier and the DSB. The CD during optical fiber propagation is inevitable, and the relative phase among the optical carrier and the DSB is shifted due to the effect of CD. Therefore, the CD induces the relative phase shift between the DSB, which may result in decrease of the amplitude-modulation index [36]–[38]. The RF output power P_{RF} considering the relative phase shift between DSB is given by the following equation [36];

$$P_{RF} = A\cos^2\left(\frac{\pi L D \lambda_{RF}^2 f_{RF}^2}{c}\right), \quad (2.2)$$

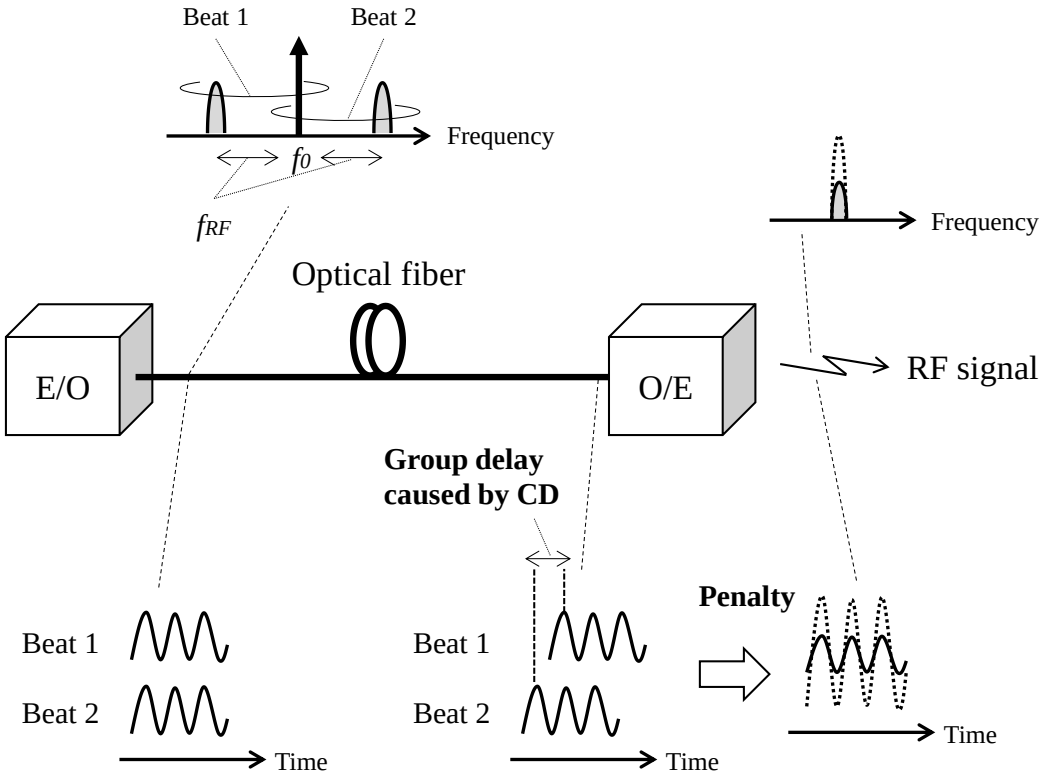

Fig. 2-3. Mechanism of dispersion-induced RF transmission penalty in a RoF link.

where A is a constant number, L is a length of transmission fiber, D is a dispersion parameter of the transmission fiber, which is typically in the range of 16–18 ps/nm/km, λ_{RF} is a wavelength of the RF signal, and c is the light velocity in optical fiber. The RF modulation components are canceled out when the phase shift, which is the phase term of $\cos^2$ in Eq. (2.2), reaches π.

Figure 2-4 shows the RF output power as a function of the transmission fiber length, which was calculated by using Eq. (2.2). In this calculation, the dispersion parameter was set as 17 ps/nm/km, and the RF carrier frequency f_{RF} was changed to be 10, 20, and 60 GHz. When the f_{RF} is 10 GHz, the RF transmission penalty is within 3 dB even after 15 km-long fiber transmission. When the f_{RF} is 20 GHz, however, the effect of

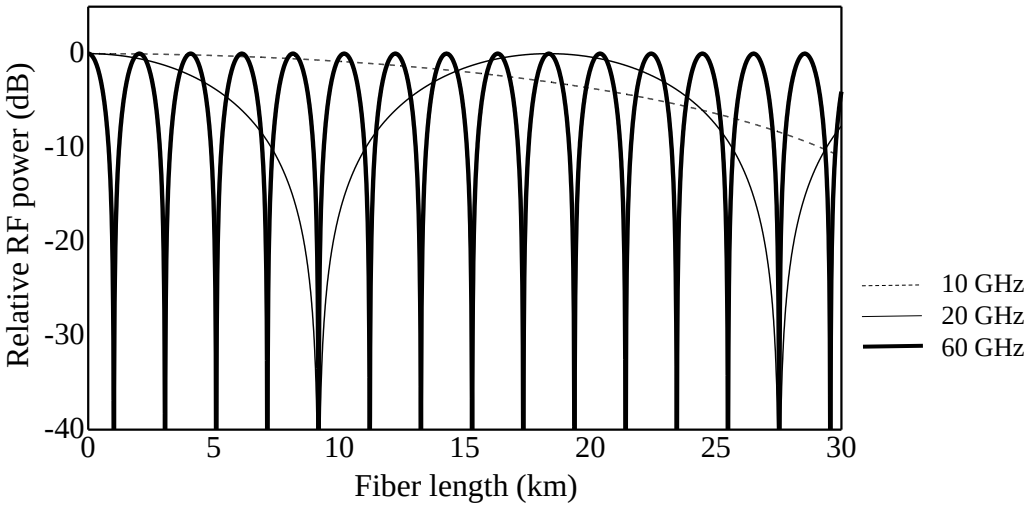

Fig. 2-4. RF output power as a function of transmission fiber length.

CD becomes large and the RF output power is canceled out after about 9-km fiber transmission. In the case of f_{RF} = 60 GHz, the CD has a significant impact on the RF output power. The RF output power periodically changes depending on the fiber length, and therefore, it may seem to be strict to transmit 60-GHz RoF signal over several km-long fiber. To overcome this issue, the dispersion compensation (DC) fiber or module equipped in the CO will be one of the solutions. The use of low or zero dispersion wavelength for the light source of RoF signal and of low or zero dispersion fiber can also avoid the problem of RF transmission penalty.

Figure 2-5 shows the relationship between RF carrier frequency and fiber length considering the CD-induced RF transmission penalty, where the penalty was calculated from Eq. (2.2). The gray-highlighted areas indicate that the penalty becomes more than 3 dB, and these areas periodically appear depending on the RF carrier frequency and the fiber length as explained above in Fig. 2-4. As shown in Fig. 2-5, the transmission fiber length in 60 GHz seems to be restricted within 0.5 km in order to keep the transmission penalty less than 3 dB. As the RF output power periodically

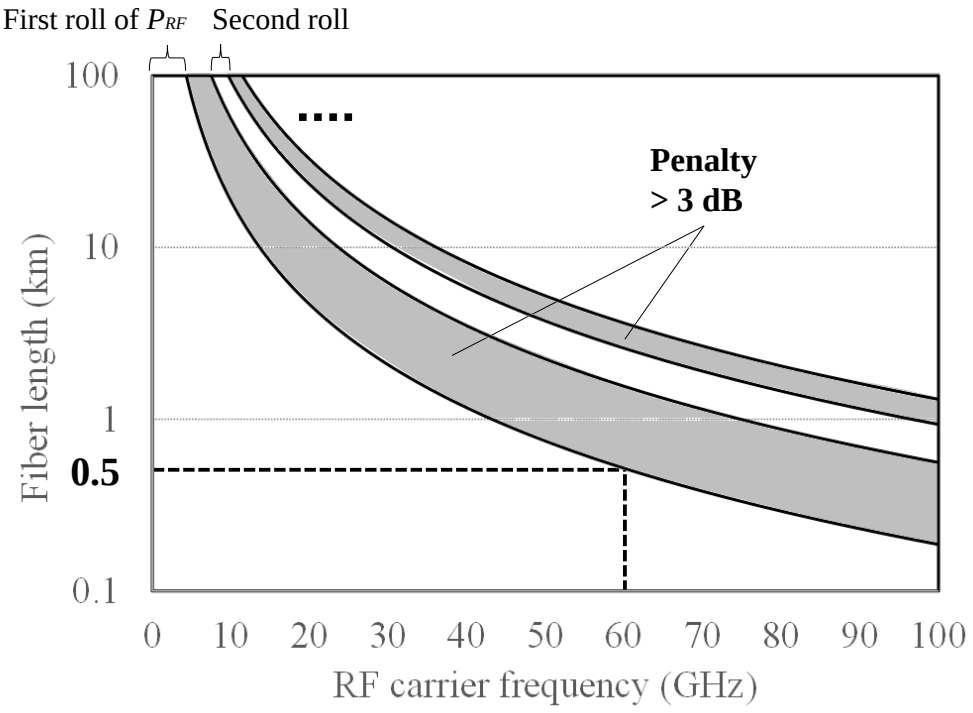

Fig. 2-5. Relationship between RF carrier frequency and fiber length considering the CD-induced RF transmission penalty.

changes, the fiber length can be extended even in the 60 GHz. However, it will be preferable that the fiber length is within the range below the first roll of P_{RF}, because the selection of higher-order roll of P_{RF} induces the gradual deviation of data symbols and it may result in the degradation of signal quality. As a consequence, if the required fiber length is longer than the penalty limit, the adoption of DC fibers or modules should be considered. Thus, the RF transmission penalty is one of the most important issues for designing the parameters in practical RoF transmission system, which is experimentally investigated in detail in Chapters 4 and 5.

2.4 Conclusion

This chapter introduced the overview of RoF transmission technique. It was explained that the RoF transmission was promising for accommodating mobile BSs because of its seamless optical and radio signal conversion feature. The RoF technique can be also expected to be applied to new applications, such as rapid disaster recovery, quick installation of communication links, and so on.

In addition, the CD-induced RF transmission penalty was introduced as one of the undesired effects on the RoF transmission. The numerical analysis confirmed that the RF transmission penalty became significant especially in millimeter-wave band such as 60 GHz. When the required fiber length is longer than the penalty limit, the adoption of DC fibers or modules equipped in the CO will resolve the restriction of fiber length. The RF transmission penalty due to the effect of CD must be considered when we design the parameters of RoF transmission system.

Chapter 3

Seamless Optical and Radio Transmission System

3.1 Introduction

RoF-based seamless optical and radio communication system is effective for rapid disaster recovery, where failed optical fiber links are switched to backup radio links. In this chapter, an autonomous self-healing technique utilizing a self-injection-locked Fabry-Perot laser (FP-LD) is proposed. It is experimentally confirmed that the switching operation can be completed within the required restoration time for network lifelines. In addition, the signal quality degradation caused by switching operation is quantitatively evaluated by RoF transmission experiments with the proposed technique.

3.2 Seamless Optical and Radio Communication System

A conceptual diagram of the seamless optical and radio communication systems is shown in Fig. 3-1, where backup radio links are preliminarily installed at plural sections in an optical fiber transmission line between the COs-1 and 2. The optical transmission bit-rate and the total distance between the COs-1 and 2 are assumed to be 100 Gbit/s or more and several tens of kilometers, respectively. When optical fiber failures occur, the bit-rate should be decreased due to the restriction of RoF transmission capacity in radio sections, and thus, it is assumed that the bit-rate in the case of fiber failures is decreased to 10 Gbit/s or more. The distance of backup radio links is assumed to be 1 km or less, corresponding to the distance of optical fiber links between the nodes-1 and 2. When optical fiber failures are caused by a disaster at the sections-1 and 2 as shown in Fig. 3-1, the failed links are switched to backup radio links. It is preferable that the switching can be completed as soon as possible, within the order of seconds for example, in order to recover lifeline utilities provided on the network such as safety confirmation systems, emergency calls, and so on. For switching to backup radio links reliably and rapidly, the following operations are required;

(i) All the switching process including the failure detection should be completed only in physical layer to reduce the complexity of the configuration and the latency caused by signaling.

(ii) The switching should be autonomously operated to save the time that network operators go to the failed sections.

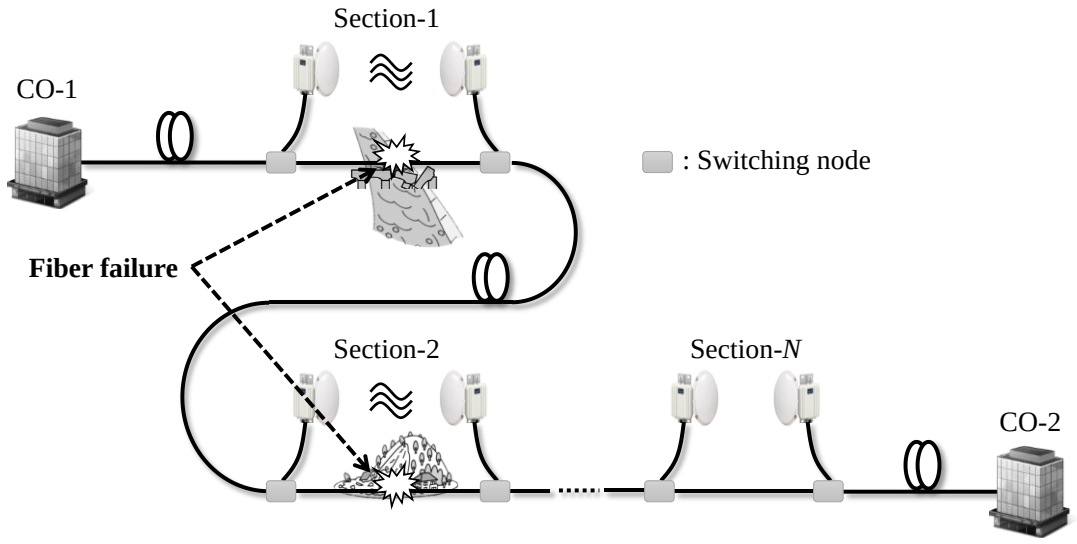

Fig. 3-1. Seamless optical and radio communication system.

(iii) The switching should be independently operated in each section to avoid the isolation from the COs. For example, in the case that link failures occur in sections-1 and 2 as shown in Fig. 3-1, the section between the node-2 in section-1 and the node-1 in section-2 is isolated and these nodes cannot communicate with the COs.

As for the failure detection technique in physical layer described in the requirement (i), an optical time domain reflectometer (OTDR) is a promising candidate [39]. However, it cannot satisfy the requirements (ii) and (iii) because it detects only the first failure point closest to the COs. While there is another type of detection technique monitoring the change of states-of-polarization (SOP) [40], the configuration is too complicated to fulfill the requirement (i), because it needs monitoring the temporal variation of SOP precisely. From these reasons, a new technique that can meet all the requirements (i) to (iii) is proposed, and the details of the proposed technique are explained in the next section.

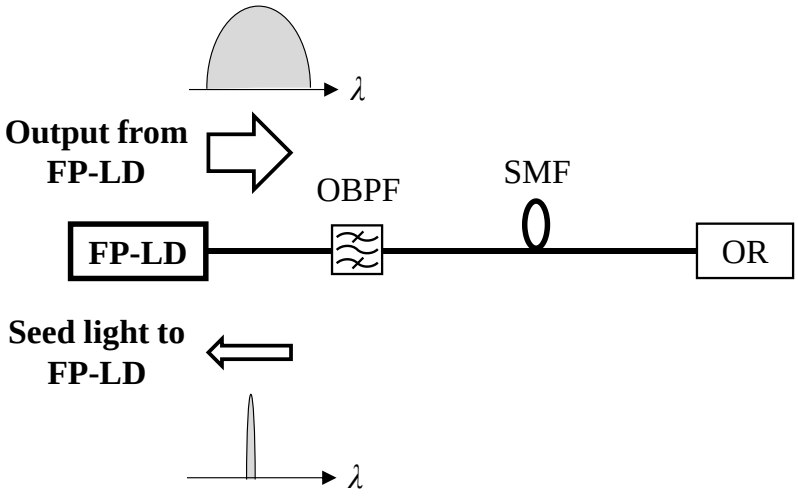

Fig. 3-2. Schematic illustration of a self-injection-locked FP-LD.

3.3 Autonomous Self-Healing Technique for Optical Fiber Failures

As a technique to autonomously backup plural optical fiber failures with high reliability, a novel self-healing technique utilizing a self-injection-locked FP-LD is proposed.

3.3.1 Self-injection-locking of Fabry-Perot Laser

In general, an FP-LD emits light with plural longitudinal modes in a wavelength range. When a light injects into the FP-LD, the physical phenomenon of “injection-locking” is occurred, where the FP-LD emits light with being locked in the wavelength of the

injection light [41], [42]. A schematic diagram of the self-injection-locked FP-LD is shown in Fig. 3-2. An FP-LD and an optical reflector (OR) are connected to the both terminals of a single-mode fiber (SMF), and an optical band-pass filter (OBPF) is inserted between the FP-LD and the OR. The light output from the FP-LD is spectrum-sliced by the OBPF and injected into the FP-LD itself after being reflected by the OR, and thus, the self-injection-locking state of the FP-LD can be created.

3.3.2 Proposed Technique for Autonomous Self-Healing Operation

The proposed autonomous self-healing technique is based on the detection of the state change of an injection-locked FP-LD. The self-healing operation is simple because it does not require complicated signal processing, and thus, the high reliability of self-healing operation can be ensured.

Figure 3-3 shows a schematic diagram of the proposed autonomous self-healing technique utilizing a self-injection-locked FP-LD. In this technique, the FP-LD is not utilized for data transmission but just for monitoring the state of fiber link between two switching nodes. When the optical fiber between nodes-1 and 2 is cut off, the failed link is switched to a backup radio link. An optical and radio switching node consists of an FP-LD for monitoring the state of the fiber link, an optical coupler (CPL) for dividing the light emitted from the FP-LD, a wavelength division multiplexing (WDM) coupler for combining an optical data signal and the light emitted from the FP-LD, an OR for inducing the self-injection-locking state of the FP-LD, an optical notch filter and a PD for monitoring the locking state of the FP-LD, and an optical switch (SW) for switching the path according to the monitored result. The FP-LD in the node-1 emits light around the wavelength of λ_1, which are different from the optical data signal wavelength of λ_0, at the free-running state. The light at λ_1 is then spectrum-sliced by the WDM coupler that operates as the OBPF explained in Fig. 3-2, and is reflected by

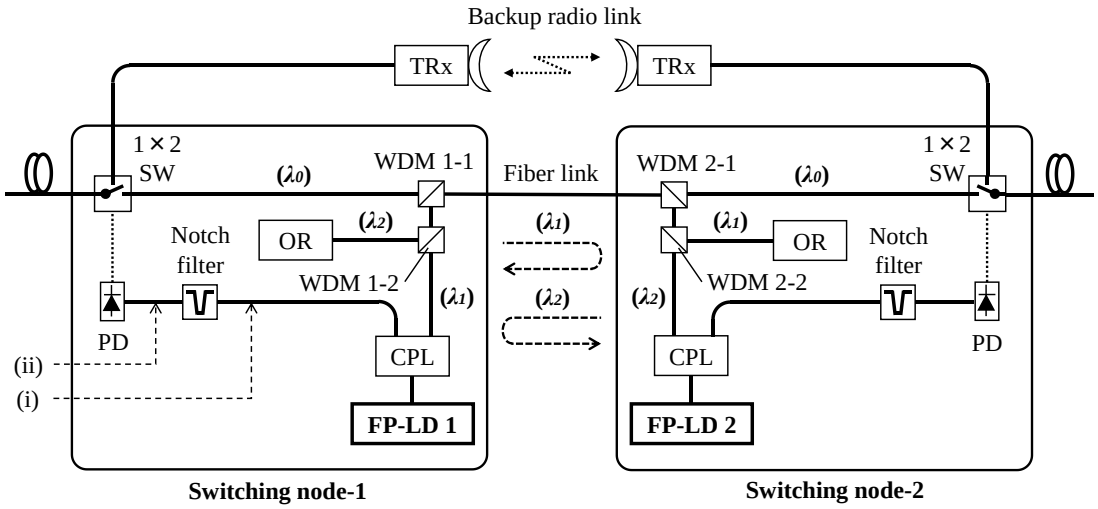

Fig. 3-3. Schematic diagram of the proposed autonomous self-healing technique.

the OR in the node-2. The reflected light is returned to the FP-LD in the node-1, and thus, the self-injection-locking state of the FP-LD is created.

The optical spectra of the injection-locked or unlocked FP-LD monitored at the points (i) and (ii) designated in Fig. 3-3 are shown in Figs. 3-4(a) to (d), respectively. In the injection-locking state, the FP-LD emits light with a narrow spectrum at 1550 nm (Fig. 3-4(a)), and the optical power passing through the notch filter is too low to be detected by the PD (Fig. 3-4(b)). On the other hand, when an optical fiber failure occurs, the FP-LD is turned to the unlocking state (Fig. 3-4(c)), and the light passing through the notch filter is injected into the PD (Fig. 3-4(d)). A trigger signal, which is generated by a simple analog circuit for the adjustment of the output from the PD, drives the SW to change the connection path from the fiber link to the backup radio link. Hence, the self-healing operation can be autonomously completed.

The proposed technique has high reliability for failure detection because it detects the light emitted from the FP-LD only in the case that optical fiber failures occur. The self-healing operation employing the proposed technique can be completed only in the

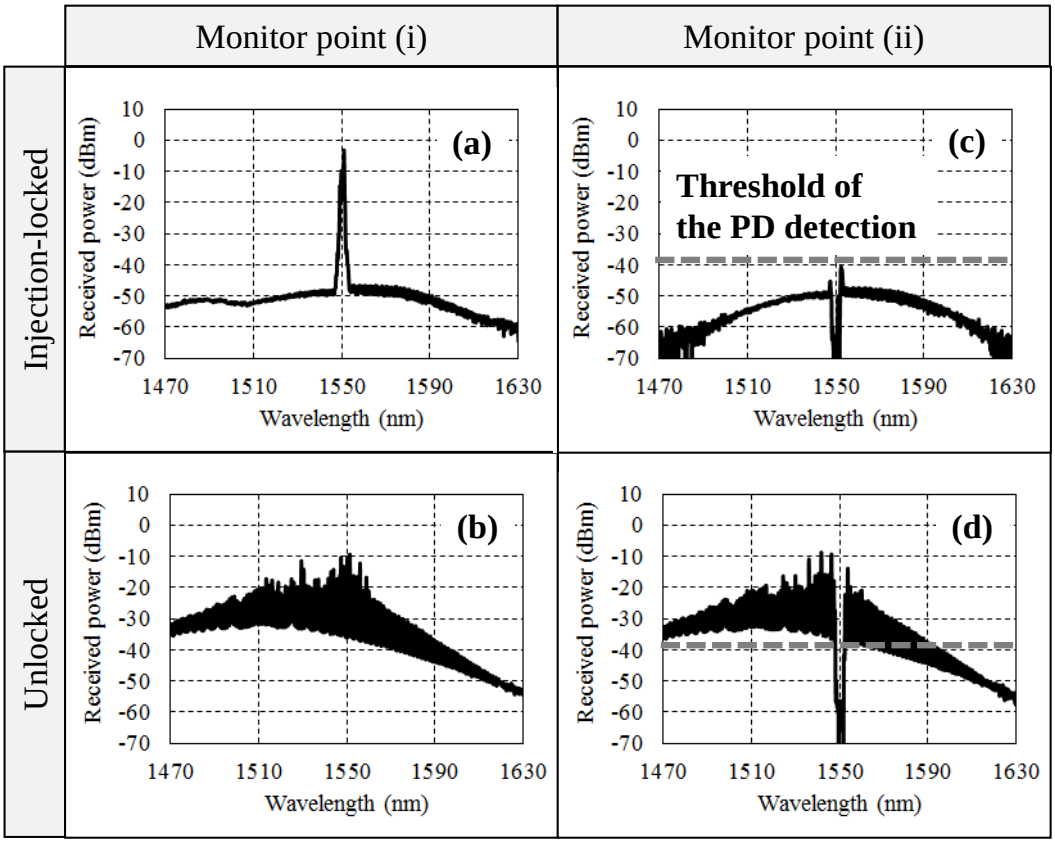

Fig. 3-4. Optical spectra measured at the points (i) and (ii) before and after optical fiber failure.

physical layer. In higher layers, a function of monitoring the switching node status in control plane will be necessary in the COs for changing the bit-rate. Thus, the total time to complete the switching of the whole system would be long, compared to the switching time in the physical layer.

3.3.3 Comparison among Related Techniques

Figures 3-5(a) and (b) show the alternative self-healing techniques based on the

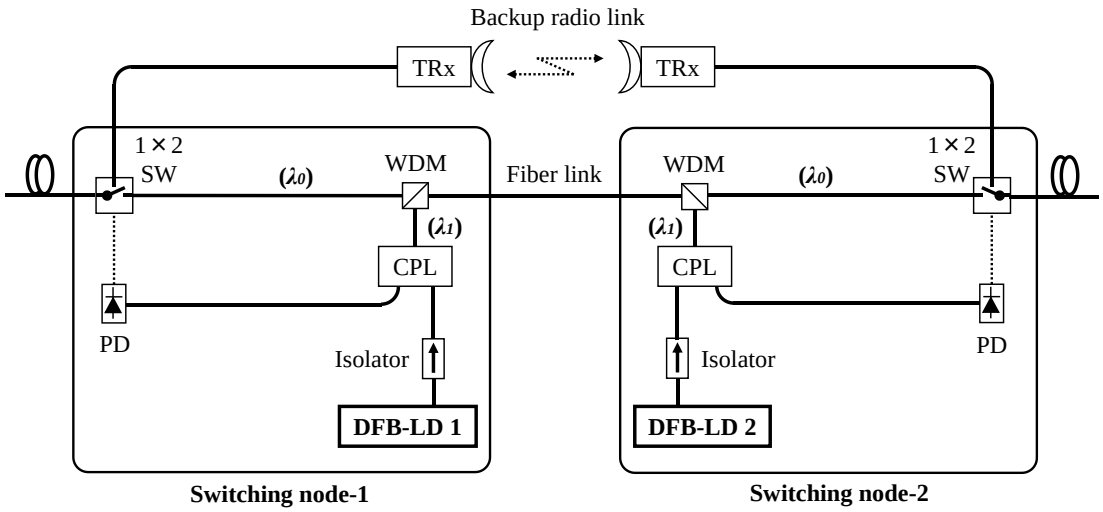

(a)

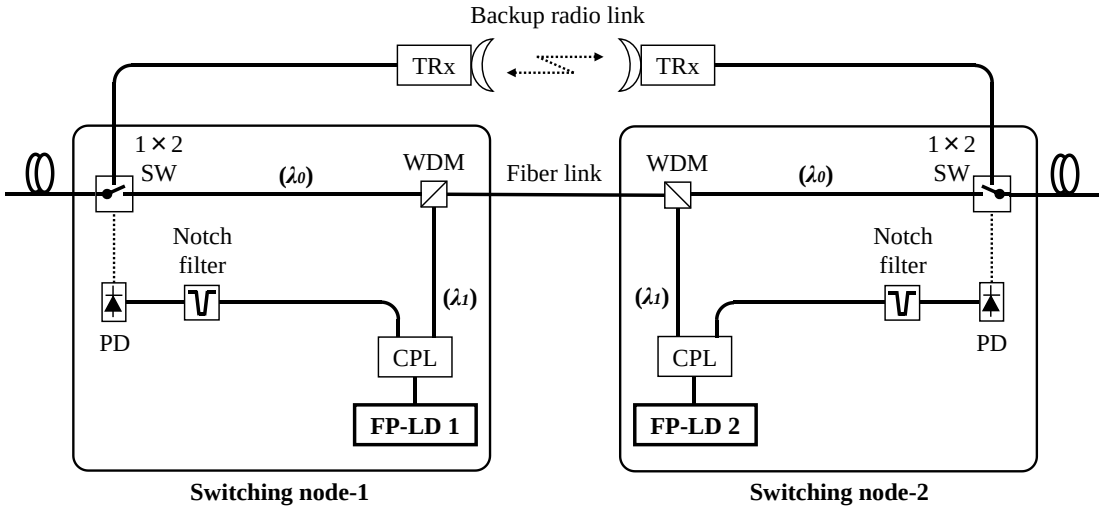

(b)

Fig. 3-5. Alternative configurations of self-healing techniques;
(a) DFB-LDs, (b) Mutual-injection-locked FP-LDs.

distributed feedback lasers (DFB-LDs) and on the mutual-injection-locked FP-LDs, respectively. In the configuration (a), the DFB-LDs-1 and 2 in the nodes-1 and 2 emits light toward the nodes-2 and 1, respectively, and the optical fiber failure can be detected

by monitoring optical received power at the PDs-2 and 1. In the configuration (b), the FP-LDs-1 and 2 in the nodes-1 and 2 are mutually injection-locked with each other, and the optical fiber failure can be detected by monitoring the change of the locking state of FP-LDs [44].

The result of comparison among three techniques in terms of the reliability for self-healing operation is summarized in Table 3-I. It is desired for the autonomous switching to operate only when optical fiber failures occur. In the DFB-LD-based technique, however, the switch is falsely operated in the cases of the DFB-LD and/or PD failures. As for the mutual-injection-locked FP-LDs, the false operation is caused in the case of the laser failure, and consequently, the self-healing operations based on these two techniques are not sufficiently reliable against disasters. For the mutual-injection-locking scheme, the temperature of the two FP-LDs must be adaptively controlled to keep the locking state. When the difference of the temperature between the two FP-LDs becomes large, the state is falsely changed to be unlocked.

Table 3-I. Comparison among three self-healing techniques.

Techniques	Switching operation in the case of each failure		
	Fiber failure	LD failure	PD failure
DFB-LDs	**Switch**	Switch	Switch
Mutual-injection-locked FP-LDs	**Switch**	Switch	**Hold**
Self-injection-locked FP-LD	**Switch**	**Hold**	**Hold**
Desired operation	Switch	Hold	Hold

On the other hand, even in the cases of the optical component failures such as the FP-LD and PD, the self-injection-locked scheme can properly operate because it uses a loop-back configuration. In addition, it does not require the temperature control of the FP-LD since it can be injection-locked by the light emitted from itself. Hence,

compared to the other two techniques, the self-healing technique based on the self-injection-locked FP-LD is the most promising because of its high reliability and simple configuration.

3.4 Seamless Optical and Radio Transmission Experiments

In this section, the proof-of-concept experiments of the proposed autonomous self-healing technique is conducted. In addition, the signal degradation caused by the switching operation from optical to radio links is quantitatively evaluated though the seamless optical and radio transmission experiments employing the proposed self-healing technique.

3.4.1 Experiment for Autonomous Self-Healing Operation

The proof-of-concept experiments of autonomous self-healing operations employing the detection technique utilizing a self-injection-locked FP-LD were conducted. Figure 3-6 shows the experimental setup. An FP-LD at the central wavelength of 1550 nm was located in the node-1 for monitoring the state of 1 km-long SMF. The DFB-LD emitted light at the wavelength of 1535 nm as a light source emulating an optical data signal. The light emitted from the FP-LD looped back to the node-1 after being reflected by the OR in the node-2, and the FP-LD was self-injection-locked. The pass-bands of the WDM couplers for slicing the spectrum of the light emitted from the

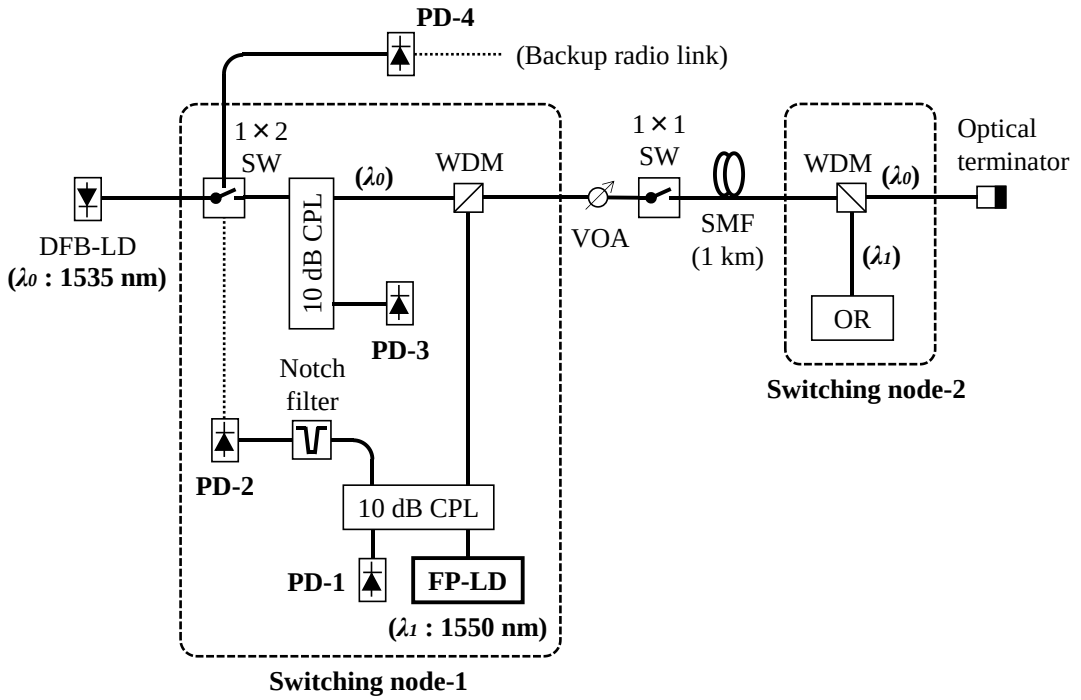

Fig. 3-6. Experimental setup for optical fiber failure detection and switching.

FP-LD were 1550 ± 1.5 nm, and the rejection bandwidth of the optical notch filter was 3 nm. The PDs-1, 2, 3, and 4 monitored the optical powers of the injection light into the FP-LD, that after the optical notch filter, that output from the 1 × 2 SW to the SMF, and that output from the 1 × 2 SW to the backup radio link, respectively. The failure of the SMF was emulated by switching a 1 × 1 SW placed between the nodes-1 and 2, and the evolution of optical powers monitored by the PDs-1 to 4 were measured.

The optical power received by the PD-2 as a function of the optical injection power into the FP-LD is shown in Fig. 3-7. The horizontal and vertical axes are "the injection power into the FP-LD" and "the optical power measured by the PD-2 designated in Fig. 3-6," respectively. The injection power into the FP-LD was changed by adjusting the variable optical attenuator (VOA) inserted between the node-1 and 1 ×1 SW in the experiment. It is shown that the state of the FP-LD gradually varies from

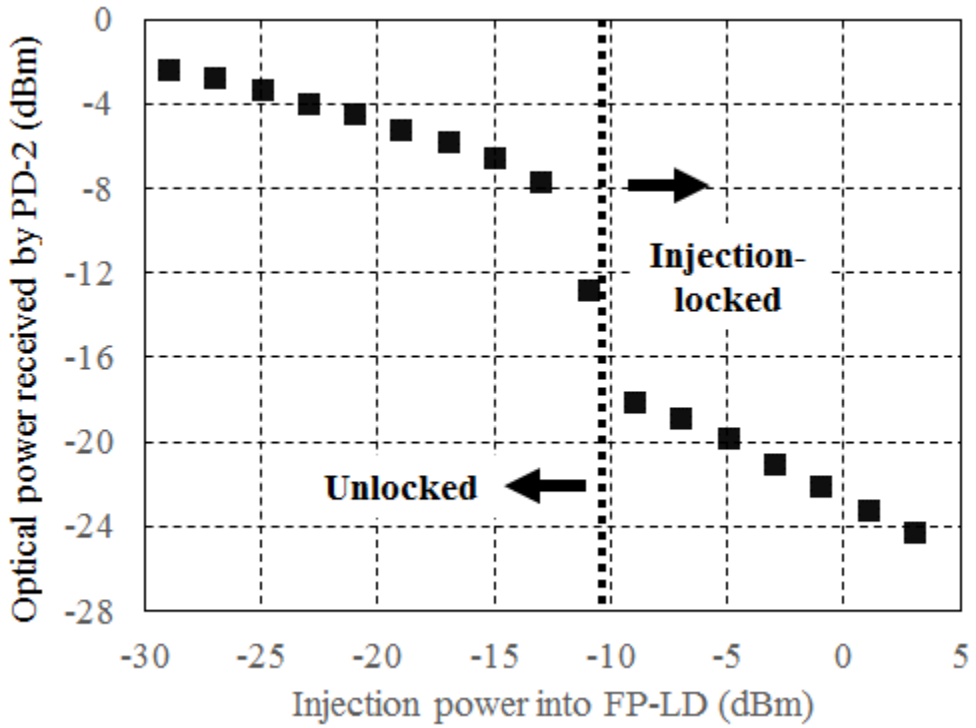

Fig. 3-7. Optical power received by the PD-2 as a function of the injection power into the FP-LD.

the injection-locking state to the unlocking state when the injection power becomes less than about –10 dBm. As the optical output power from the FP-LD used in the experiment was +8 dBm, the round-trip optical transmission loss can be allowed up to 18 dB for keeping the injection-locking state, and thus, the power budget between the nodes-1 and 2 corresponds to a half of 18 dB. The polarization dependence of the reflected light for the injection-locking was measured to be 0.9 dB, which is a relatively small value although the FP-LD is not specially designed nor optimized. Therefore, the self-healing technique can be applied to the systems with an optical power budget of 8 dB after subtracting 1-dB polarization dependence. As the polarization dependence loss (PDL) of the FP-LD may be larger than 1 dB in the actual situation, it is preferabe

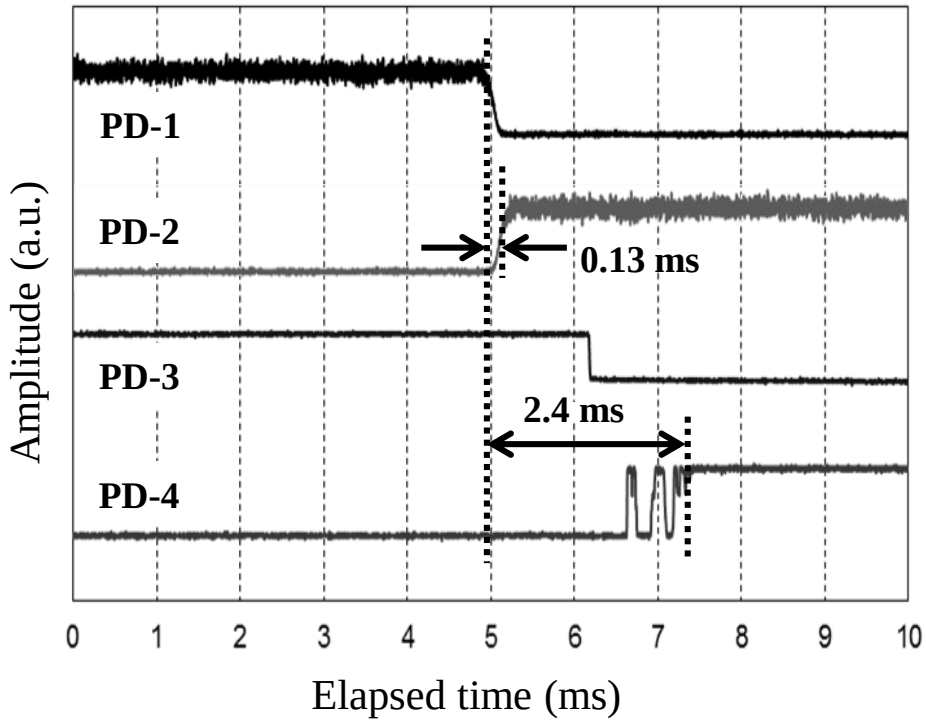

Fig. 3-8. Optical power received by the PD-1 to the PD-4.

to adopt the FP-LD with low-PDL characteristic in a practical use.

As the optical injection power required for creating the injection-locking state of the FP-LD is high (more than –10 dBm in this experiment), the proposed technique is unlikely to falsely operate by some unintended lights reflected at fiber connection points. In addition, while each FP-LD has the individual characteristics on the injection-locking operation, there is no technical problems in a practical use once the system operators measure the required parameters of each FP-LD as references and configure them remotely for the equipment in the switching nodes. In order to suppress operating and testing expenditure, some techniques that enables us to automatically measure the parameters of FP-LDs will be needed.

Figure 3-8 shows the optical powers received by the PDs-1 to 4 as a function of

elapsed time. These results indicate that the FP-LD turned to the unlocking state by the optical fiber failure, subsequently the received power at the PD-2 increased, and finally, the 1 × 2 SW was correctly switched from the failed optical fiber link to the backup radio link. As the 1 × 2 SW used in the experiment mechanically switches the optical paths, a chattering of the received optical power at the PD-4 was observed when the optical path was switched. The optical fiber failure detection time was as small as 0.13 ms, and the total self-healing time including the stabilization of the 1 × 2 SW was 2.4 ms. The switching speed would be sufficiently rapid to be adopted in seamless optical and radio communication systems. Thus, it was confirmed that the proposed technique can rapidly recover the failed optical fiber links with high reliability and simple configuration. The optical fiber failure detection time of 0.13 ms results from the injection-locking state change of the FP-LD, and it may be difficult to be shortened due to the restriction on physical phenomena. However, by using the switching devices quicker than the SW used in the experiment, the total self-healing time of 2.4 ms will be able to be shortened.

The application of the proposed technique is not necessarily limited to seamless optical and radio communication systems. For example, in future passive optical networks (PONs) that provide broadband services to hundreds of subscribers via an optical fiber [45]–[47], failure at a single point should have a significant impact. In such a case, the fiber failure can be promptly recovered by deploying the self-healing nodes at critical points along the optical fiber line, while the redundant links are not necessarily limited to radio links.

3.4.2 Experiment for Seamless Radio-over-Fiber Transmission

In order to design parameters such as the number of backup radio links and optical fiber transmission length in the seamless optical and radio communication system, it is

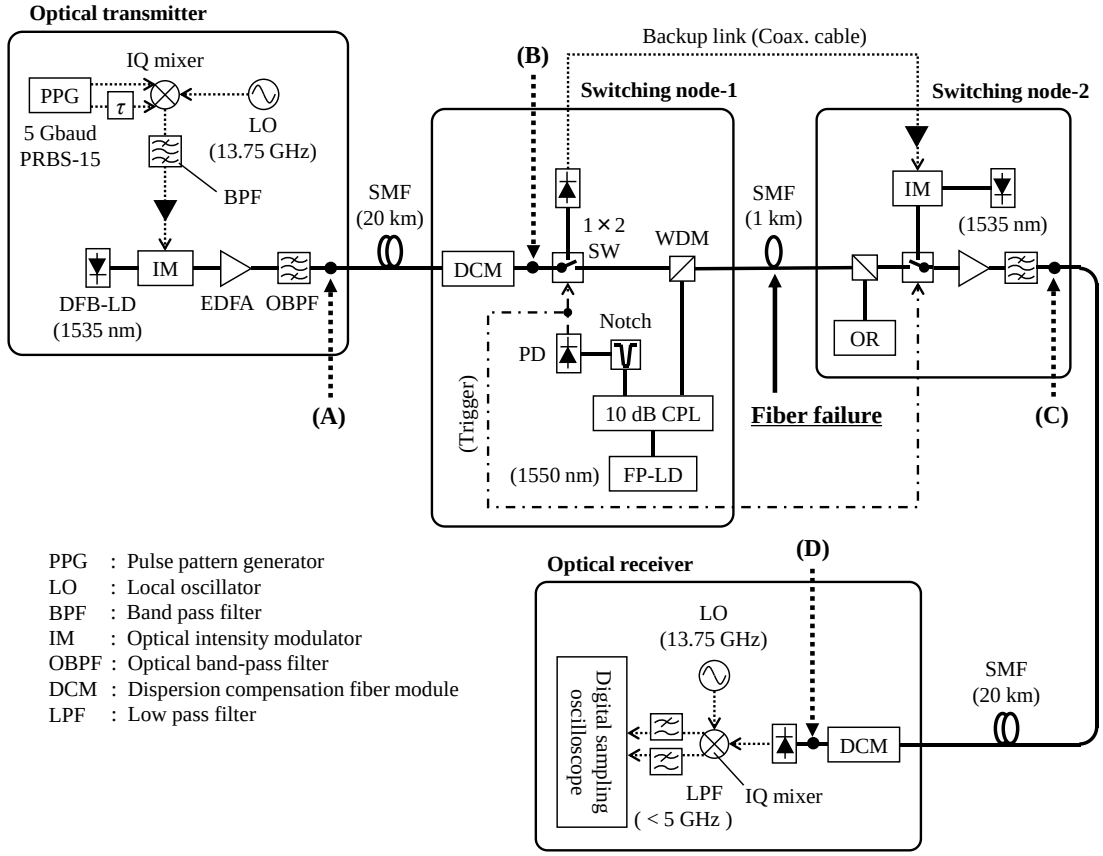

Fig. 3-9. Experimental setup for seamless RoF transmission.

necessary to quantitatively analyze the degradation of signal quality when the optical fiber links are switched to the backup radio links. Therefore, seamless RoF transmission experiments including the proposed self-healing technique were conducted.

The experimental setup for seamless RoF transmission is shown in Fig. 3-9. The switching nodes-1 and 2 based on the proposed self-healing technique were inserted between the optical transmitter and receiver. The optical transmitter and receiver were connected to the switching node-1 and 2 by 20 km-long SMFs, respectively. When the 1-km SMF between the switching nodes-1 and 2 is cut-off, the two switching nodes will autonomously switch the failed fiber link to the backup link. In order to quantitatively

measure the transmission penalty caused by the switching operation for the 1-km SMF failure, the backup radio link was emulated by a coaxial cable between the PD and the IM. Therefore, the undesired effect of the level fluctuation in the radio transmission sections was not considered in this experiment.

In the optical transmitter, a 5-Gbaud pseudo random bit sequence with the length of 2^{15} (PRBS-15) was converted to a 10-Gbit/s QPSK signal with 13.75-GHz intermediate frequency by using an I/Q mixer. The 10-Gbit/s QPSK signal was injected to the IM and then converted to a RoF signal of which central wavelength was 1535 nm. The OMI of the RoF signal was about 25%. After being amplified by an erbium-doped fiber amplifier (EDFA), the RoF signal was injected into the switching node-1 via the 20-km SMF. For compensating the RF transmission penalty caused by fiber chromatic dispersion [36], a dispersion compensation fiber modules (DCMs) of –340 ps/km, which corresponded to the chromatic dispersion of 20-km SMF, were inserted in the switching node-1 and optical receiver.

When the 1-km SMF was not failed, the RoF signal reached the switching node-2 via the 1-km SMF, and the RoF signal was injected into the optical receiver via 20-km SMF. When the 1-km SMF is cut off, the switching nodes-1 and 2 autonomously switched the failed SMF link to the backup link. The 10-Gbit/s QPSK signal received by the PD in the switching node-1 was re-converted to the 1535-nm RoF signal by the IM in the switching node-2, and the RoF signal arrived at the optical receiver via the 20 km-long SMF. In the optical receiver, the RoF signal was directly detected as a 10-Gbit/s QPSK signal after compensating the effect of the fiber chromatic dispersion by the DCM, and the 10-Gbit/s QPSK signal was converted to the two 5-Gbaud baseband signals by being mixed with a 13.75-GHz RF tone in the I/Q mixer. After an off-line signal processing in the oscilloscope, the signal-to-noise ratio (SNR) of the received baseband signals was measured.

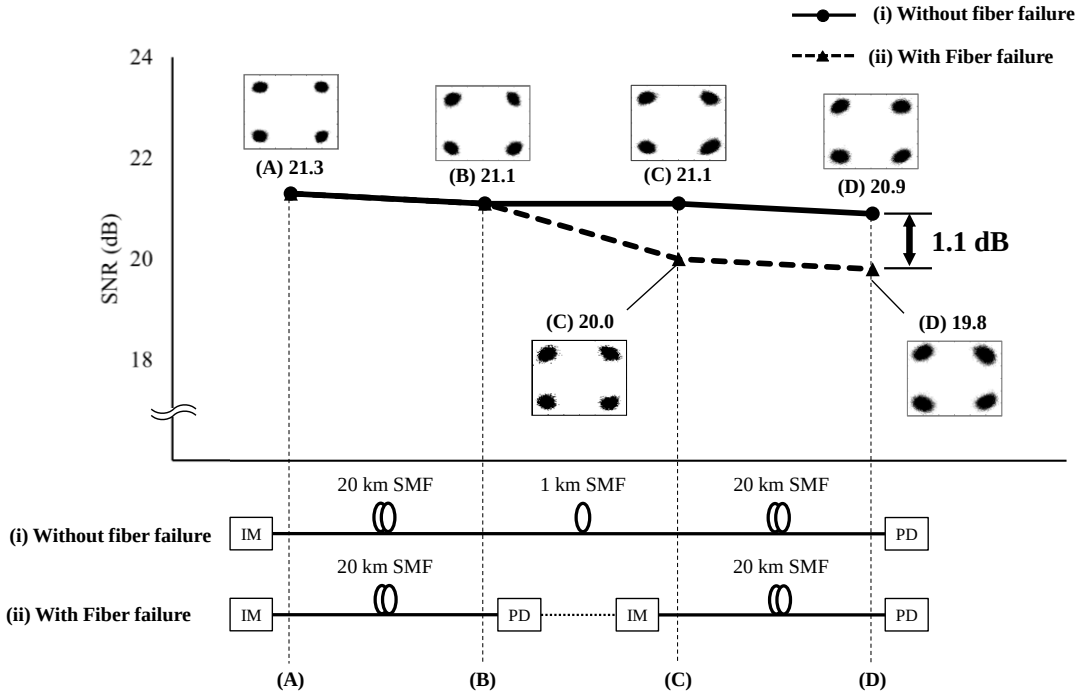

Fig. 3-10. SNR diagram and constellations with and without fiber failure.

In order to analyze the degradation of the signal quality by the switching operation, the SNR values with and without fiber failure were measured at four representative points as shown in Fig. 3-9; (A) just after the EDFA in the optical transmitter, (B) just after the DCM in the switching node-1, (C) just after the EDFA in the switching node-2, and (D) just after the DCM in the optical receiver, respectively. Figure 3-10 shows the SNR diagram and the corresponding constellations with and without fiber failure. In the section from (A) to (B) that corresponded to the 20-km SMF transmission span from the optical transmitter to the switching node-1, it can be confirmed that the SNR was degraded from 21.3 to 21.1 dB (0.2-dB SNR degradation). It can be assumed that this SNR degradation was caused by the disproportion of dispersion compensation of the DCM. In the section from (B) to (C), there was no SNR degradation when the fiber failure did not occur. On the other hand, the SNR was degraded from 21.1 to 20.0 dB

(1.1-dB SNR degradation), which may be caused by the re-modulation from the RF signal to the RoF signal, in the case of fiber failure. Finally, in the section from (C) to (D) which corresponded to the 20-km SMF transmission span from the switching node-2 to the optical receiver, the SNR degradation was 0.2 dB in both cases with and without fiber failure.

From the above-described results, the SNR degradation of 10-Gbit/s QPSK signal transmission can be estimated to be only 0.1 dB per 10-km SMF, and therefore, it has no large impact on the total system of seamless optical and radio communication. While the SNR degradation caused by the switching operation was 1.1 dB, the effect on the total system is not so large because sufficient SNR margin can be ensured in considering the forward error correction (FEC) limit of SNR = 8.5 dB with 7% overhead (the corresponding bit error rate is 3.8×10^{-3}) [48].

This experiment was conducted in terms of unidirectional communication from CO-1 to 2, and the SNR degradation was not observed even when the monitoring light emitted from the FP-LD was multiplexed with the RoF signal. When we consider the real system of bidirectional communication, it is necessary to carefully consider the nonlinear optical effects in the SMF transmission [49]. In this experiment, the wavelengths for the monitoring light and data signal light were set as 1550 and 1535 nm, respectively, due to the restriction of experimental apparatus, while the wavelength for monitoring light should be within 1.3-μm band and that of data signal light should be 1.5-μm band, from a practical point of view. By adopting such a wavelength allocation, we can ensure enough wavelength spacing of more than 120 nm to avoid the stimulated Raman scattering (SRS) [50] that is one of the nonlinear optical fiber effects.

Figure 3-11 shows the relationship between the SNR and the number of backup radio links. The solid and dotted lines show the measurement result in the experiment and the calculation result estimated from the experimental results, respectively. As the SNR just after the optical transmitter was 21.3 dB and the SNR degradation caused by

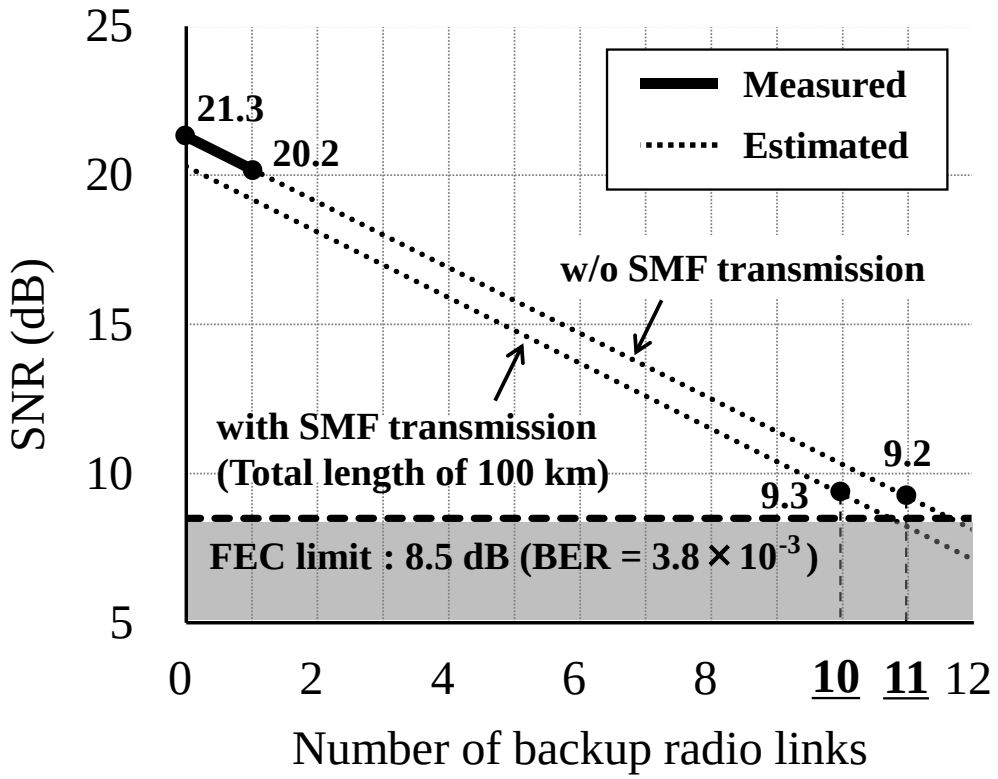

Fig. 3-11. Relationship between SNR and the number of backup radio links.

the switching operation was 1.1 dB, the SNR will be 20.2 dB when one failed fiber link is switched to the backup radio link. When the signal degradation due to SMF transmission is not taken into account, it can be estimated that the number of backup radio links will be up to 11 because the FEC limit is 8.5 dB (the SNR after recovering 11 sections is 9.2 dB). In this calculation, it was assumed that there is no noise source in each radio section and the noises caused by optical re-modulation in each backup link were completely based on the white Gaussian noise distribution [51]. Therefore, the SNR degradation in each backup section becomes 1.1 dB without any deviations. In the practical system where the total transmission fiber length from the CO-1 to the CO-2 is 100 km at the longest, the transmission penalty should be considered. From

the experimental results shown in Fig. 3-10, the SNR degradation caused by the 100-km SMF transmission can be estimated to be about 1 dB. Therefore, when the transmission penalty is also taken into account, the number of backup radio links will be up to ten (the SNR after 100-km SMF transmission and recovering ten sections is 9.3 dB). As the performance of each optical and RF component used in this experiment were optimized as much as possible, it may be difficult to drastically improve the SNR values and increase the number of backup radio links.

In actual backup radio links, there is a concern about RF power fluctuation during the radio transmission, which may depend on the radio propagation characteristics in each frequency range used in the system. As there is no large noise component in each radio transmission section, the SNR degradation in radio sections will not be so large. For example, when we assume the SNR degradation in one radio section is 0.5 dB at the maximum, it can be calculated that the number of backup radio links will decrease to seven links. From these experimental results, the required parameters for designing the seamless optical and radio communication system can be clarified.

3.5 Conclusion

In this chapter, an autonomous self-healing technique utilizing a self-injection-locked FP-LD was proposed for seamless optical and radio communication systems. Compared to the other techniques with a similar configuration, the proposed technique is the most promising for the self-healing operation because of its high-reliability and simple configuration. The failure detection time of 0.13 ms and the total self-healing operation of 2.4 ms were experimentally confirmed, which are rapid enough to be

adopted in the practical systems.

In addition, the signal quality degradation caused by switching operation was quantitatively evaluated throughout the 10-Gbit/s RoF transmission experiment employing the proposed self-healing technique. It was experimentally confirmed that more than ten backup radio links including 100-km fiber transmission was achievable. The obtained results in this chapter enable us to design seamless optical and radio communication systems with plural backup radio links.

Chapter 4

Optical Beam Forming Scheme for Phased Array-Antenna

4.1 Introduction

In this chapter, a simple and practical technique for beam forming of the phased array-antennas by RoF transmission technique is studied. A new scheme to detect the direction of mobile terminals is proposed, which is expected to be employable in a practical system, and the feasibility of the proposed detection technique is confirmed by bidirectional RoF transmission experiments. In addition, a two-dimensional beam forming in the millimeter-wave band is experimentally demonstrated for targeting a future high-speed radio communication system. The system parameters required for a practical system in the microwave and millimeter-wave bands are also designed by investigating the effect of CD on RoF transmission.

4.2 Fundamental Architecture of Proposed Scheme

In this section, the fundamental mechanism of beam forming for phased array antennas based on RoF transmission is introduced, and a scheme for detecting the direction of mobile terminals is proposed.

4.2.1 Phased Array-Antenna

A conventional phased array-antenna is schematically illustrated in Fig. 4-1. It consists of *N* pairs of an RF phase shifter and an antenna element. An RF signal input to the array-antenna is divided and fed to each RF phase shifter for arbitrarily shifting the RF phase, and the RF signal injected into each antenna element forms a beam defined by the relative RF phases.

When the RF signals injected into each antenna element are totally in-phase, the array-antenna radiates a straightforward beam toward the observation angle of 0 degree. In contrast, when the relative RF phases are changed, the beam radiated from the array-antenna is steered as shown in Fig. 4-1. The array factor (AF), which indicates the total directivity of the array-antenna, is expressed as;

$$AF(\theta) = \sum_{k=1}^{N} \exp\left\{ -j\left(\frac{2\pi}{\lambda_{RF}} d_k \sin\theta + \beta_k \right) \right\}, \tag{4.1}$$

where λ_{RF} is the wavelength of RF carrier, d_k is the distance of each antenna element, θ is the observation angle, and β_k is the phase shift among input RF signals to the array-antenna [51]. A numerically calculated result of the AF in the case of two

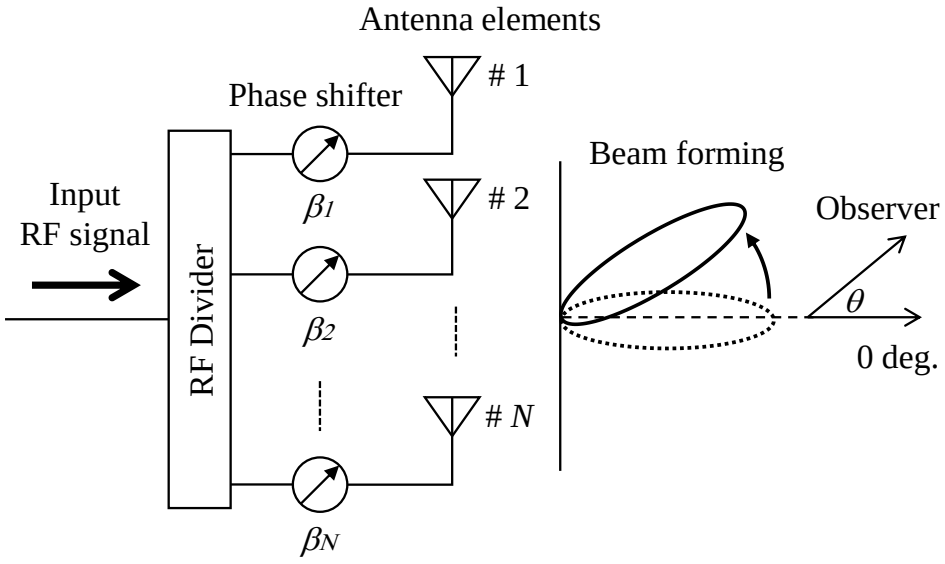

Fig. 4-1. Schematic illustration of the phased array-antenna with *N* elements.

antenna elements is shown in Fig. 4-2. In the calculation, the phase shift of antenna element #1 was fixed at 0, while that of antenna element #2 (β) was changed as 0, $\pi/2$ and π. The distance between two elements was set as d = 0.7 λ_{RF}. As formerly described, when β equals to 0, the phases of the RF signals fed to two antennas are synchronized and the peak of the AF appears at the observation angle of 0 degree. In the case of $\beta = \pi/2$, the peak point shifts at around –15 degree. In the case of $\beta = \pi$, a null point of the AF appears at 0 degree and the peak point shifts at around ±30 degrees. Thus, beam forming of the array-antenna will be achieved by changing the relative RF phase.

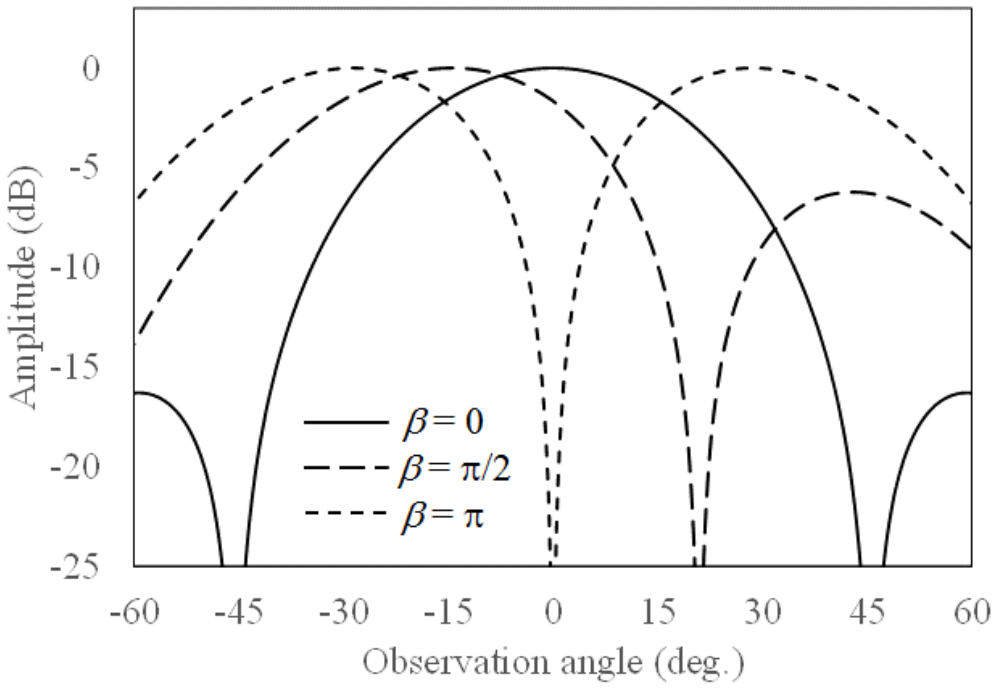

Fig. 4-2. Numerically calculated result of the array-factor with RF phase shift.

4.2.2 Antenna Beam Forming by Radio-over-Fiber

A beam forming technique by RoF transmission is one of the promising candidates for the simplification of the phased array-antenna architecture. In the beam forming scheme by RoF, the relative RF phases can be generated by precisely controlling the wavelengths of light sources. Figures 4-3(a) and (b) show a schematic illustration how the antenna beam is steered by RoF transmission, in which two RoF signals at the wavelengths of λ_1 and λ_2 are transmitted from the E/O at the CO and received by the O/E in the antenna site, and finally fed to respective antenna elements #1 and #2. At

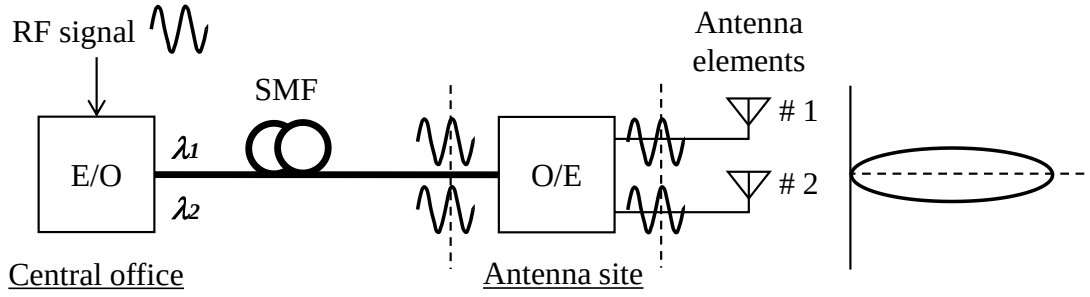

(a)

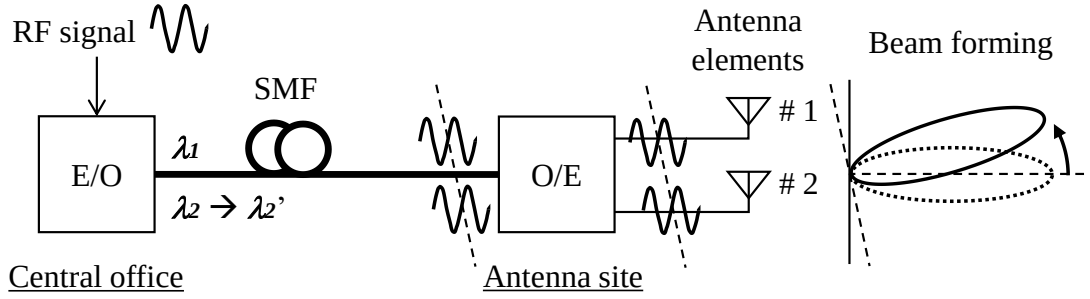

(b)

Fig. 4-3. Schematic illustration of antenna beam forming by RoF;
(a) RF signals are in-phase, (b) RF phase is relatively shifted.

the initial condition where the phases of the RF signals fed to two antenna elements are synchronized, the array-antenna radiates a straightforward beam as shown in Fig. 4-3(a). The initial phase offset due to the different wavelengths between λ_1 and λ_2 can be compensated by, for example, optical delay lines in the central office, which are utilized for the experiments described in the following sections. In contrast, when the wavelength λ_2 is changed to λ_2', the phase of the RoF signal at λ_2' is shifted because of the CD, and it results in steering of the RF beam radiated from the array-antenna as shown in Fig. 4-3(b). By controlling the wavelengths in the CO according to the predetermined CD of the SMF, which has a typical dispersion parameter of D = 16–18

ps/nm/km in the wavelength range of 1.5 μm [53], the antenna beam can be remotely steered. The required wavelength shift ($\Delta\lambda$) in order to attain π phase shift of the RF signal is given by the following equation;

$$\Delta\lambda = 1 \Big/ \left(2LDf_{RF}\right), \tag{4.2}$$

where L is the length of the SMF and f_{RF} is the RF carrier frequency [22]. This scheme can simplify the phased array-antenna architecture by eliminating the RF phase shifters at the antenna site. In this scheme, the controllable parameter is only the wavelength of lasers because the fiber length, dispersion parameter, and RF carrier frequency are uniquely determined.

4.2.3 Proposed Scheme to Detect the Mobile Terminal Direction

While the RoF-based beam forming of the array-antenna can be achieved as described in Sect. 4.2.2, the method to detect the direction of mobile terminals is indispensable in practical radio access systems. For detecting the direction of mobile terminals, a novel scheme to transmit RoF uplink signals received from the antenna is proposed.

When considering the laser diodes (LDs) are used for array-antennas as uplink light sources that are located at the antenna site, it is inevitable that the configuration of the BS becomes greatly complicated due to the required functionalities such as the wavelength control, the wavelength stabilization, and the output power stabilization. Therefore, we propose an uplink transmission scheme utilizing reflective-semiconductor optical amplifiers (RSOAs). Owing to the loop-back architecture with RSOAs [54], [55], the wavelengths of RoF uplink signals are remotely controllable from the CO, and the RSOAs can be “colorless” owing to their wide operational range in wavelength. In

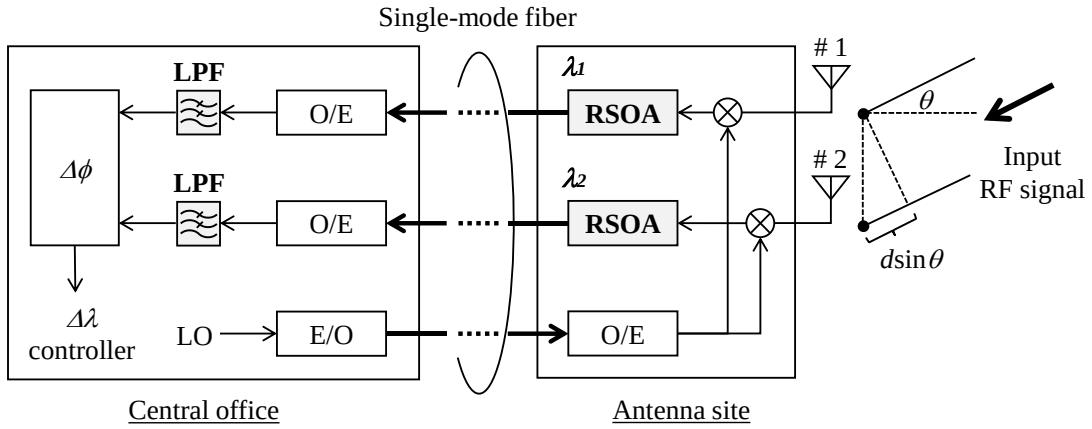

Fig. 4-4. Schematic diagram of the proposed RoF uplink transmission.

addition, the wavelengths of RoF uplink signals are not affected by the outside environment because of reusing the optical downlink signals that are originally generated at the CO. When we consider the time division duplex (TDD)-based mobile systems, however, the reuse of downlink signals may cause a degradation of uplink signal quality due to the residual modulation tone of the downlink signal [56]. To avoid the signal quality degradation, an uplink frequency conversion technique is applied to the proposed scheme [56].

A schematic diagram of the RSOA-based RoF uplink transmission is depicted in Fig. 4-4. The frequency of RF uplink signals is down-converted by being mixed with an RF tone from a local oscillator (LO). For further simplification of the antenna site, the LO should be also located in the CO, where the RF tone from the LO is transmitted as a RoF signal to the antenna site. RSOAs are re-modulated by down-converted RF uplink signals. The RF uplink signals transmitted to the CO are then passed through low-pass filters (LPFs), and thus, the frequency component of the residual modulation tone can be extracted. By utilizing the frequency down-conversion technique, the

undesired interference with uplink signal can be avoided.

The procedure for detecting the direction of mobile terminals is described in detail as follows. The RF phase difference ($\Delta\phi$) is calculated for the angle estimation of an input RF uplink signal at the CO. The $\Delta\phi$ consists of the RF path difference ($\Delta\phi_1$) and the phase shift caused by the CD ($\Delta\phi_2$). The $\Delta\phi_1$ can be derived from the path difference of $d\sin\theta$, and the $\Delta\phi_2$ can be compensated by calculating the phase shift yielded by the CD, because the optical fiber length and the wavelengths of downlink signals are preliminarily known at the CO. The arrival angle of the RF uplink signal (θ) is expressed by the following equation:

$$\theta = \sin^{-1}\left(c \cdot \frac{\Delta\phi - DL|\lambda_1 - \lambda_2|}{d} \right), \tag{4.3}$$

where c is the light velocity in an optical fiber, and d is the distance between two antenna elements. By calculating the Eq. (4.3), the arrival angle corresponding to the direction of mobile terminals can be estimated at the CO. Finally, it is possible to properly control the wavelengths of RoF downlink signals toward the detected direction of the mobile terminal.

4.3 Experiments for Proposed Detection Scheme

As the proof-of-concept demonstration of the scheme described in Sect. 4.2, experiments for antenna beam forming in 2-GHz band, which is the frequency band used for current mobile or Wi-Fi systems [58], are conducted.

4.3.1 Experiment for Antenna Beam Forming

A beam forming experiment of a 2 GHz-band array-antenna was conducted by using the experimental setup as shown in Fig. 4-5. Two wavelengths at λ_1 = 1550 and λ_2 = 1530 nm were modulated by a 2.1-GHz continuous wave (CW) RF signal. After propagating a 5 km-long SMF, two optical downlink signals were converted to RF signals in O/Es, and they were fed to two antenna elements. Figure 4-6 shows the pictures of the array-antenna used in the experiment. The array-antenna consists of two patch antennas at the central frequency of 2.1 GHz. The two patch antenna elements are separated by 1.3 λ_{RF}, which is wider than the 0.7-λ_{RF} separation used for the calculation in Sect. 4.2, in order to observe clear null points. At the initial condition, the phases of the RF signals fed to two antennas were synchronized. For steering the beam, λ_2 was changed from 1530 to 1533 nm because the $\Delta\lambda$ for π RF phase shift of the 2.1-GHz RF signal was estimated to be approximately 3 nm from Eq. (4.2). The radio transmission distance was 8 m. It should be noted that the antenna site in Fig. 4-5 was set up in an anechoic chamber to exclude unintentional interference of reflected or external signals.

Figures 4-7(a) to (c) show the measured beam patterns for the RF phase shifts of 0, $\pi/2$ and π, respectively, where the 3-nm wavelength change along the 5 km-long SMF transmission was preliminarily confirmed to yield the relative RF phase shift of π. The result corresponds to the actual value of the CD parameter of 16.7 ps/nm/km. It is observable that a null point appears at 0 degree in the case of π phase shift. The measured beam patterns almost coincide with the numerical calculation results obtained from Eq. (4.1). Thus, the feasibility of the RoF-based antenna beam forming scheme was experimentally confirmed.

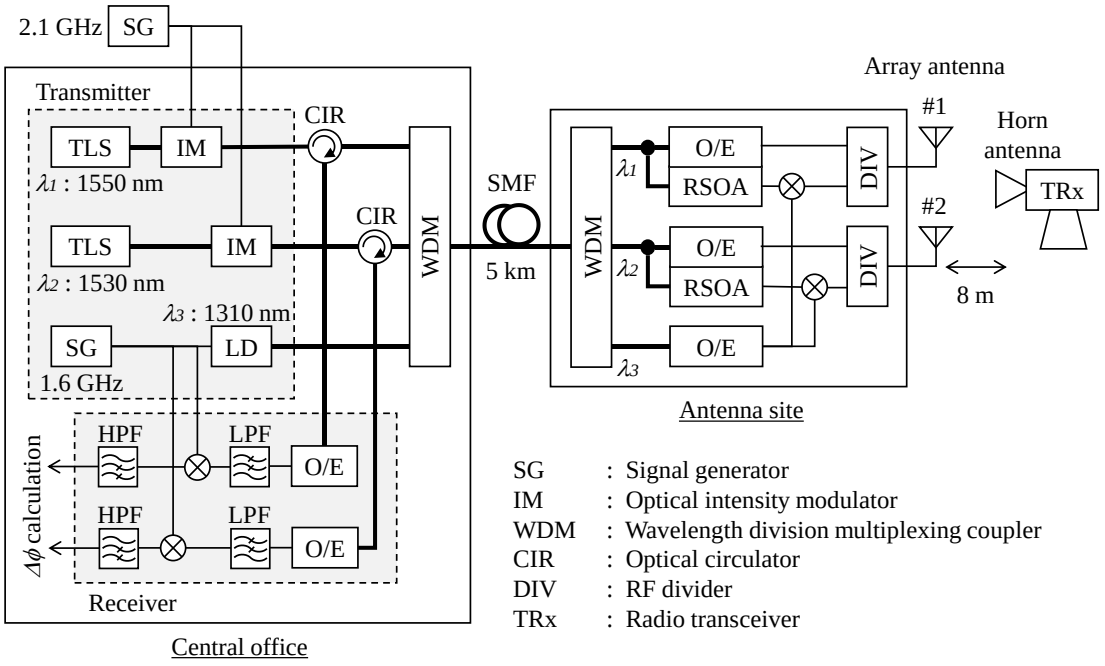

Fig. 4-5. Experimental setup for beam forming of the 2-GHz array-antenna.

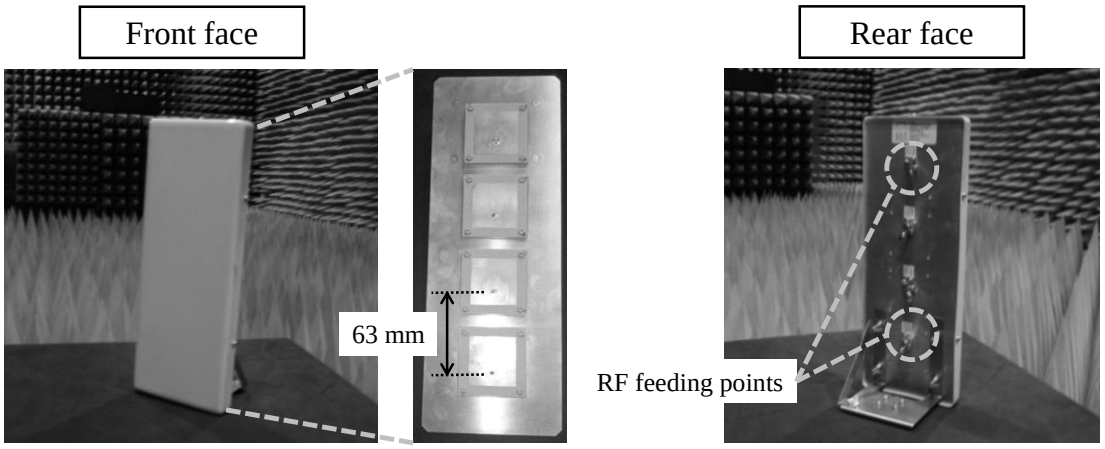

Fig. 4-6. Pictures of the array-antenna used in the experiment.

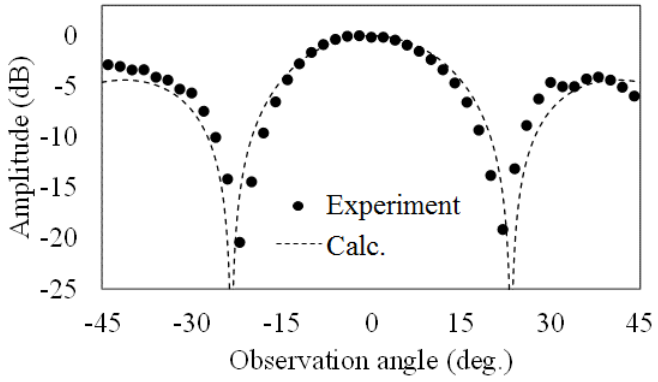

(a)

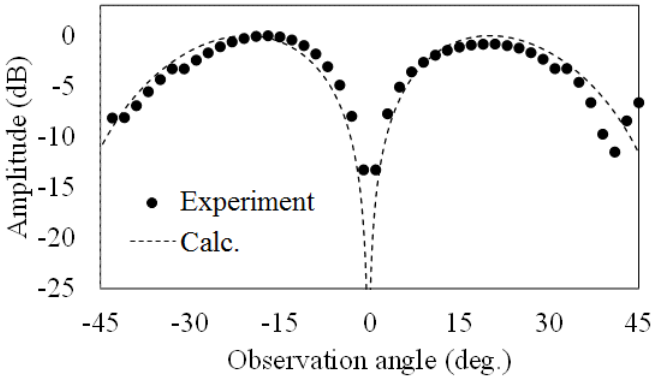

(b)

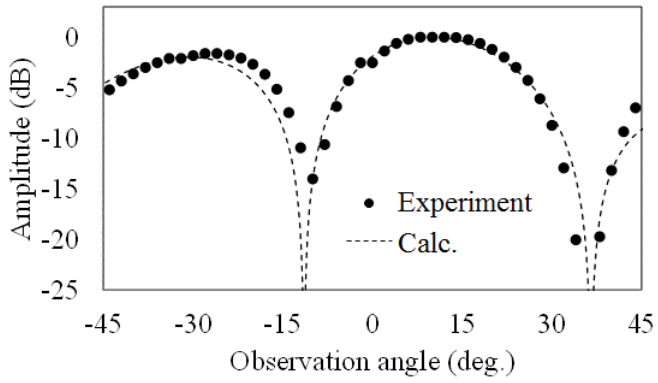

(c)

Fig. 4-7. Beam patterns when the λ_2 was (a) 1530, (b) 1531.5, and (c) 1533 nm.

4.3.2 Experiment for Detecting the Direction of Mobile Terminals

An experiment for detecting the direction of mobile terminals based on the proposed scheme was conducted. The experimental setup is shown in Fig. 4-5, which is the same as the downlink beam forming experiment. A part of the optical downlink signal was tapped and injected into the RSOA. The 2.1-GHz RF uplink signal from the RF transceiver (TRx) was down-converted to 500 MHz by being mixed with a 1.6-GHz RF tone, and two optical downlink signals were re-modulated by the RSOAs with the down-converted RF uplink signals. The frequency component of 500 MHz was extracted by LPFs at the CO. The 2.1-GHz original RF uplink signals were restored after up-conversion by being mixed with an 1.6-GHz RF tone, and then, the phase difference ($\Delta\phi$) between two RF uplink signals was measured by changing the angle of the array-antenna from –60 to 60 degrees.

Figures 4-8(a) and (b) show the RF phase shift generated by the wavelength change of the downlink and uplink, respectively. The relative RF phase shift was π in the downlink by changing the wavelength of λ_2 by 3 nm, while the 3-nm wavelength shift for the uplink yielded $\pi/4$ RF phase shift because of the frequency down-conversion to 500 MHz corresponding to $f_{RF}/4$. Therefore, it is confirmed that the beam control scheme accurately operates in both directions. Figure 4-9 shows the measured $\Delta\phi$ as a function of the incident angle of the RF uplink signal. The numerical calculation result obtained from Eq. (4.3) is inset in Fig. 4-9. The $\Delta\phi$ was linearly changed according to the incident angle of the RF uplink signal and the experimental result almost coincides with the calculation result. The result indicates that the arrival angle of the RF uplink signal, i.e., the direction of mobile terminals, can be estimated, and that the wavelength of TLSs for the optical downlink transmission can be properly controlled toward the detected direction of the mobile terminal. Throughout the experiments in both downlink and uplink directions, the feasibility of the proposed antenna beam control

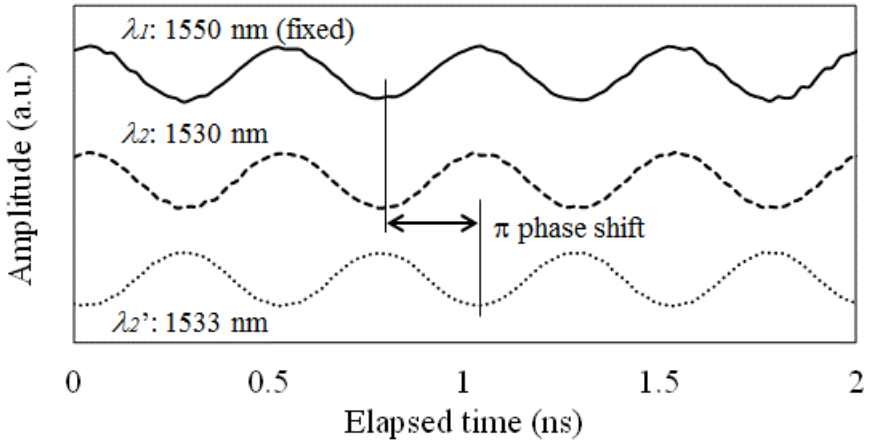

(a)

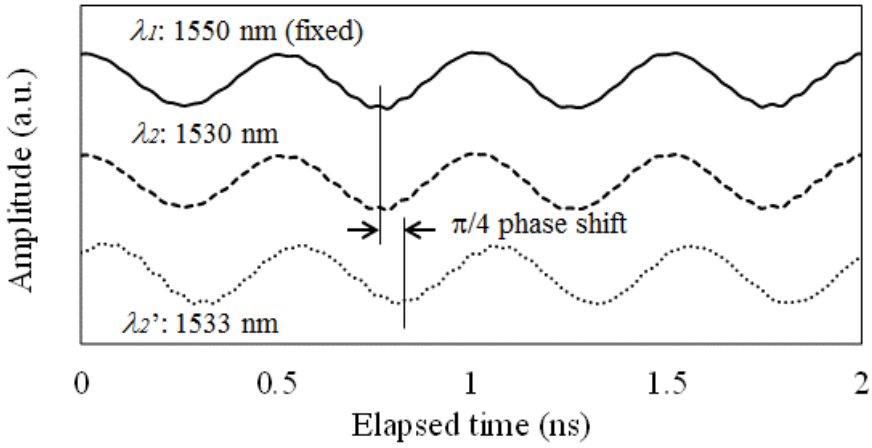

(b)

Fig. 4-8. Relationship of RF phase shift between (a) downlink and (b) uplink.

scheme was successfully demonstrated. The scheme will be also applicable to radio access systems in the millimeter-wave band.

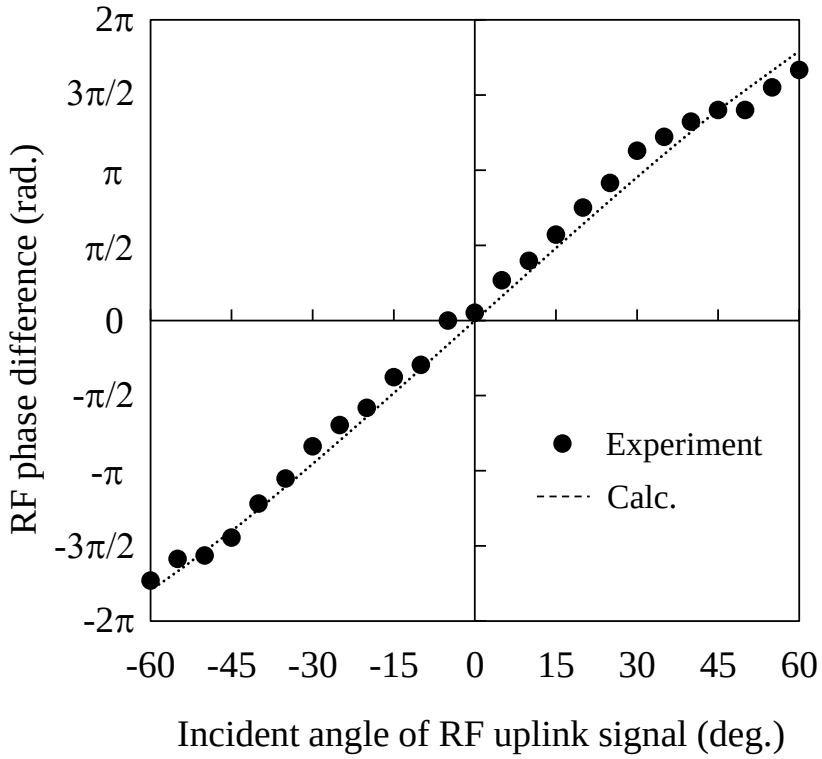

Fig. 4-9. Measured phase difference $\Delta\phi$ as a function of the incident angle of RF uplink signal.

For TDD-based mobile systems with antenna beam forming, the efficiency of the time slot allocation for each antenna site should be considered. In future RoF-based mobile systems that accommodate many antenna sites in a single CO, the time allocation efficiency may be degraded due to the difference of transmission fiber distance among antenna sites. In such a case, a new scheduling algorism will be able to efficiently allocate the time slot for each antenna site. Although the TDD-based mobile systems were assumed in the experiment, the proposed RoF uplink transmission and user position estimation scheme can be also used for the frequency division duplex (FDD)-based mobile systems without changing any operations.

4.4 Millimeter-Wave-Band Operation

The feasibility of the antenna beam forming scheme in the 2-GHz band was confirmed in the previous section. For a further progress in the transmission speed, it is promising to apply the scheme to the millimeter-wave band having a capability of 10 Gbit/s-class radio transmission [59]. To date, several RoF transmission experiments in the millimeter-wave band have been reported. However, they mainly focused on the fixed wireless access (FWA) systems [59]–[63], while the millimeter-wave-band RoF transmission focusing on mobile access systems is not reported to the author's knowledge. The antenna beam forming in the millimeter-wave band by RoF has not been investigated in detail, and thus it is important to validate that the beam forming scheme is also applicable to a higher RF carrier frequency such as the millimeter-wave band. The fabrication of an antenna using typical RF components is difficult in the millimeter-wave band because the size of each antenna element is too small for the RF signals to be directly fed. Therefore, we used SMP connectors for direct feeding of the RF signals from PDs to the antenna elements [64]. In addition, as a two-dimensional array operation will be preferable to control the antenna beam more flexibly for future advanced mobile applications, we fabricate a 2 × 3 millimeter-wave array- antenna. In this section, a two-dimensional beam forming of the fabricated array- antenna is experimentally demonstrated.

Figures 4-10(a) and (b) show the picture and schematic illustration of the fabricated patch array-antenna, respectively. The antenna consists of 2 × 3 patch antenna elements, and each element is directly connected to a photodiode with an SMP connector. The RF return loss (S_{11} parameter) of each antenna element is less than –15 dB in the targeting frequency range around 37 GHz. The square patches are 2.4-mm (0.3 λ_{RF}) wide and each antenna element is separated by 5.7 mm (0.7 λ_{RF}). The

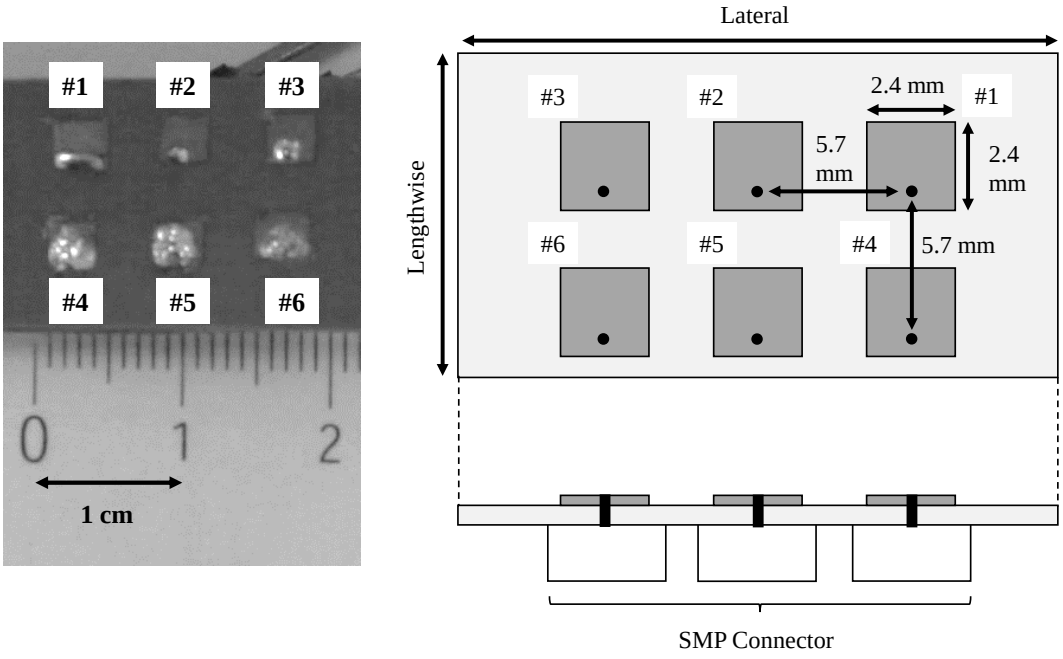

(a) (b)

Fig. 4-10. Picture and schematic illustration of the 2 × 3 array-antenna in 37 GHz.

number of antenna elements for the lengthwise and lateral directions is asymmetric because the beam in the lateral direction should be more flexibly steered than that in the lengthwise direction.

The experimental setup for two-dimensional beam forming of the 2 × 3 array-antenna is depicted in Fig. 4-11. The wavelengths of three optical signals, λ_1 = 1560, λ_2 = 1550, and λ_3 = 1530 nm, were determined by the pass-bands of the WDM couplers used in this experiment, and they can be flexibly decided according to applications in a practical use. The three optical signals were modulated by a 37-GHz CW RF signal. In order to boost the optical power, an EDFA was inserted just after wavelength multiplexing. After propagating a 1 km-long SMF, three optical signals were injected into UTC-PDs at the antenna site. The RF signals output from the UTC-PDs were directly fed to the array-antenna without using any electrical amplifiers.

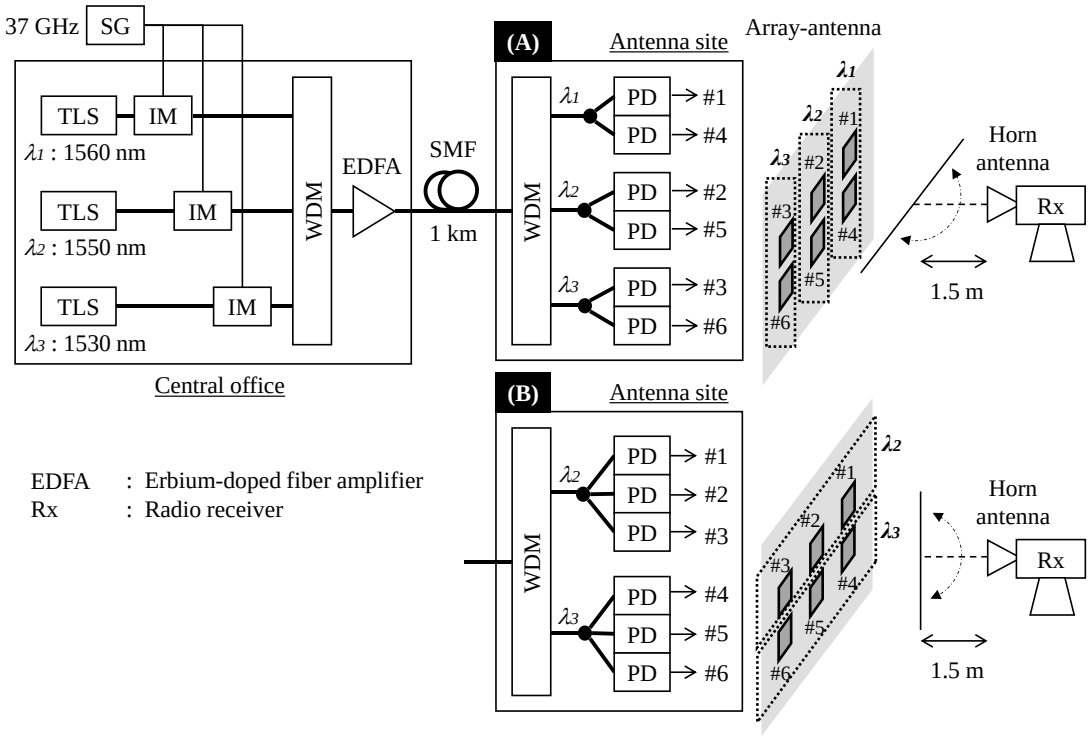

Fig. 4-11. Experimental setup for two-dimensional antenna beam forming in 37-GHz band.

For beam forming in the lateral direction, the optical signals were fed to the RoF receiver (A) shown in Fig. 4-11 and injected into the three sets of two UTC-PDs via optical couplers. The wavelength of λ_1 was fixed at 1560 nm, while the λ_2 and λ_3 were respectively changed by $\Delta\lambda$ and $2\Delta\lambda$ for antenna beam forming. As for the lengthwise direction by contrast, the λ_1 optical signal was not used and two optical signals at λ_2 and λ_3 were fed to the RoF receiver (B). The wavelength of λ_2 was changed by $\Delta\lambda$ while the λ_3 was fixed at 1530 nm. The wavelength variable range $\Delta\lambda$ for π RF phase shift in the experiment was estimated to be about 0.8 nm from Eq. (4.2). The beam radiated from the array-antenna was received by the horn antenna located at the fixed point. The radio transmission distance in the anechoic chamber was 1.5 m.

Figures 4-12(a) and (b) show the received power radiated from the 37 GHz-band array-antenna and received at an observation angle of 0 degree in the lateral and lengthwise directions, respectively. The experimental results almost coincide with the results numerically calculated from Eq. (4.1). In the lateral direction, it was clearly seen that the null points of the received power appeared when the λ_2 was changed by ±0.6 nm corresponding to the RF phase shift $\beta = \pm 2\pi/3$. Similarly, in the lengthwise direction, the null points appeared when the λ_2 was changed by ±0.8 nm, which corresponds to the RF phase shift $\beta = \pi$ as preliminarily estimated. The experimental results also mean that the more antenna elements are used, the sharper the antenna beam can be formed, and the more precise pointing to the on-target mobile terminal is possible. Thus, a two-dimensional beam forming of the array-antenna in the millimeter-wave band was experimentally demonstrated. Furthermore, there seems to be no reason that prevents us from employing the detection technique of mobile terminal direction using the RoF uplink transmission scheme as described in the previous section. Thus, the future high-speed and smart radio access systems using the millimeter-wave band should be feasible.

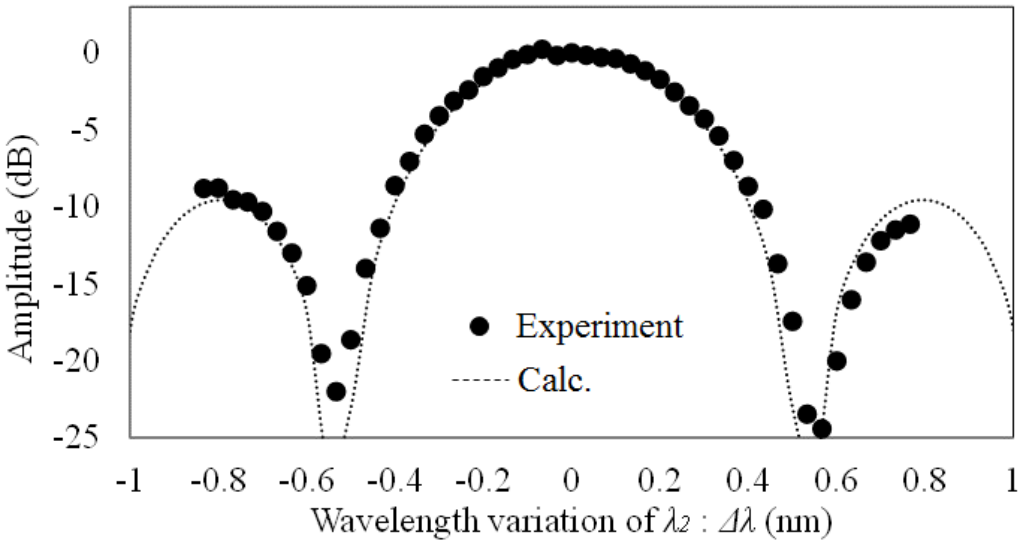

(a)

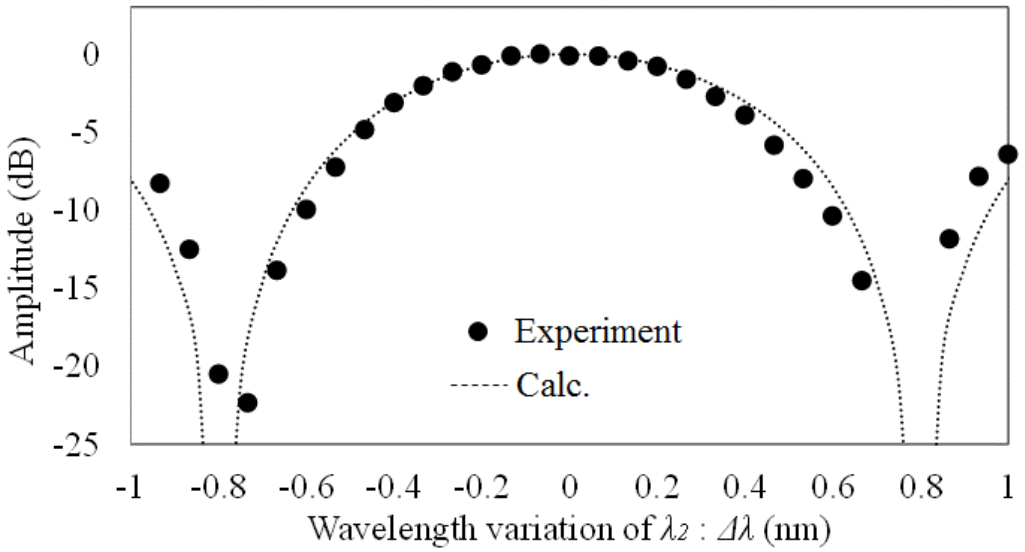

(b)

Fig. 4-12. RF received power as a function of the optical wavelength variation; (a) lateral direction, (b) lengthwise direction.

4.5 System Parameters for the Millimeter-Wave Band

While the CD is useful for phase shift generation to steer the antenna beam as proved in the previous sections, an undesired effect induced by the CD has to be taken care of. In this section, an adverse effect caused by the CD is investigated, and the requirements for system parameters considering the effect are discussed.

The optical spectrum of the RoF signal amplitude-modulated by an RF signal consists of an optical carrier at the central wavelength of λ_0 and two sidebands that are respectively separated by the RF carrier frequency of f_{RF} from λ_0. The CD induces the relative phase shift between the sidebands, which may result in RF transmission penalty as described in Chapter 2. The decrease of the amplitude-modulation index determines the RF transmission penalty. Therefore, it is one of the critical issues to determine the parameters of the beam forming system.

Figure 4-13 shows the fiber length requirement for π RF phase shift as a function of RF carrier frequency calculated from Eq. (4.2). The RF transmission penalty calculated from Eq. (2.2) is also depicted in Fig. 4-13. The two solid circles indicate the points verified in the experimental demonstrations described in Sects. 4.3 and 4.4. The solid and dashed lines show the required fiber length for π RF phase shift with a wavelength change $\Delta\lambda$ of 0.8 or 3 nm and an RF transmission penalty of 1 or 3 dB, respectively. As a consequence, the fiber length is sufficiently long to have the $\Delta\lambda$ as small as 3 nm or smaller in the microwave frequency up to 10 GHz. In the millimeter-wave band above 30 GHz, however, the fiber length should be short enough to avoid the penalty or the wavelength variable range ($\Delta\lambda$) must be larger in order to precisely operate the beam forming. As for 37-GHz band, the fiber length should be shorter than 1 km and the $\Delta\lambda$ should be larger than 1 nm. From Fig. 4-13, the RF

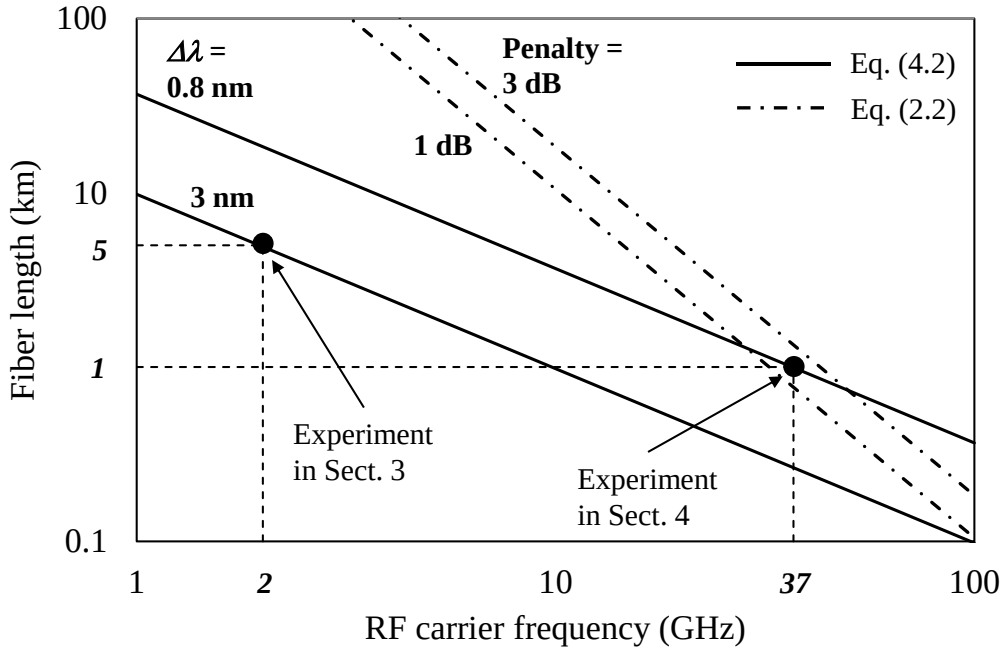

Fig. 4-13. Fiber length requirement for obtaining π RF phase shift and transmission penalty as a function of RF carrier frequency.

transmission penalty in the experiment described in Sect. 4.4 is estimated to be a few dB.

Figure 4-14 shows the measurement result of 37-GHz RF throughput as a function of transmission optical fiber length L in the range from 0 to 10 km. The numerical calculation result from Eq. (4.4) considering the RF transmission penalty is also shown in Fig. 4-14 by the dashed line. The RF throughput periodically changed according to the fiber length. It was confirmed that the actual measurement value of the transmission penalty at L = 1 km was about 1.8 dB. When we consider an actual fiber network, the fiber length may be within the range below the first roll-off point of the RF throughput. Therefore, in order to keep the penalty small enough, it is necessary to shorten the L and expand the $\Delta\lambda$. Thus, by properly selecting the L and the $\Delta\lambda$, the beam forming scheme will be applicable to the millimeter-wave radio access systems.

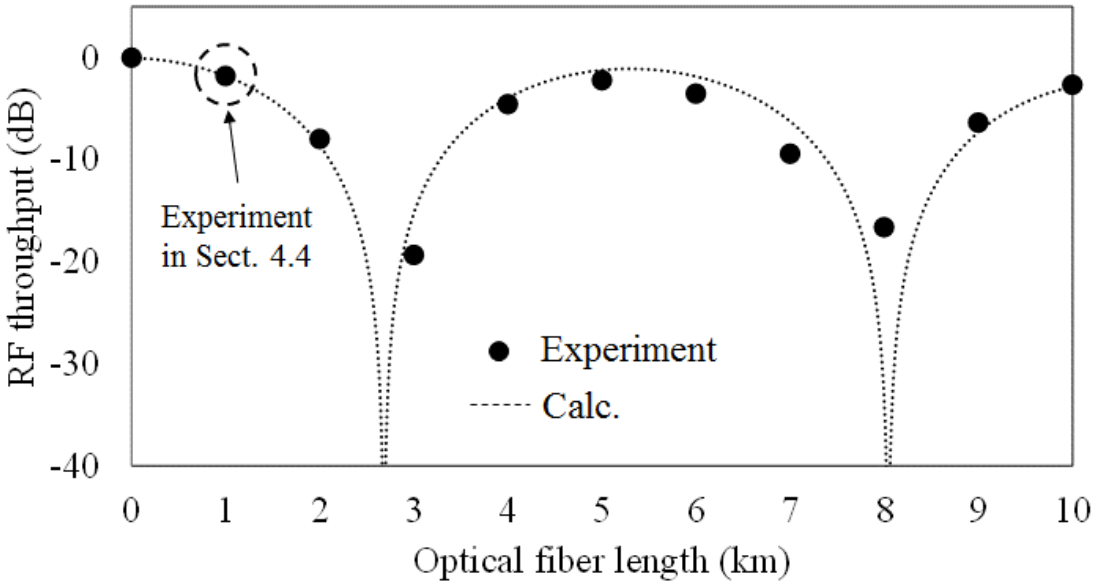

Fig. 4-14. Measurement result of 37-GHz RF throughput as a function of the optical fiber length.

In the beam forming scheme presented in this thesis, the round-trip time (RTT) between the CO and the array-antenna should be taken into account. As the RTT of 20 km-long fiber transmission is 200 μs for example, the antenna beam should be controlled with a ms-order or longer interval so as not to disconnect communications with user terminals. If the beam forming with higher speed than the current operation is required in the future, some additional techniques should be studied for overcoming the restriction on the RTT.

4.6 Conclusion

In this chapter, a simple and practical scheme to determine the direction of a phased array-antenna beam in radio access systems utilizing the RoF technique was proposed. It was experimentally confirmed that the proposed scheme feasibly operated and would be applicable to practical RoF-based radio access systems in the microwave band such as 2 GHz.

Moreover, a two-dimensional beam steering operation in 37-GHz band was experimentally demonstrated for future high-speed and smart radio access systems. The required system parameters were also provided by evaluating the RF transmission penalty caused by the CD. It was confirmed that the beam forming scheme including the detection of the target will be applicable to the millimeter-wave band by properly designing the fiber length and the wavelength variable range.

Chapter 5

Integrated Photonic Array-Antenna Beam Forming

5.1 Introduction

In this chapter, the performance of 3.5-Gbit/s QPSK signal RoF transmission with beam forming of the 60 GHz-band integrated photonic array-antenna (IPA) is studied. The beam forming operation for the IPA is experimentally demonstrated by using a QPSK signal assuming real mobile data traffic, and the quality of the QPSK signal during the beam forming operation is quantitatively evaluated. The expandability for more advanced quadrature amplitude modulation (QAM) formats is also studied. Finally, the required parameters for practical use in 60-GHz band are provided by investigating the induced transmission penalty.

5.2 Integrated Photonic Array-Antenna

The antenna beam forming scheme described in Chapter 4 can simplify the architecture of the phased array-antenna by eliminating RF phase shifters from the antenna site, which are required in the conventional array-antennas. When high-power PDs such as UTC-PDs are adopted in the antenna site, RF amplifiers that are generally required in the conventional array-antenna can be also eliminated. For further simplification of the antenna site, an IPA was proposed and fabricated [31]. While some photonic-integrated techniques have been reported [65]–[67], the integration of PDs and array-antenna elements such as the IPA has not been investigated. In this section, the design of the IPA and its fundamental characteristics are explained.

An overall structure of the IPA is shown in Fig. 5-1, and the pictures of the IPA, which was used for the experiments in the following sections, are also shown in Figs. 5-2(a) and (b). The IPA consists of a PD-integrated patch antenna substrate (Fig. 5-1(a)) and an optical signal feeding substrate (Fig. 5-1(b)). The PD-integrated antenna substrate has 4 × 2 patch antennas in the front side and UTC-PD chips in the rear side. The optical signal feeding substrate is used for optically connecting fibers to the UTC-PDs of the PD-integrated antenna substrate.

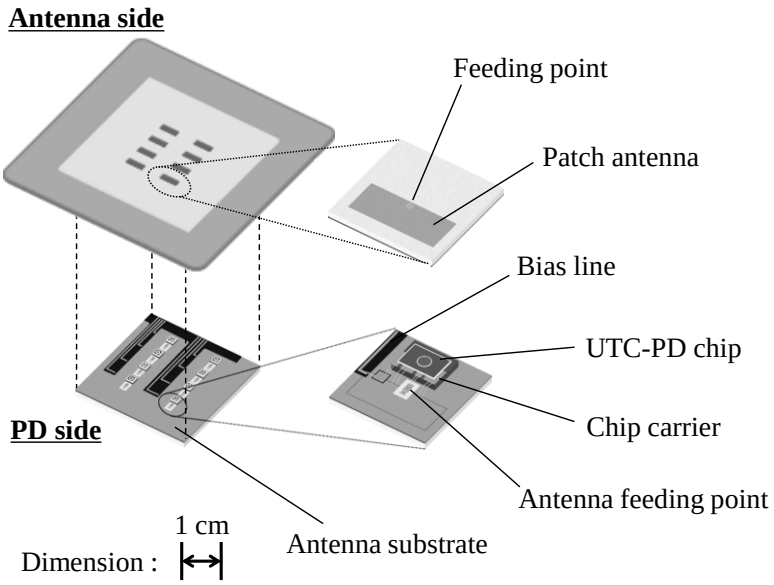

(a)

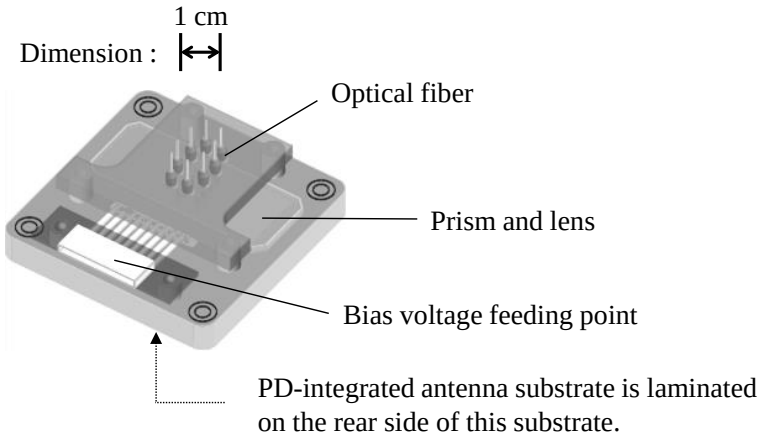

(b)

Fig. 5-1. Overall structure of the integrated photonic array-antenna;
(a) PD-integrated antenna substrate, (b) optical signal feeding substrate.

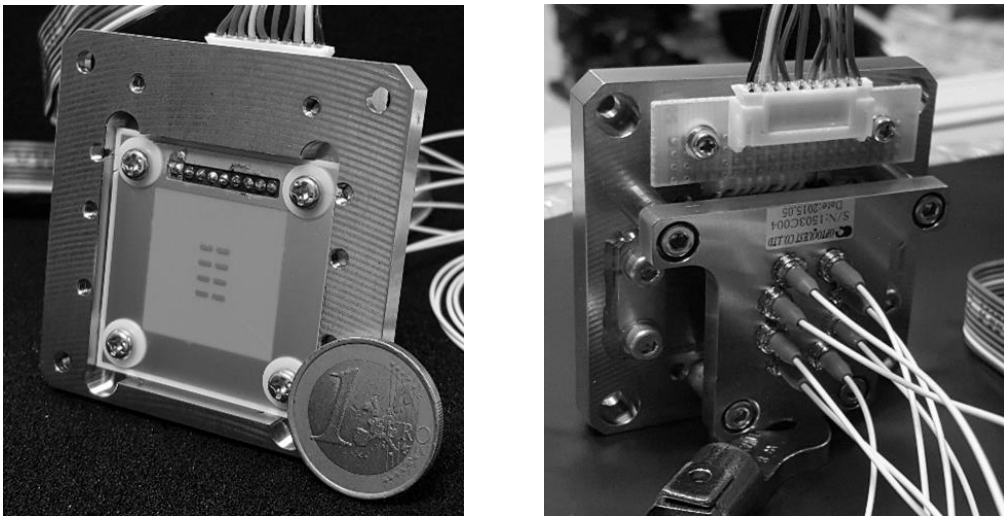

(a) (b)

Fig. 5-2. Pictures of the fabricated IPA; (a) front side, (b) rear side.

The PD-integrated antenna substrate consists of 60 GHz-band patch antenna elements, an antenna substrate, chip carriers, co-planer lines, bias voltage lines for each PD, and UTC-PD chips. The size of one patch antenna element is 0.66 × 2.1 mm, and the separation between each adjacent antenna element is 2.5 mm (0.5 λ_{RF} at 60 GHz) in the direction of four patch antennas and 3.0 mm (0.6 λ_{RF} at 60 GHz) in the direction of two patch antennas, respectively. The UTC-PD chips corresponding to the 4 × 2 patch antenna elements are mounted on each chip carrier via co-planer lines. The co-planer lines are electrically connected to the antenna substrate by the method of wire-bonding, and an antenna feeding point is also electrically connected to each patch antenna through a via-hole. The optical signal feeding substrate consists of optical fibers, prisms, and lenses. Optical signals through fibers are focused on the optical receiving areas of each UTC-PD chip by the prisms and lenses. The coupling efficiency between each optical input and RF output power is more than 70 %, and therefore it is high enough to radiate RF beam from the array-antenna.

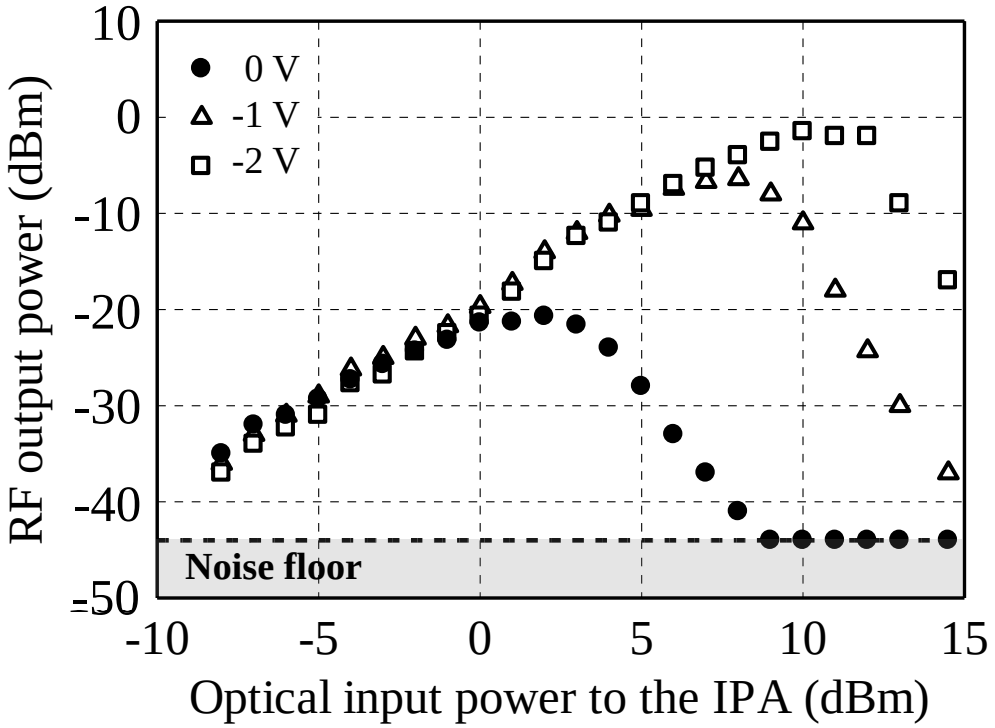

Fig. 5-3. Measured RF power output from the IPA as a function of optical input power to the IPA.

The fabricated IPA can emit sufficient RF power without supplying bias voltages for each UTC-PD chip, which would be one of the advantageous points of the IPA. Figure 5-3 shows the measurement result of the RF output power as a function of optical injection power into the IPA, where the reverse bias voltage for the IPA was changed to be 0, –1, and –2 V. In this measurement, the RoF signal modulated by a 60-GHz CW RF tone was injected into the IPA, and the IPA emitted the 60-GHz RF signal to the receiver horn antenna. The RF propagation distance between the IPA and the horn antenna was fixed to be 0.45 m. The RF power received by the horn antenna was measured, and the RF power output from the IPA was estimated by compensating the RF propagation loss. It should be noted that the result shown in Fig. 5-3 was

measured by using just one set of UTC-PD chip and antenna element in the IPA. As shown in Fig. 5-3, the IPA can emit sufficient RF power even in the case of the bias voltage = 0 V. This feature of the IPA enables us to simplify the configuration of the antenna site because RF amplifiers can be removed from the antenna site. The bias voltage for the IPA was set to be 0 V in the experimental demonstrations described in the following sections. In the case of zero bias voltage, the RF output power was saturated when the optical input power to the IPA was more than +2 dBm due to the limitation of the IPA responsivity as shown in Fig. 5-3. Therefore, the optical input power to each UTC-PD chip in the IPA was set to be about 0 dBm so as not to occur the RF output power saturation in the experiments described in the following sections.

Figure 5-4 shows the beam forming capability of the IPA for 60-GHz RF tone, where four independent tunable lasers were used in the experimental demonstration. The four RoF signals with the wavelengths of λ_1 (1560 nm), λ_2 (1555 nm), λ_3 (1550 nm), and λ_4 (1545 nm) were provided for each 1 × 2 patch antenna element as depicted in Fig. 5-4, and totally in-phase at the initial condition. The λ_2, λ_3, and λ_4 were then changed by +0.125, +0.25, and +0.375 nm, which corresponded to $+\pi/2$, $+\pi$, and $+3\pi/2$ RF phase shifts, respectively. The solid and dotted lines in Fig. 5-4 are the AF that indicates the total directivity of the array-antenna, and can be calculated from Eq. (4.1). The experimental results almost coincided with the calculated results. Hence, the IPA will create various beam patterns by increasing the number of independent lasers.

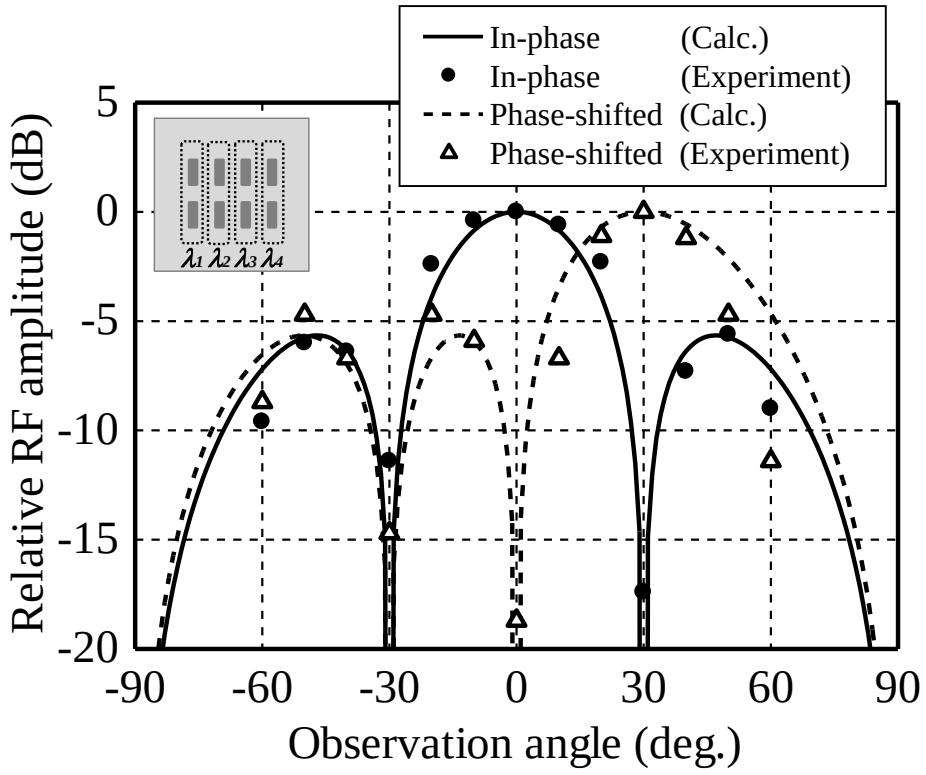

Fig. 5-4. Beam forming capability of the fabricated IPA for 60-GHz RF tone with four independent lasers.

The fabricated IPA can output sufficient RF power without supplying any bias voltages, because the UTC-PDs have a bias-free characteristic owing to a build-in field in the p-n junction [68], and experiments in the following section were conducted without any bias voltages for all the PDs. In addition, devices and components for amplifying RF signals are not necessary in the antenna site because RoF signals can be transmitted from the CO with much lower propagation loss than coaxial cables. These features enable us to simplify the configuration of the antenna site drastically because the IPA needs only RoF signals.

5.3 Transmission Experiments with Beam Forming of IPA

5.3.1 Experimental Setup

In order to evaluate the signal quality with beam forming operation for the fabricated IPA, RoF signal transmission experiments were conducted. The experimental setup for 3.5-Gbit/s QPSK signal RoF transmission is shown in Fig. 5-5. In the CO, a 1.76-Gbaud QPSK signal (the corresponding bit-rate is 3.5 Gbit/s), of which intermediate frequency was 4.0 GHz, was generated from an arbitrary waveform generator (AWG). The 4.0-GHz QPSK signal was then frequency-converted up to 60.48 GHz, which was the IEEE-standardized central frequency of 60 GHz-band channel 2 [69], by being mixed with a 56.48-GHz RF tone from an LO. In order to suppress undesired harmonic noises, a band-pass filter (BPF), of which central frequency and pass-bandwidth were 60.48 and 1.76 GHz, was inserted just after the mixer. After passing through the BPF, the 60.48-GHz QPSK RF signal was injected into an IM. Two light sources output from TLSs with different wavelengths of λ_1 = 1550 and λ_2 = 1545 nm were multiplexed by a WDM coupler and simultaneously modulated by the 60.48-GHz QPSK RF signal, and thus, 60.48-GHz QPSK RoF signals with two wavelengths were created. The wavelength tuning speed of the TLS used in the experiment was less than 200 ms, and the wavelength stability of the TLS was within ±100 MHz. After being boosted by an EDFA, the two RoF signals were transmitted toward the antenna site. The transmission length L and dispersion parameter D of the SMF between the CO and the antenna site were 2 km and 16.7 ps/nm/km. From these parameters, the required wavelength change $\Delta\lambda$ for obtaining π RF phase shift can be estimated to be 0.25 nm from Eq. (4.2). Figure 5-6 shows the

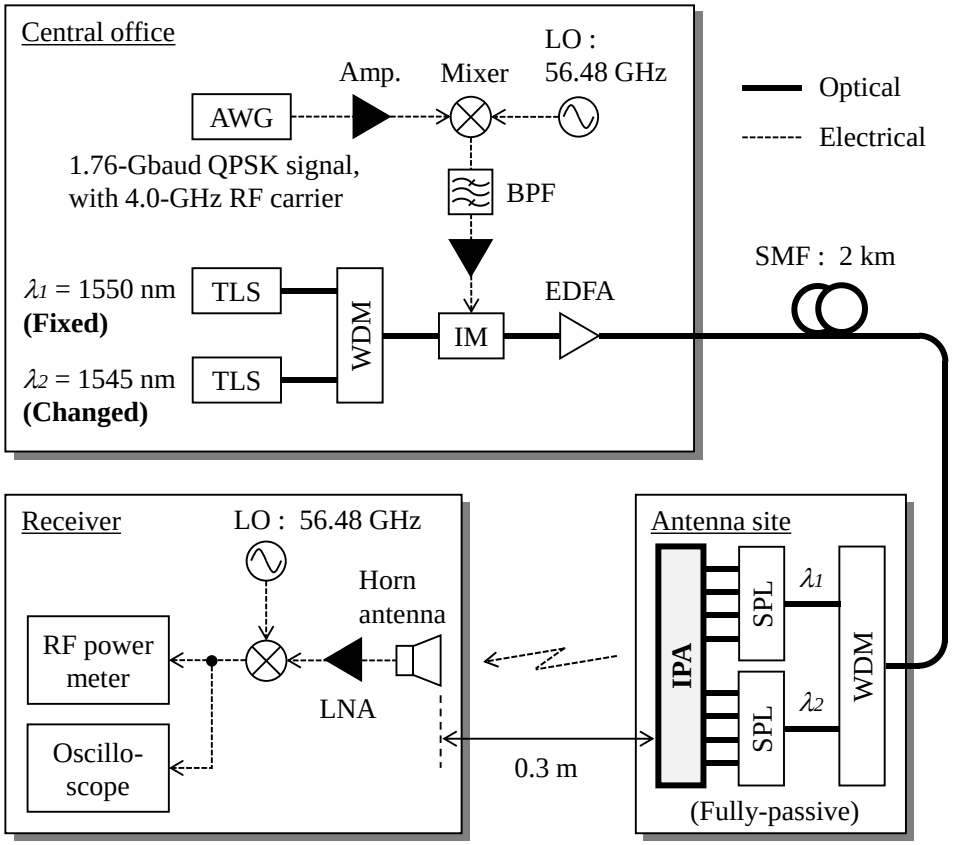

Fig. 5-5. Experimental setup for RoF transmission with beam forming of the IPA.

optical spectrum measured just after the EDFA in the CO, where two RoF signals with DSB components separated by 60.48 GHz from the optical carrier can be observed. The pass-bandwidth of the WDM coupler in the CO is also described in Fig. 5-6. It can be observed that the bandwidth of the λ_2 port was wide enough for changing the λ_2 by $\Delta\lambda$ = 0.25 nm or more.

In the antenna site, the two RoF signals were de-multiplexed by a WDM coupler with the same characteristics as the WDM coupler in the CO, and each wavelength RoF signal was injected into the IPA after being divided into four branches by an optical splitter (SPL). The RoF signals with the wavelengths of λ_1 and λ_2 were provided for the left- and right-side 2 × 2 patch antenna elements, respectively. All the optical input

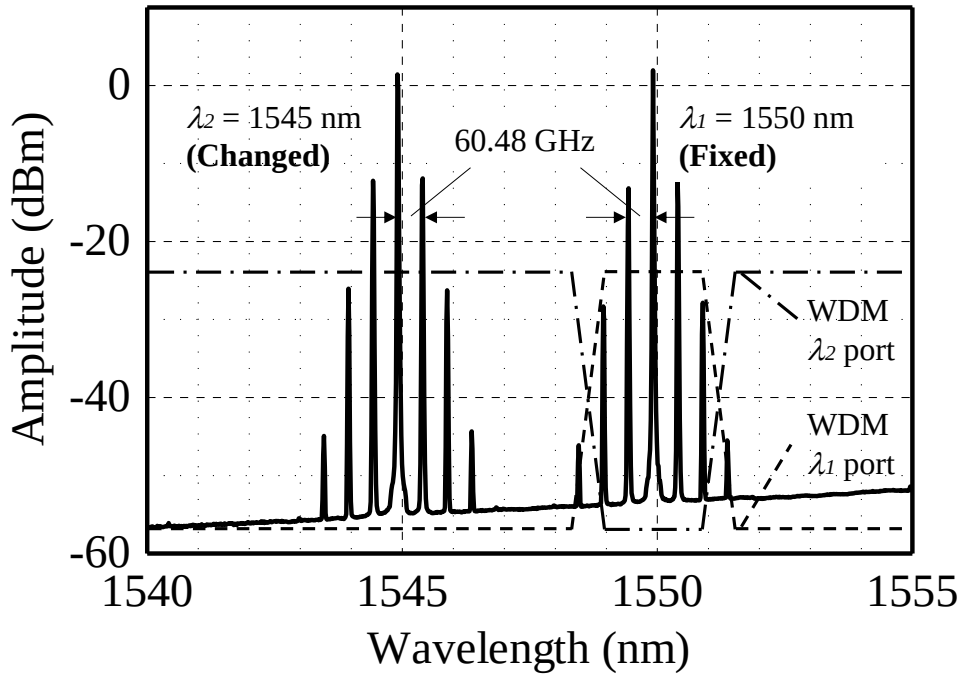

Fig. 5-6. Optical spectrum measured just after the EDFA.

power to the IPA via eight fibers were adjusted to be ±0 dBm by optical attenuators just before optical input points to the IPA. The IPA converted the RoF signals to 60.48-GHz QPSK RF signals and radiated them from the 4 × 2 patch antenna elements. It should be noted that the bias voltage was not applied to the IPA, which means that the antenna site was under a fully-passive condition in this experiment. The propagation distance between the IPA and a V-band receiver horn antenna was set as 0.3 m, which meets the requirement for far-field electromagnetic wave [52]. After being received by the horn antenna with 15-dBi antenna gain and amplified by a low-noise amplifier (LNA), the RF signals were frequency-converted down to 4.0 GHz, and then provided for an RF power meter and an oscilloscope. An off-line signal processing was utilized for the QPSK signal received by the oscilloscope.

The two-tone technique, where two optical tones are extracted by OBPFs from the

amplitude-modulated RoF signal, is one of the candidate techniques for generating 60-GHz RoF signals [70]. In this technique, the one tone is used as an optical carrier and another tone is as a data-modulated sideband signal, which enables us to avoid the CD-induced RF transmission penalty owing to the single-sideband modulation. However, the configuration of the two-tone-based RoF transmitter in the CO is more complicated than that of the SCM-based RoF transmitter. When the wavelength of the RoF transmitter is changed for antenna beam forming, the OBPFs for extracting two optical tones must be also controlled at the same time, which will complicate the whole RoF transmission system. Therefore, the simple SCM-based technique was used in this experiment.

In this experiment, the phases of the two RoF signals were adjusted preliminarily so as to synchronize RF carrier phases and QPSK-data symbols at the optical input point to the IPA. The beam of the IPA was then controlled by changing the wavelength of λ_2, while the λ_1 was fixed at the 1550 nm. The received RF power and the SNR of the QPSK signal were measured by using the RF power meter and the oscilloscope with controlling the beam of the IPA.

5.3.2 Results and Discussion

Figure 5-7 shows the measurement results of the received RF power and SNR of the QPSK signal at the observation angle of 0 degree. In this measurement, the λ_2 was changed by just ±0.5 nm from the initial wavelength of 1545 nm, because the $\Delta\lambda$ for obtaining π RF phase shift was theoretically estimated to be 0.25 nm. The SNR values, error vector magnitude (EVM) values, and constellations [72] for the QPSK signal are also shown in Fig. 5-7, which were measured at the three representative points of $\Delta\lambda$ = (i) 0, (ii) 0.2, and (iii) 0.25 nm. It can be confirmed that the received RF power periodically changed as the $\Delta\lambda$ was swept from –0.5 to +0.5 nm, which indicates that

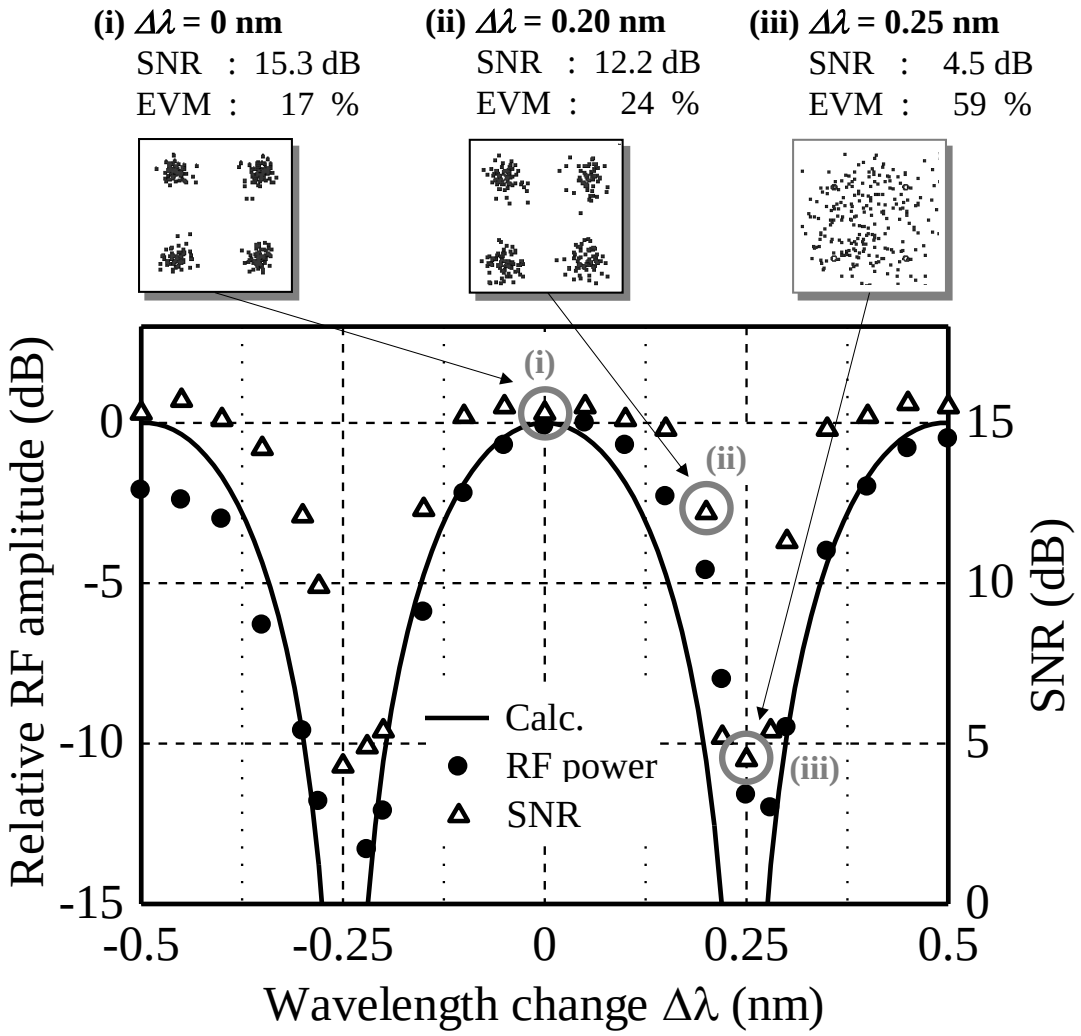

Fig. 5-7. Relationship between the received RF power and SNR of the QPSK signal when the IPA beam is controlled.

beam forming of the IPA was successfully demonstrated. The solid line in Fig. 5-7 is the AF calculated from Eq. (4.1), and the received RF power almost coincided with the AF. The difference between the received RF power and the theoretical curve of the AF was possibly caused by the multipath due to RF reflections and scattering, because the present experimental environment for the antenna site and RF receiver was not completely anechoic. The change of SNR also coincided with that of the received RF

power, and the SNR value degraded from 15.3 to 4.3 dB as the AF shifted from the peak to the null point. Thus, the quality of the QPSK signal during the IPA beam forming operation was experimentally confirmed. From a practical point of view, it may need to stabilize the wavelengths of TLSs for properly operating the IPA beam forming, for example, within ±0.01 nm that corresponds to ±1.25 GHz. Therefore, the temperature in the CO should be constant for stabilizing the wavelengths.

The change of signal quality was measured at the fixed observation angle in this experiment. It would be also important to measure the change of SNR value at other observation angles and to evaluate the impact of the deviation of data symbol on signal quality, which is considered as one of the future works. In this experiment, as the RF carrier frequency of 60 GHz is sufficiently wide compared to the data symbol rate of 1.76 Gbaud, the impact of the deviation of data symbol is negligible.

Figure 5-8 shows the received RF powers and SNR values for the 1.76-Gbaud QPSK signal that were measured by changing the RF propagation distance between the IPA and the receiver horn antenna from 0.4 to 1.4 m. In the present experimental setup, the achievable RF propagation distance was 1.0 m because the required SNR for error-free transmission with a low-density parity-check (LDPC) code was 9.8 dB [69]. It should be noted that the received RF power and the SNR in the Figs. 5-7 and 5-8 have been limited by the performance of the IM, EDFA, and PDs used in the experiment. While the output power from the UTC-PD in the experiment was about –30 dBm, a new UTC-PD that is optimized to output RF power of more than 0 dBm at zero bias voltage has been reported [73], [74]. Therefore, if we use such a PD and compensate the RF propagation loss, the RF propagation distance can be extended to 10 m or much longer, and it will be long enough to be adopted in practical systems such as mobile BSs and Wi-Fi access points (APs).

The expandability for more advanced modulation formats such as a multiple-QAM was also studied. Figure 5-9 shows the SNR values at the observation angle of 0

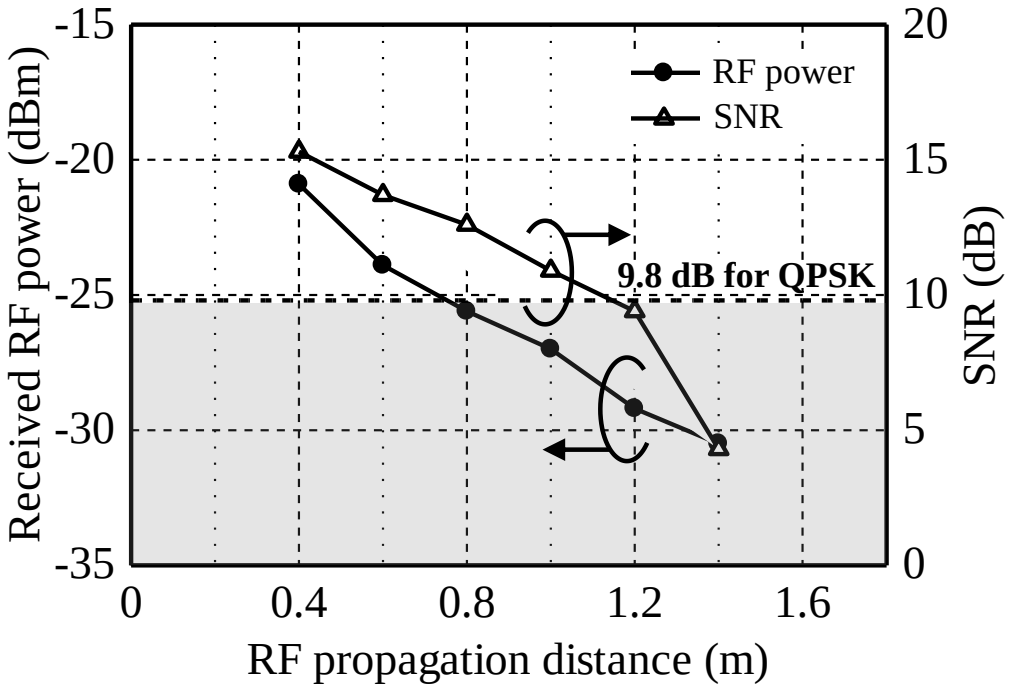

Fig. 5-8. Received RF powers and SNR values for the QPSK signal as a function of the RF propagation distance.

degree as a function of the baud-rate of the AWG, which were measured without controlling the IPA beam. In this measurement, the modulation format of output signal from the AWG was set as QPSK or 16-QAM, and the baud-rate was changed from 0.2 to 1.76 Gbaud that was the highest speed of the present experiment due to the restriction on the bandwidth of the BPF. The RF propagation distance was fixed at 0.3 m in this measurement. An example of constellation for a 1.0-Gbaud 16-QAM signal is shown in Fig. 5-9. In the case of QPSK signal, there is a margin of more than 5 dB for the required SNR of 9.8 dB even at 1.76 Gbaud. In the case of 16-QAM signal, however, it is difficult to ensure enough SNR margin for the required SNR of 16.5 dB, and therefore, it may be strict to adopt further more advanced modulation formats such as 32- or 64-QAM. In this experimental environment, the SNR for the total system was

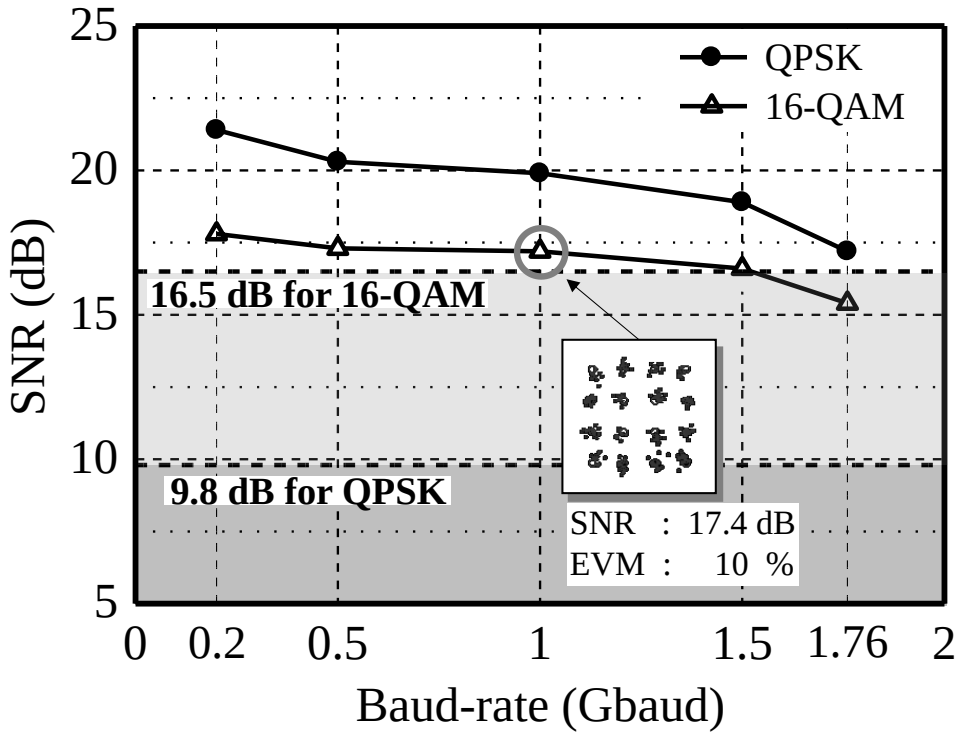

Fig. 5-9. Measured SNR values for QPSK and 16-QAM signals as a function of baud-rate of the AWG.

not completely optimized because the bulky and discrete off-the-shelf devices were used for a part of sections. Therefore, by using optimally engineered and integrated devices such as the IPA for all the sections, the RF power and SNR for the total system can be improved drastically, and the RoF transmission system with the IPA beam forming can be enhanced to several 10 Gbit/s-class speed by applying more advanced modulation formats than QPSK or 16-QAM.

5.3.3 Design of System Parameters for 60 GHz-Band IPA

As formerly described in Chapters 2 and 4, the RF transmission penalty due to the effect

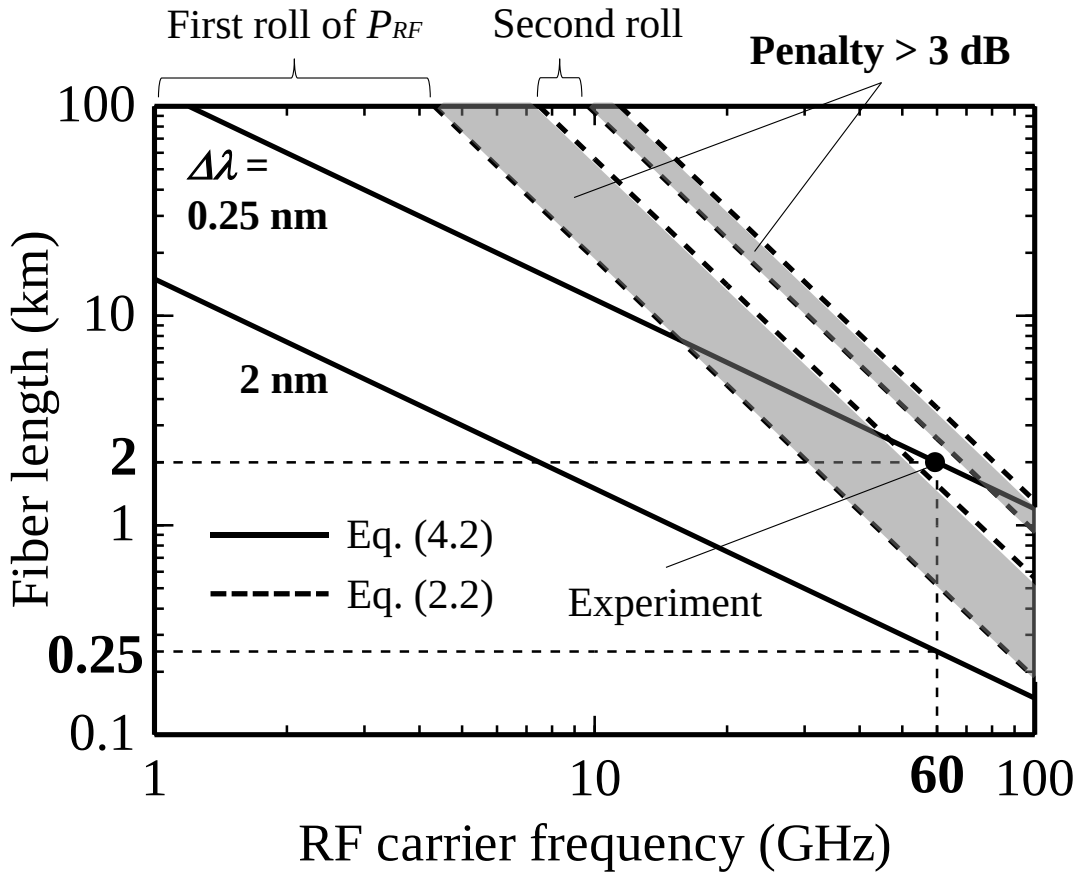

Fig. 5-10. Fiber length requirement for π RF phase shift as a function of RF carrier frequency.

of CD must be considered to design the system parameters in RoF transmission system. The RF transmission penalty in 60 GHz-band RoF systems especially becomes larger than microwave band. Therefore, the system parameters such as optical fiber length (L) and wavelength variable range ($\Delta\lambda$) should be carefully selected in order to avoid the undesired effect of the CD.

Figure 5-10 shows the fiber length requirement for π RF phase shift as a function of RF carrier frequency calculated from Eq. (4.2), where the RF transmission penalty due to the CD calculated from Eq. (2.2) is also depicted in Fig. 5-10. The solid and dotted

lines show the required fiber length for π RF phase shift with $\Delta\lambda$ of 0.25 or 2 nm and the transmission penalty of 3 dB, respectively. The gray-highlighted areas, which periodically appear according to the fiber length and RF carrier frequency, indicate that the penalty becomes more than 3 dB. As a consequence, the L and the $\Delta\lambda$ should be properly selected so as to avoid the penalty especially in 60 GHz. The penalty in the experiment is estimated to be only 0.05 dB from the solid circle in Fig. 5-10, which is in the second roll of the P_{RF}. When we consider a practical fiber network, it may be preferable that the fiber length is within the range below the first roll of the P_{RF}. Therefore, in order to keep the penalty small enough, it is necessary to shorten the fiber length and expand the $\Delta\lambda$. If the $\Delta\lambda$ is set to be 2 nm, the fiber length may seem to be limited to 0.25 km as shown in Fig. 5-10. When the required fiber length is longer than the RF penalty limit, the adoption of dispersion compensation (DC) fibers or modules equipped in the CO will resolve the restriction on the transmission distance, and the use of the DC fibers or modules compensating for an extra dispersion is independent of the RoF-based beam forming scheme using the CD.

The fabricated IPA has eight sets of UTC-PD chips and array-antenna elements, which would be enough to be adopted in the pico/femto-cells and Wi-Fi APs. However, when we consider other applications such as macro-cell BSs and satellite communications, several ten or hundred array-antenna elements will be required in the future. In the RoF-based antenna beam forming scheme, the number of array-antenna elements is restricted by the number of available wavelengths of the TLSs. In the case of 60-GHz RoF signals, a 200 GHz-grid WDM coupler such as an arrayed-waveguide grating (AWG) multiplexer [75], which corresponds to 1.6-nm grid, will be applicable in considering the $\Delta\lambda$ of 0.25 nm. In this situation, more than 80 wavelengths can be utilized for array-antenna elements when we assume the use of S/C/L-band, where the wavelength range of 130 nm from 1460 to 1590 nm is divided by 1.6-nm grid of the WDM coupler and the number of available array-antenna elements can be calculated to

be about 80. On the other hand, when we set the parameters to be L = 0.25 m and $\Delta\lambda$ = 2 nm, the pass-bandwidth of the WDM coupler should be extended, for example, to be 5 nm considering the $\Delta\lambda$ of 2 nm. In such a case, the number of array-antenna elements is decreased to be 26. Hence, the parameters of the L and $\Delta\lambda$ should be selected according to the applications including the number of array-antenna elements. If we want to increase the number of array-antenna elements and shorten the L, the use of high-dispersion fiber or modules equipped in the CO may resolve the problem.

As another technique for increasing the number of array-antenna elements, the use of some optical multiplexing techniques is promising. For example, when we adopt a multi-core fiber (MCF) in a transmission fiber between the CO to the array-antenna, the number of available wavelengths can be increased according to the number of fiber cores in the MCF. The feasibility of MCF-based RoF transmission and antenna beam forming operation has been reported in Ref. [76].

The experimental demonstration focused just on the RoF downlink transmission, while the bidirectional RoF transmission including the uplink must be considered from a practical viewpoint. As a technique to transmit the RoF uplink signal and decide the direction of mobile terminal, the proposed scheme presented in Chapter 4 can be adopted even in the 60-GHz antenna beam forming system [77]. Figure 5-11 shows the schematic diagram of 60-GHz RoF-based antenna beam forming system, where the IPA is utilized for downlink RF radiation and the proposed scheme using the RSOA is adopted in the RoF uplink transmission. As shown in Fig. 5-11, the receiver (Rx) array-antenna at the antenna site is separated from the IPA because the transmitter (Tx) array-antenna elements are integrated with the UTC-PDs for the RoF downlink transmission. In the CO, the RoF transmitter consists of the TLSs for the RoF downlink transmission, of which wavelengths are λ_1 to λ_N, and an LD for supplying an RF tone for the antenna site. The wavelength of the LD (λ_0) should be 1.3 μm in terms of the simplicity of the total system. In the antenna site, the IPA receives the RoF

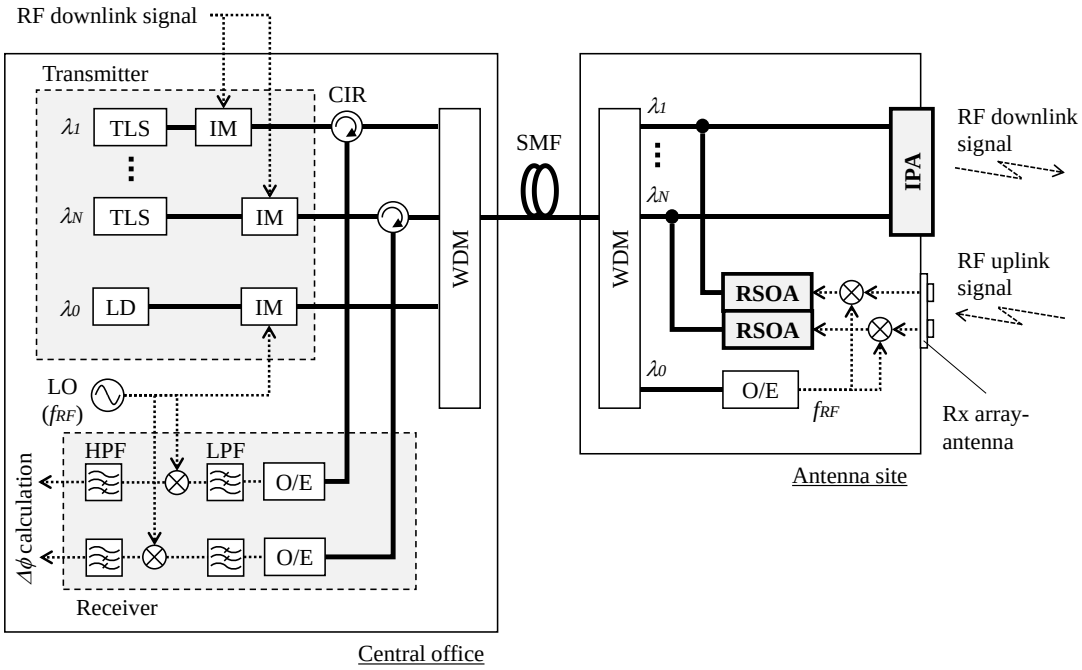

Fig. 5-11. Schematic diagram of 60-GHz RoF-based antenna beam forming.

signals from the CO and radiates the RF downlink signal. A part of RoF signals at the antenna site is tapped, and the RoF signals are injected into the RSOAs to reproduce the RoF uplink signals. The RF uplink signal received by the Rx array-antenna is down-converted by being mixed with the RF tone of f_{RF}, and the RoF uplink signals are created by the amplitude modulation in the RSOAs. The RoF uplink signals are extracted by the optical circulators (CIRs) in the CO, and the RoF uplink signals are utilized for estimating the direction of the mobile terminal by the same manner as the scheme proposed in Chapter 4. As for the number of array-antenna elements for RF uplink transmission, two elements will be enough to decide the direction of mobile terminal, and the two elements will not have a large impact on the simplicity of the total system. Therefore, the RoF beam forming scheme proposed in Chapters 4 and 5 of

this thesis will be applicable to the existing microwave and future millimeter-wave BSs and Wi-Fi APs.

5.4 Conclusion

The performance of signal transmission by RoF with beam forming of the 60 GHz-band IPA was experimentally studied. The beam forming operation for the IPA was successfully demonstrated by using the 3.5-Gbit/s QPSK signal assuming the real mobile data traffic, and the relationship between beam forming operation and quality of the QPSK signal was quantitatively evaluated. The expandability for more advanced modulation formats such as 16-QAM was also experimentally studied. In addition, the system parameters for a practical use were also designed by investigating the transmission penalty induced by the CD. Finally, the schematic diagram of the bidirectional 60-GHz RoF transmission with antenna beam forming capability is presented, where the same scheme presented in Chapter 4 can be adopted. The obtained results in this chapter enable us to design next generation radio access networks based on 60 GHz-band RoF transmission technique.

Chapter 6

Conclusion

This thesis studied the optical and radio integrated network utilizing RoF transmission technique for future optical and radio access systems with the capabilities of highly resilient disaster recovery and array-antenna beam forming. The main results obtained in this thesis are summarized as follows.

In Chapter 3, an autonomous self-healing technique utilizing a self-injection-locked FP-LD was proposed for seamless optical and radio communication systems. The failure detection time of 0.13 ms and the total switching time of 2.4 ms were experimentally confirmed, which would be rapid enough to be adopted in the practical systems. The signal quality degradation caused by the switching operation was quantitatively evaluated by the experiment of the 10-Gbit/s QPSK signal RoF transmission employing the proposed self-healing technique. It was experimentally confirmed that more than ten backup radio links including 100 km-long SMF transmission was achievable. The obtained results in Chapter 3 enable us to design seamless optical and radio communication systems with plural backup radio links.

In Chapter 4, a simple and practical scheme to determine the direction of phased

array-antenna beam in RoF-based radio access systems was proposed. It was experimentally confirmed that the proposed scheme feasibly operated and would be applicable to practical RoF-based radio access systems in a microwave band such as 2 GHz. The two-dimensional beam forming operation for the 2 × 3 array-antenna in millimeter-wave band of 37 GHz was experimentally demonstrated for targeting future high-speed and smart radio access systems. The required system parameters were also provided by evaluating the RF transmission penalty caused by the CD. It was confirmed that the beam forming scheme including the detection of the target will be applicable to the millimeter-wave band by properly designing the fiber length and the wavelength variable range.

In Chapter 5, the performance of RoF signal transmission with beam forming of the 60 GHz-band IPA was experimentally studied. The beam forming operation for the IPA was successfully demonstrated by using the 3.5-Gbit/s QPSK signal assuming the real mobile data traffic, and the relationship between beam forming operation and quality of the QPSK signal was quantitatively evaluated. The expandability for more advanced modulation formats such as 16-QAM was also experimentally studied. In addition, the system parameters for practical radio access systems in 60 GHz were also designed by investigating the CD-induced transmission penalty. The schematic diagram of the 60-GHz RoF-based antenna beam forming system that includes bidirectional RoF transmission links was also shown. The obtained results in this chapter enable us to design next generation radio access networks based on 60 GHz-band RoF transmission technique.

From the above-described results, it was confirmed that the RoF transmission technique was a promising solution for designing the optical and radio integrated network with the capabilities of rapid disaster recovery and remote beam forming for the phased array-antenna. The future works on this study are considered as follows;

(1) In the seamless optical and radio communication system presented in Chapter 3, the total network design including higher-layer operation than the physical layer should be studied. The detailed operation how to switch the bit-rate and transmission links in higher layer should be clarified. In addition, the feasibility of RoF transmission with plural radio sections should be experimentally confirmed by using the field fibers and radio sections in actual situations.

(2) In the antenna beam forming scheme presented in Chapter 4, the simplification of antenna site for RoF uplink transmission should be studied. In the uplink direction, RF amplifiers may be required for boosting weak RF uplink signals, and therefore, it is one of the technical issues how to simplify the configuration of RF and RoF uplink transmission in the antenna site. While it is assumed that the antenna beam is controlled with a ms-order interval considering the RTT between the CO and the array-antenna, some additional techniques will be needed for the high speed beam forming with a μs-order interval in the future.

(3) In the IPA-based beam forming scheme presented in Chapter 5, the actual demonstration of RF beam forming with data transmission using eight or much more independent sets of light sources and array-antenna elements should be conducted. In addition, the impact of the deviation of data symbol on signal quality during antenna beam forming should be experimentally clarified. Furthermore, the feasibility of advanced optical multiplexing techniques for increasing the number of array-antenna elements should be experimentally confirmed.

Finally, the author believes that the whole works in this thesis will contribute to the design and development of future optical and radio integrated network utilizing the RoF transmission technique.

Bibliography

[1] Cisco Visual Network Index: Global mobile data traffic forecast update, 2013-2018. [Online]. Available: http://www.cisco.com/c/en/us/solutions/collateral/service-provider/visual-networking-index-vni/white_paper_c11-520862.html

[2] A. Khandekar, N. Bhushan, J, Tingfang, and V. Vanghi, “LTE-advanced: heterogeneous networks,” in *Proc. the 2010 European Wireless Conference (EW’10)*, pp. 978-982, Lucca, Italy, 2010.

[3] K. Sakaguchi, E. M. Mahmoud, H. Kusano, M. Mizukami, S. Miyamoto, R. E. Rezagah, K. Takinami, K. Takahashi, N. Shirakawa, H. Peng, T. Yamamoto, and S. Nanba, “Millimeter-wave wireless LAN and its extension toward 5G heterogeneous networks,” *IEICE Trans. Commun.*, vol. E98-B, no. 10, pp. 1932-1948, Oct. 2015.

[4] C-RAN: The road toward green RAN, White paper. [Online]. Available: http://labs.chinamobile.com/report/view_59826

[5] S. Nanba, T. Matsunaka, T. Warabino, S. Kaneko, and Y. Kishi, “Colony-RAN architecture for future cellular network,” in *Proc. Future Network & Mobile Summit*, pp. 1-8, Berlin, Germany, July 2012.

[6] Common Public Radio Interface (CPRI): Interface specification V6.0. [Online]. Available: http://www.cpri.info/spec.html

[7] ETSI GS ORI 002-1 V4.1.1 (2014-10), “Open radio equipment interface (ORI); ORI interface specification; Part 1: Low layers (Release 4).” [Online]. Available: http://www.etsi.org/deliver/etsi_gs/ORI/001_099/00201/04.01.01_60/gs_ORI00201v040101p.pdf, 2014.

[8] ITU-T Recommendation J.185, “Transmission equipment for transferring multi-channel television signals over optical access networks by frequency modulation conversion,” 2012.

[9] M. Maeda, T. Nakatogawa and K. Oyamada, “Optical fiber transmission

technologies for digital terrestrial broadcasting signals," *IEICE Trans. Commun.*, vol. E88-B, no. 5, pp. 1853-1860, 2005.

[10] P. B. Ozmar, "A look at optical fiber CATV," *IEEE Trans. on Cable Television*, vol. CATV-4, no. 1, pp. 43-46, 1979.

[11] M. L. Yee, L. C. Ong, C. K. Sim, B. Luo and A. Alphones, "Low-cost radio-over-fiber in-building distribution network for WLAN, UWB and digital TV broadcasting," in *Proc. Asia-Pacific Microwave Conference (APMC'06)*, pp. 95-98, Yokohama, Japan, Dec. 2006.

[12] T. Iwakuni, K. Miyamoto, T. Higashino, K. Tsukamoto, S. Komaki, T. Tashiro, Y. Fukada, J. Kani, N. Yoshimoto and K. Iwatsuki, "Analysis of wireless channel capacity in RoF-DAS over WDM-PON system," *IEICE Trans. Electron.*, vol. E96-C, no. 2, pp. 171-179, 2013.

[13] H. Al-Raweshidy and S. Komaki, Radio over fiber technologies for mobile communications networks, Artech House, 2002.

[14] Y. Yizhuo, C. Lim and A. Nirmalathas, "Radio-over-Fiber as the energy efficient backhaul option for mobile base stations," in *Proc. the 2011 Int'l. Topical Meeting on Microwave Photonics (MWP'11)*, pp. 242-245, Singapore, Oct. 2011.

[15] T. Kuri, K. Ikeda, H. Toda, K. Kitayama and Y. Takahashi, "A compact remote antenna base station for microwave/millimeter-wave dual-band radio-on-fiber systems," in *Proc. the 17th Annual Meeting of the IEEE Lasers and Electro-Optics Society (LEOS'04)*, pp. 59-60, Nov. 2004.

[16] M. Hosokawa, "The disaster caused by the 2011 Great East Japan Earthquake and fire fighting operation by Japanese fire service," *IEICE Commun. Society Global News Lett.*, vol. 35, no. 4, pp. 7-8, Dec. 2011.

[17] K. Kinoshita, Y. Ito, H. Kimura and Y. Maeda, "Technologies and emergency management for disaster recovery – With focus on the Great East Japan Earthquake," *IEICE Trans. Commun.*, vol. E95-B, no. 6, pp. 1911-1914, June 2012.

[18] ITU-T Recommendation G.8032/Y.1344, "Ethernet ring protection switching," 2010.

[19] A. Kanno, K. Inagaki, I. Morohashi, T. Sakamoto, T. Kuri, I. Hosako, T.

Kawanishi, Y. Yoshida and K. Kitayama, "20-Gb/s QPSK W-band (75-110 GHz) wireless link in free space using radio-over-fiber technique," *IEICE Electronics Express,* vol. 8, no. 8, pp. 612-617, April 2011.

[20] X. Pang, J. V. Olmos, A. Lebedev and I. T. Monroy, "A 15-meter multi-gigabit W-band bidirectional wireless bridge in fiber-optic access network," in *Proc. the 2013 IEEE Int'l Topical Meeting on Microwave Photonics (MWP'13)*, pp. 37-40, Alexandria, VA, Oct. 2013.

[21] M. Y. Frankel and R. D. Esman, "True time-delay fiber-optic control of an ultra wideband array transmitter/receiver with multibeam capability," *IEEE Trans. on Microw. Theory and Techn.*, vol. 43, no. 9, pp. 2387-2394, Sep. 1995.

[22] M. Tadokoro, T. Taniguchi and N. Sakurai, "Optically-controlled beam forming for 60 GHz-ROF system using dispersion of optical fiber and DFWM," in *Proc. 2007 IEEE/OSA Optical Fiber Communication Conference (OFC'07)*, paper OWN2, Anaheim, CA, Mar. 2007.

[23] H. Lee, J. Hyun-Bin and W. J. Ji, "Optical true time-delay beam-forming for phased array antenna using a dispersion compensating fiber and a multi-wavelength laser," in *Proc. the 2011 4th Annual Caneus Fly by Wireless Workshop (FBW'11)*, pp. 1-4, Montreal, QC, June 2011.

[24] D. Takeuchi, W. Nakajo, S. Yamamoto and Y. Oyamada, "Phase control and calibration characteristics of optically controlled phased array antenna feed using multiple SMFs," *IEICE Trans. Electron.*, vol. E94-C, no. 10, pp. 1634-1640, 2011.

[25] L. Zhuang, A. Meijerink, C. G. H. Roeloffzen, D. A. I. Marpaung, R. G. Heideman, M. Hoekman, A. Leinse and W. V. Etten, "Novel ring resonator-based optical beamformer for broadband phased array receive antennas," in *Proc. the 2008 21st Annual Meeting on the IEEE Lasers and Electro-Optics Society (LEOS'08)*, pp. 20-21, Acapulco, Mexico, Nov. 2008.

[26] S. Akiba, M. Oishi, and H. Matsuno, "Effects of chromatic dispersion on RF power feeding to array antenna through fiber," in Proc. *the 17th Opto-Electronics Communication Conference (OECC'12)*, pp. 323-324, Busan, Korea, July 2013.

[27] S. Akiba, M. Oishi, Y. Nishikawa, J. Hirokawa, and M. Ando, "Photonic approach to beam steering of phased array antenna," in *Proc. the 2013 URSI*

Int'l. Symposium on Electromagnetic Theory (EMTS'13), pp. 448-451, Hiroshima, Japan, May 2013.

[28] L. A. Colden, S. C. Nicholes, L. Johansson, S. Ristic, R. S. Guzzon, E. J. Norberg and U. Krishnamachari, "High performance InP-based photonic ICs," *IEEE/OSA J. Lightw. Technol.*, vol. 29, no. 4, pp. 554-570, Feb. 2011.

[29] M. J. Wale, "PICs for next generation access systems," in *Proc. 2012 IEEE/OSA Optical Fiber Communication Conference (OFC'12)*, paper OTh1F.7, Los Angeles, CA, Mar. 2012.

[30] H. Ito, T. Ohno, H. Fushimi, T. Furuta, S. Kodama and T. Ishibashi, "60GHz high output power uni-traveling-carrier photodiodes with integrated bias circuit," *Electron. Lett.*, vol. 36, no. 8, pp. 747-748, April 2000.

[31] T. Hirasawa, K. Furuya, M. Oishi, S. Akiba, J. Hirokawa, and M. Ando, "Integrated photonic array-antennas in RoF system for MMW-RF antenna beam steering," in *Proc. the 2015 IEEE Int'l. Topical Meeting on Microwave Photonics (MWP'15)*, paper TuP-14, Paphos, Cyprus, Oct. 2015.

[32] "Text proposal on data compression to Rel-3 requirements spec.," ETSI Open Radio Interface (ORI), ORI(13)M18016, 2013.

[33] A. Agata, S. Nanba, M. Oishi, and K. Tanaka, "Nonlinear quantization-based I/Q data compression technique for C-RAN fronthaul link," *IEICE Trans. Electron.*, vol. J98-C, no. 8, pp. 158-166, Aug. 2015.

[34] K. Nishimura, M. Oishi, N. Kamiya, A. Bekkali, and K. Tanaka, "[Invited talk] W-band seamless optical and radio transmission system – Aiming for application to disaster recovery –," *IEICE Technical Report*, vol. 114, no. 287, MWP2014-43, pp. 7-12, Nov. 2014.

[35] R. Olshansky, V. A. Lanzisera, and P. M. Hill, "Subcarrier multiplexed lightwave systems for broad-band distribution," *IEEE/OSA J. Lighw. Technol.*, vol. 7, no. 9, pp. 1329-1342, Sep. 1989.

[36] G. J. Meslener, "Chromatic dispersion induced distortion of modulated monochromatic light employing direct detection," *IEEE J. Quantum Electron.*, vol. 20, no. 10, pp. 1208-1216, Oct. 1984.

[37] H. Schmuck, "Comparison of optical millimeter-wave system concepts with regard to chromatic dispersion," *Electron. Lett.*, vol. 31, no. 21, pp. 1848-1849,

Oct. 1995.

[38] U. Gliese, S. Norskov, and T. N. Nielsen, “Chromatic dispersion in fiber-optic microwave and millimeter-wave links,” *IEEE Trans. on Microw. Theory and Techn.*, vol. 44, no. 10, pp. 1716-1724, Oct. 1996.

[39] N. Tomita, H. Takasugi, N. Atobe, I. Nakamura, F. Takaetsu and S. Takashima, “Design and performance of a novel automatic fiber line testing system with OTDR for optical subscriber loops,” *IEEE/OSA J. Lightw. Technol.*, vol. 12, no. 5, pp. 717-726, May 1994.

[40] J. Pesic, E. L. Rouzic, N. Brochier and L. Dupont, “Proactive restoration of optical links based on the classification of events,” in *Proc. the 15th Int’l. Conference on Optical Network Design and Modeling (ONDM’11)*, paper S3-2, Bologna, Italy, Feb. 2011.

[41] S. Kobayashi and T. Kimura, “Injection locking characteristics of an AlGaAs semiconductor laser,” *IEEE J. Quantum Electron.*, vol. QE-16, no. 9, pp. 915-917, Sep. 1980.

[42] K. Hsu and S. Yamashita, “Performance of self-injection locked fiber Fabry-Perot laser with short feedback cavity,” in *Proc. 2000 IEEE/OSA Optical Fiber Communication Conference (OFC’00)*, pp. 14-16, Baltimore, MD, Mar. 2000.

[43] M. Oishi, and K. Nishimura, “A detection technique of optical line failures utilizing mutually injection-locked Fabry-Perot lasers,” in *Proc. IEICE General Conf.*, B-10-65, Gifu, Japan, Mar. 2013.

[44] M. Oishi, N. Kamiya, T. Murakami, K. Nishimura, and K. Tanaka, “Highly resilient optical and radio seamless communication systems with agile deployment capability (2) －Optical link failure detection and switching technique－,” *IEICE Technical Report*, vol. 113, no. 397, MWP2013-55, pp. 7-10, Jan. 2014.

[45] K. Suzuki, M. Fujiwara, K. Taguchi, T. Imai, H. Ishii, N. Yoshimoto, and H. Hadama, “128 × 8 split and 80 km long-reach dual-rate 10G-EPON transmission using ALC hybrid burst-mode optical fiber amplifier and SOA pre-amplifier,” in *Proc. the 37th European Conference on Optical Communication (ECOC’11)*, paper Mo.1.C.3, Geneva, Switzerland, Sep. 2011.

[46] M. Noda, N. Suzuki, S. Yoshima, T. Suehiro, S. Ihara, S. Shirai, M. Nogami, H. Aruga, S. Kozaki, and J. Nakagawa, "Super-splits 10G-EPON: 256 ONU passive splits with 240 ns dual-rate burst-mode 3R synctime and bi-directionally extended 35.9 dB loss budgets," in *Proc. 2012 IEEE/OSA Optical Fiber Communication Conference (OFC'12)*, paper PDP5B, Los Angeles, CA, Mar. 2012.

[47] M. Oishi, T. Tsuritani, and K. Nishimura, "Extended-reach 10G/1G-EPON over 80 km and 1024 split with optical amplifier-based hybrid repeater," in *Proc. 2012 IEEE/OSA Optical Fiber Communication Conference (OFC'12)*, paper NTu1.J.1, Los Angeles, CA, Mar. 2012.

[48] ITU-T Recommendation G.975.1, "Forward error correction for high bit-rate DWDM submarine systems," 2004.

[49] I. P. Kaminow, and T. L. Koch, Optical fiber telecommunications, 3rd ed., vol. A, Academic Press, 1997.

[50] C. Yijiang and A. W. Snyder. "Depletion and saturation effect of stimulated Raman scattering," *Electron. Lett.*, vol. 24, no. 23, pp. 1450-1452, Nov. 1988.

[51] P. Frost and T. Kailath, "An innovations approach to least-square estimation – Part III: Nonlinear estimation in white Gaussian noise," *IEEE Trans. on Automatic Control*, vol. 16, no. 3, pp. 217-226, Jun. 1971.

[52] H. Jasik and R. C. Johnson, Antenna Engineering Handbook, 3rd ed., McGraw-Hill, 1993.

[53] ITU-T Recommendation G.652, "Characteristics of a single-mode optical fiber and cable," 2009.

[54] W.R. Lee, M.Y. Park, S.H. Cho, J. Lee, B.W. Kim, G. Jeong and B.W. Kim, "Bidirectional WDM-PON based on gain-saturated reflective semiconductor optical amplifiers," *IEEE Photon. Technol. Lett.*, vol. 17, no. 11, pp. 2460-2462, Nov. 2005.

[55] J. H. Yu, N. Kim, and B. W. Kim, "Remodulation scheme with reflective SOA for colorless DWDM PON," *IEEE J. Opt. Commun. Netw.*, vol. 6, no. 8, pp. 1041-1054, 2007.

[56] J. Watanabe, S. Ebisawa, and J. Maeda, "A proposal of upstream signal generation in high speed WDM-PON using re-modulation of downstream

signal," in *Proc. IEICE General Conf.*, B-10-95. Okayama, Japan, Mar. 2012.

[57] M. Oishi, K. Nishimura, and S. Akiba, "Study of uplink transmission for array-antenna beam forming by radio over fiber," in *Proc. IEICE General Conf.*, B-10-67, Gifu, Japan, Mar. 2013.

[58] IEEE Std. 802.11-2007, "Part 11: Wireless LAN medium access control (MAC) and physical layer (PHY) specifications," 2007.

[59] H. Suzuki, M. Fujiwara, K. Iwatsuki, A. Hirata, and T. Nagatsuma, "Photonic millimeter-wave generator using intensity and phase modulators for 10 Gbit/s wireless link," *Electron. Lett.*, vol. 41, no. 6, pp. 355-356, Mar. 2005.

[60] S. Koening, F. Boes, D. Lopez-Diaz, J. Antes, R. Hunneberger, R. Schmogrow, D. Hillerkuss, R. Palmer, T. Zwick, C. Koos, W. Freude, O. Ambacher, I. Kallfass, and J. Leuthold, "100Gbit/s wireless link with mm-wave photonics," in *Proc. 2013 IEEE/OSA Optical Fiber Communication Conference (OFC'13)*, paper PDP5B.4, Anaheim, CA, March 2013.

[61] A. Kanno, K. Inagaki, I. Morohashi, T. Sakamoto, T. Kuri, I. Hosako, T. Kawanishi, Y. Yoshida and K. Kitayama, "40 Gb/s W-band (75-110 GHz) 16-QAM radio-over-fiber signal generation and its wireless transmission," *Optics Express*, vol. 19, no. 26, pp. B56-B63, 2011.

[62] T. Taniguchi, N. Sakurai, K. Kumozaki, and T. Imai, "Full-duplex 1.0 Gbit/s data transmission over 60 GHz radio-on-fiber access system based on the loop-back optical heterodyne technique," *IEEE/OSA J. Lightw. Technol.*, vol. 26, no. 13, pp. 1765-1776, July 2008.

[63] X. Pang, A. Lebedev, J. J. Vegas, and I. T. Monroy, "Seamless optical fiber-wireless millimeter-wave transmission link for access networks," in *Proc. the 18th Opto-Electronics Communication Conference (OECC'13)*, paper TuPP-12, Kyoto, Japan, June/July 2013.

[64] Type SMP connectors product catalog [Online]. Available: http://www.mouser.com/pdfdocs/Emerson_SMP_Connectors.pdf

[65] K. Wu, Y. J. Cheng, T. Djerafi, X. P. Cheng, N. Fonseca, and W. Hong, "Millimeter-wave integrated waveguide antenna arrays and beamforming networks for low-cost satellite and mobile systems," in *Proc. the 4th European Conference on Antenna and propagation (EuCAP'10)*, pp. 1-5, Barcelona,

Spain, April 2010.

[66] J. F. Coward, T. K. Yee, C. H. Chalfant, and P. H. Chang, "A photonic integrated-optic RF phase shifter for phased array antenna beam-forming applications," *IEEE/OSA J. Lightw. Technol.*, vol. 11, no. 12, pp. 2201-2205, Aug. 2002.

[67] J. Stulemeijer, D. H. P. Maat, I. Moerman, F. E. V. Vliet, and M. K. Smit, "Photonic integrated beamformer for a phased array antenna," in *Proc. 24th European Conference on Optical Communication (ECOC'98)*, pp. 637-638, Madrid, Spain, Sep. 1998.

[68] H. Ito, S. Kodama, Y. Muramoto, T. Furuya, T. Nagatsuma, and T. Ishibashi, "High-speed and high-output InP-InGaAs unitraveling-carrier photodiodes," *IEEE J. Selected Topics in Quantum Electron.*, vol. 10, no. 4, pp. 709-727, July/Aug. 2004.

[69] IEEE Std. 802.11ad-2012.

[70] K. Minoguchi, Y. Nishikawa, M. Oishi, S. Akiba, J. Hirokawa, and M. Ando, "Beam steering scheme of photonic array-antennas for 60 GHz RF signals generated by optical two-tone technique," in *Proc. the 19th Opto-Electronics and Communications Conference (OECC'14)*, paper Th10A3, Melbourne, Australia, July 2014.

[71] A. Alvarado, E. Agrell, D. Lavery, and P. Bayvel, "LDPC codes for optical channels: Is the "FEC limit" a good predictor of post-FEC BER?," in *Proc. 2015 IEEE/OSA Optical Fiber Communication Conference (OFC'15)*, paper Th3E.5, Los Angeles, CA, Mar. 2015.

[72] B. Nebendahl, R. Schmogrow, T. Dennis, A. Josten, D. Hillerkuss, S. Koenig, J. Meyer, M. Dreschmann, M. Winter, M. Huebner, W. Freude, C. Koos, and J. Leuthold, "Quality metrics in optical modulation analysis: EVM and its relation to Q-factor, OSNR, and BER," in *Proc. the 2012 Asia Communications and Photonics Conference (ACP'12)*, pp. 1-3, Guangzhou, China, Nov. 2012.

[73] T. Umezawa, K. Akahane. N. Yamamoto, K. Inagaki, A. Kanno, and T. Kawanishi, "Ultra-broadband UTC-PD beyond 110 GHz at 0 V for future photonic integration," in *Proc. the 2014 Int'l Topical Meeting on Microwave Photonics (MWP'14)*, pp. 450-453, Sendai, Japan, Oct. 2014.

[74] T. Umezawa, K. Akahane, N. Yamamoto, A. Kanno, K. Inagaki, and T. Kawanishi, “Zero-bias operational ultra-broadband UTC-PD above 110 GHz for high symbol rate PD-array in high-density photonic integration,” in *Proc. 2015 IEEE/OSA Optical Fiber Communication Conference (OFC’15)*, paper M3C.7, Los Angeles, CA, Mar. 2015.

[75] Y. Inoue, A. Kaneko, F. Hanawa, H. Takahashi, K. Hattori, and S. Sumida, “Athermal silica-based arrayed-waveguide grating (AWG) multiplexer,” in *Proc. the 11th European Conference on Optical Communication (ECOC’97)*, pp. 33-36, Edinburgh, UK, Sep. 1997.

[76] Y. Nishikawa, M. Oishi, S. Akiba, J. Hirokawa, and M. Ando, “Antenna beam steering in millimeter-wave band by radio over fiber using multi-core fiber,” in *Proc. IEICE Society Conf.*, B-10-79, Fukuoka, Japan, Sep. 2013.

[77] K. Furuya, T. Hirasawa, M. Oishi, S. Akiba, J. Hirokawa, and M. Ando, “Estimation of handset position in 60 GHz-band antenna beam steering system by radio-over-fiber,” in *Proc. IEICE General Conf.*, C-14-19, Fukuoka, Japan, Mar. 2016.

Acronyms

AF	array factor
AP	access point
AWG	arbitrary waveform generator
AWG	arrayed-waveguide grating
BPF	band-pass filter
BS	base station
CD	chromatic dispersion
CIR	optical circulator
CO	central office
CPL	coupler
C-RAN	centralized radio access network
CW	continuous wave
DCF	dispersion compensation fiber
DCM	dispersion compensation fiber module
DFB-LD	distributed feedback laser diode
D-RAN	distributed radio access network
DSB	double sidebands
EDFA	erbium-doped fiber amplifier
E/O	electrical-to-optical converter
EVM	error vector magnitude
FDD	frequency division duplex

FP-LD	Fabry-Perot laser diode
FWA	fixed wireless access
HPF	high pass filter
IM	intensity modulator
IPA	integrated photonic array-antenna
I/Q	in-phase and quadrature-phase
LDPC	low-density parity-check
LNA	low noise amplifier
LO	local oscillator
LPF	low pass filter
MCF	multi-core fiber
OBPF	optical band-pass filter
O/E	optical-to-electrical converter
OR	optical reflector
OTDR	optical time domain reflectometer
PD	photodiode
PDL	polarization dependence loss
PON	passive optical network
PPG	pulse pattern generator
PRBS	pseudo random bit sequence
QAM	quadrature amplitude modulation
QPSK	quadrature phase shift keying
RF	radio frequency
RoF	radio-over-fiber

RS	Reed-Solomon
RSOA	reflective semiconductor optical amplifier
RTT	round-trip time
SCM	sub-carrier multiplexing
SMF	single-mode fiber
SNR	signal-to-noise ratio
SOP	state-of-polarization
SPL	splitter
SRS	stimulated Raman scattering
SW	switch
TDD	time division duplex
TLS	tunable laser source
UTC-PD	uni-traveling carrier photodiode
VDL	variable optical delay line
VOA	variable optical attenuator
WDM	wavelength division multiplexing

Acknowledgement

This research has been carried out during my tenure at the Department of Electrical and Electronic Engineering, Graduate School of Engineering, Tokyo Institute of Technology, under the guidance of Profs. Makoto Ando and Jiro Hirokawa.

First of all, I would like to express my sincere gratitude with the deepest respect to Profs. Makoto Ando and Jiro Hirokawa for their invaluable suggestions, guidance, and contributions on this doctoral study. Their wealth of creative ideas and precise indications have always encouraged me to accomplish this work. It was a fortunate opportunity for me to work with them.

I would like to convey my sincere appreciation to Profs. Fumio Watanabe, Nobuhiko Nishiyama, Kei Sakaguchi, and Yuya Shoji of Tokyo Institute of Technology. I am grateful for their kind acceptance to be reviewers and judges of my doctoral thesis as well as their helpful advices and constructive criticism. I would also like to express my special gratitude to Prof. Shigeyuki Akiba of Tokyo Institute of Technology for giving me sufficient basic backgrounds on this study and his continued encouragement.

I wish to express my sincere appreciation to Drs. Kazunori Takeuchi, Kosuke Nishimura of KDDI R&D Laboratories, Inc., Drs. Yukio Horiuchi, Keiji Tanaka, Akira Agata, Takahide Murakami of KDDI Corporation, Dr. Abdelmoula Bekkali, and Mr. Naoyasu Kamiya of KDDI R&D Laboratories, Inc. for their fruitful discussions and great support throughout this study.

I am indebted to all the students and members of Ando & Hirokawa Laboratory in Tokyo Institute of Technology, especially Mr. Yoshihiro Nishikawa, Mr. Kyo Minoguchi, Mr. Takayoshi Hirasawa, and Ms. Kotoko Furuya of Tokyo Institute of Technology for their kind support on experiments and technical discussions.

Finally, I would like to thank my dear wife, Tomomi and my dear daughter, Miyu for their patience, deep understanding and support during the whole period of this work.

September 2016

Masayuki OISHI

List of Publications by the Author

I. Journals

[1] Masayuki Oishi, Yoshihiro Nishikawa, Kosuke Nishimura, Keiji Tanaka, Shigeyuki Akiba, Jiro Hirokawa, and Makoto Ando, “Phased array antenna beam steering scheme for future wireless access systems using radio-over-fiber transmission technique,” *IEICE Trans. Commun.*, vol. E97-B, no. 7, pp. 1281-1289, July 2014.

[2] Masayuki Oishi, Naoyasu Kamiya, Abdelmoula Bekkali, Kosuke Nishimura, and Keiji Tanaka, “Radio-over-fiber-based seamless optical and radio transmission system by autonomous self-healing technique for optical fiber failures,” *IEICE Trans. Electron.*, vol. J98-C, no. 7, pp. 144-153, July 2015 [2016 IEICE Best Paper Award].

[3] Masayuki Oishi, Takayoshi Hirasawa, Kotoko Furuya, Shigeyuki Akiba, Jiro Hirokawa, and Makoto Ando, “3.5-Gbit/s QPSK signal radio-over-fiber transmission with 60-GHz integrated photonic array-antenna beam forming,” *IEEE/OSA J. Lightw. Technol.*, to be published on Oct. 2016.

(Co-author)

[4] Akira Agata, Shinobu Nanba, Masayuki Oishi, and Keiji Tanaka, “Nonlinear quantization-based I/Q data compression technique for C-RAN fronthaul link,” *IEICE Trans. Electron.*, vol. J98-C, no. 8, pp. 158-166, Aug. 2015.

[5] Kyo Minoguchi, Takayoshi Hirasawa, Masayuki Oishi, Shigeyuki Akiba, Jiro Hirokawa, and Makoto Ando, “Beam steering of 60 GHz-band array-antenna utilizing radio-over-fiber transmission technique and effect of chromatic dispersion,” *IEICE Trans. Electron.*, to be published on Sep. 2016 [invited].

II. Letters

[1] Masayuki Oishi, Naoyasu Kamiya, Takahide Murakami, Kosuke Nishimura, and Keiji Tanaka, "Autonomous self-healing technique utilizing a self-injection-locked Fabry-Perot laser for optical and wireless communication systems," *IEICE Electronics Express*, vol. 11, no. 8, pp. 1-9, April 2014.

III. International Conferences

[1] Masayuki Oishi, Ryo Inohara, Akira Agata, and Yukio Horiuchi, "Reconfigurable multi-port EPON repeater," in *Proc. Asia Communication and Photonics Conference (ACP'09)*, paper TuDD6, Shanghai, China, Nov. 2009.

[2] Masayuki Oishi, Kazuho Ohara, and Yukio Horiuchi, "Failed ONU detection technique applicable to commercially available passive optical networks," in *Proc. the 36th European Conference on Optical Communication (ECOC'10)*, paper We.8.B.3, Torino, Italy, Sep. 2010.

[3] Masayuki Oishi, Takehiro Tsuritani, and Kosuke Nishimura, "Extended-reach 10G/1G-EPON over 80 km and 1024 split with optical amplifier-based hybrid repeater," in *Proc. 2012 IEEE/OSA Optical Fiber Communication Conference (OFC'12)*, paper NTu1.J.1, Los Angeles, CA, Mar. 2012.

[4] Masayuki Oishi, Yukio Horiuchi, and Kosuke Nishimura, "ONU tester for diagnosis of TDMA-PON using multi-point control protocol messages," in *Proc. the 10th Int'l Conference on Optical Internet (COIN'12)*, paper WE.2, Yokohama, Japan, May 2012 [COIN2012 Young Engineer Award].

[5] Masayuki Oishi, Hiromi Matsuno, Kosuke Nishimura, and Shigeyuki Akiba, "Experimental study of chromatic dispersion effects on antenna beam forming by RF over fiber," in *Proc. the 2012 IEEE Int'l Topical Meeting on Microwave Photonics (MWP'12)*, pp. 140-143, Noordwijk, the Netherlands, Sep. 2012.

[6] Masayuki Oishi, Kosuke Nishimura, and Shigeyuki Akiba, "RoF uplink

transmission scheme with reflective-SOA for remotely beam steerable photonic array-antenna," in *Proc. the 18th Opto-Electronics and Communications Conference (OECC'13)*, paper ThP3-2, Kyoto, Japan, June/July 2013.

[7] Masayuki Oishi, Yoshihiro Nishikawa, Shigeyuki Akiba, Jiro Hirokawa, and Makoto Ando, "2-dimensional beam steering by 2 × 3 photonic antenna using millimeter-wave radio over fiber," in *Proc. the 2013 IEEE Int'l Topical Meeting on Microwave Photonics (MWP'13)*, pp. 130-133, Alexandria, VA, Oct. 2013.

(Co-author)

[8] Shigeyuki Akiba, Masayuki Oishi, and Hiromi Matsuno, "Effect of chromatic dispersion on RF power feeding to array antennas through fiber," in *Proc. the 17th Opto-Electronics and Communications Conference (OECC'12)*, paper P1-8, Busan, Korea, July 2012.

[9] Naoyasu Kamiya, Masayuki Oishi, Takahide Murakami, and Kosuke Nishimura, "Dynamic ONU registration scheme for TDMA-PON with ultra-high-split," in *Proc. the 17th Opto-Electronics and Communications Conference (OECC'12)*, paper 5A3-4, Busan, Korea, July 2012.

[10] Shigeyuki Akiba, Masayuki Oishi, Yoshihiro Nishikawa, Jiro Hirokawa, and Makoto Ando, "Photonic approach to beam steering of phased array antenna," in *Proc. the 2013 URSI Int'l Symposium on Electromagnetic Theory (EMTS'13)*, pp. 448-451, Hiroshima, Japan, May 2013.

[11] Yoshihiro Nishikawa, Masayuki Oishi, Shigeyuki Akiba, Jiro Hirokawa, and Makoto Ando, "Photonic array-antenna in millimeter-wave band by wavelength division multiplexed radio over fiber," in *Proc. the 18th Opto-Electronics and Communications Conference (OECC'13)*, paper ThP3-3, Kyoto, Japan, June/July 2013.

[12] Shigeyuki Akiba, Masayuki Oishi, Yoshihiro Nishikawa, Kyo Minoguchi, Jiro Hirokawa, and Makoto Ando, "Photonic architecture for beam forming of RF phased array antenna," in *Proc. 2014 IEEE/OSA Optical Fiber Communication Conference (OFC'14)*, paper W2A.51, San Francisco, CA, Mar. 2014.

[13] Kosuke Nishimura, Masayuki Oishi, Naoyasu Kamiya, Takahide Murakami,

Yu Kawaguchi, Takehiro Tsuritani, and Keiji Tanaka, “Analogue RoF-based seamless optical and wireless transmission systems,” presented at *the 2014 Int’l Wireless Symposium (IWS’14)*, Xi’an, China, Mar. 2014 [invited].

[14] Akira Agata, Masayuki Oishi, and Keiji Tanaka, “Performance enhancement of optical access network in C-RAN using nonlinear quantization-based compression,” in *Proc. the 19th Opto-Electronics and Communications Conference (OECC’14)*, paper Tu3A2, Melbourne, Australia, July 2014.

[15] Kyo Minoguchi, Yoshihiro Nishikawa, Masayuki Oishi, Shigeyuki Akiba, Jiro Hirokawa, and Makoto Ando, “Beam steering scheme of photonic array-antennas for 60 GHz RF signals generated by optical two-tone technique,” in *Proc. the 19th Opto-Electronics and Communications Conference (OECC’14)*, paper Th10A3, Melbourne, Australia, July 2014.

[16] Naoyasu Kamiya, Masayuki Oishi, Abdelmoula Bekkali, Kosuke Nishimura, and Keiji Tanaka, “Study on signal modulation scheme for millimeter-wave band RoF transmission systems with optical signal re-modulation,” in *Proc. the 2014 IEEE Int’l Topical Meeting on Microwave Photonics (MWP’14)*, paper TuB-1, Sapporo, Japan, Oct. 2014.

[17] Abdelmoula Bekkali, Masayuki Oishi, Kosuke Nishimura, and Keiji Tanaka, “First demonstration of seamless optical and radio transmission with plural W-band wireless sections,” in *Proc. 2015 IEEE/OSA Optical Fiber Communication Conference (OFC’15)*, paper W2A.65, Los Angeles, CA, Mar. 2015.

[18] Takayoshi Hirasawa, Kyo Minoguchi, Masayuki Oishi, Shigeyuki Akiba, Jiro Hirokawa, and Makoto Ando, “Amplitude modulated digital signal transmission in RoF system for MMW-RF antenna beam steering,” in *Proc. the 20th Opto-Electronics and Communications Conference (OECC’15)*, paper JMoD.42, Shanghai, China, June/July 2015.

[19] Takayoshi Hirasawa, Kotoko Furuya, Masayuki Oishi, Shigeyuki Akiba, Jiro Hirokawa, and Makoto Ando, “Integrated photonic array-antenna in RoF system for MMW-RF antenna beam steering,” in *Proc. the 2015 IEEE Int’l Topical Meeting on Microwave Photonics (MWP’15)*, paper TuP-14, Paphos, Cyprus, Oct. 2015.

[20] Ken-ichi Kitayama, Yuki Yoshida, Yuya Yamaguchi, Hirochika Nakajima, Kosuke Nishimura, Abdelmoula Bekkali, Masayuki Oishi, Hidenori Iwai,

Kazuya Ota, Norihiko Sato, Naoyasu Kamiya, Keiji Tanaka, Yoichi Oikawa, Kazukiyo Joshin, Nobuhiko Shibagaki, Kaoru Higuma, Satoshi Oikawa, Junichiro Ichikawa, Atsushi Kanno, and Tetsuya Kawanishi, "High-speed optical and millimeter-wave wireless link for disaster recovery," presented at *the 2015 IEEE Globecom Workshops*, San Diego, CA, Dec. 2015.

[21] Kotoko Furuya, Takayoshi Hirasawa, Masayuki Oishi, Shigeyuki Akiba, Jiro Hirokawa, and Makoto Ando, "3.5-Gbit/s QPSK signal transmission in beam forming of 60-GHz integrated photonic array-antenna," in *Proc. the 21st Opto-Electronics and Communications Conference (OECC'16)*, paper TuA2-1, Niigata, Japan, July 2016 [OECC2016 Best Paper Award].

IV. Domestic Conferences

[1] Masayuki Oishi, Ryo Inohara, Akira Agata, and Yukio Horiuchi, "Proposal of Reconfigurable multi-port EPON repeater," in *Proc. IEICE Society Conf.*, B-8-18, Niigata, Japan, Sep. 2009.

[2] Masayuki Oishi, Kazuho Ohara, and Yukio Horiuchi, "Rogue ONU identification technique with standardized multi-point control protocol messages," in *Proc. IEICE Society Conf.*, B-8-22, Sakai, Japan, Sep. 2010.

[3] Masayuki Oishi, Yukio Horiuchi, and Kosuke Nishimura, "Rogue ONU isolation system with multi-point control protocol messages," in *Proc. IEICE Society Conf.*, B-10-81, Sapporo, Japan, Sep. 2011.

[4] Masayuki Oishi, Takehiro Tsuritani, and Kosuke Nishimura, "Extended-reach 10G/1G-EPON upstream signal transmission utilizing cross gain modulation of semiconductor optical amplifier," in *Proc. IEICE General Conf.*, Okayama, Japan, Mar. 2012.

[5] Masayuki Oishi, Hiromi Matsuno, Kosuke Nishimura, and Shigeyuki Akiba, "Experimental study of antenna beam forming by radio over fiber utilizing fiber chromatic dispersion," in *Proc. IEICE Society Conf.*, B-10-80, Toyama, Japan, Sep. 2012.

[6] Masayuki Oishi, and Kosuke Nishimura, “A detection technique of optical line failures utilizing mutually injection-locked Fabry-Perot lasers,” in *Proc. IEICE General Conf.*, B-10-65, Gifu, Japan, Mar. 2013 [2013 IEICE Young Researcher’s Award].

[7] Masayuki Oishi, Kosuke Nishimura, and Shigeyuki Akiba, “Study of uplink transmission for array-antenna beam forming by radio over fiber,” in *Proc. IEICE General Conf.*, B-10-67, Gifu, Japan, Mar. 2013.

[8] Masayuki Oishi, Yoshihiro Nishikawa, Shigeyuki Akiba, Jiro Hirokawa, and Makoto Ando, “2-dimensional beam steering of 2 × 3 array-antenna by millimeter-wave radio over fiber,” in *Proc. IEICE Society Conf.*, B-10-78, Fukuoka, Japan, Sep. 2013 [2013 IEICE Young Researcher’s Award].

[9] Masayuki Oishi, Naoyasu Kamiya, Takahide Murakami, Kosuke Nishimura, and Keiji Tanaka, “Optical and wireless seamless communication systems (2) －Autonomous self- healing technique for optical fiber failures－,” in *Proc. IEICE General Conf.*, C-14-2, Niigata, Japan, Mar. 2014.

[10] Masayuki Oishi, Agi Saitoh, Yukio Horiuchi, Yoshitaka Hakamada, and Shuichi Aoki, “Field transmission experiment of multi-channel 8K-broadcast signals over 10-Gbit Ethernet passive optical network,” presented at *the 15th Forum on Information Technology (FIT’16)*, Toyama, Japan, Sep. 2016 [invited].

(Co-author)

[11] Naoyasu Kamiya, Masayuki Oishi, Takahide Murakami, and Kosuke Nishimura, “Estimation of number of unregistered ONUs for TDMA-PON with ultra-high-split,” in *Proc. IEICE Society Conf.*, B-10-76, Toyama, Japan, Sep. 2012.

[12] Yoshihiro Nishikawa, Masayuki Oishi, Shigeyuki Akiba, Jiro Hirokawa, and Makoto Ando, “Enhancement to higher frequency-band (20 GHz) on antenna beam forming by radio over fiber,” in *Proc. IEICE Society Conf.*, B-10-79, Toyama, Japan, Sep. 2012.

[13] Yoshihiro Nishikawa, Masayuki Oishi, Shigeyuki Akiba, Jiro Hirokawa, and Makoto Ando, “Photonic approach to beam steering of phased array-antenna in

millimeter wavelength," in *Proc. IEICE General Conf.*, B-10-66, Gifu, Japan, Mar. 2013.

[14] Yoshihiro Nishikawa, Masayuki Oishi, Shigeyuki Akiba, Jiro Hirokawa, and Makoto Ando, "Antenna beam steering in millimeter-wave band by radio over fiber using multi-core fiber," in *Proc. IEICE Society Conf.*, B-10-79, Fukuoka, Japan, Sep. 2013.

[15] Kyo Minoguchi, Yoshihiro Nishikawa, Masayuki Oishi, Shigeyuki Akiba, Jiro Hirokawa, and Makoto Ando, "Angle estimation of handset position for photonic array-antenna by radio over fiber," in *Proc. IEICE Society Conf.*, B-10-80, Fukuoka, Japan, Sep. 2013.

[16] Kosuke Nishimura, Yu Kawaguchi, Takahide Murakami, Masayuki Oishi, Naoyasu Kamiya, Takehiro Tsuritani, and Keiji Tanaka, "Optical and wireless seamless communication systems (1) －Optical transceivers－," in *Proc. IEICE General Conf.*, C-14-1, Niigata, Japan, Mar. 2014.

[17] Akira Agata, Masayuki Oishi, Kosuke Nishimura, and Keiji Tanaka, "Optical and wireless seamless communication systems (3) －Study on dispersion compensation using equalizers－," in *Proc. IEICE General Conf.*, C-14-3, Niigata, Japan, Mar. 2014.

[18] Kyo Minoguchi, Yoshihiro Nishikawa, Masayuki Oishi, Shigeyuki Akiba, Jiro Hirokawa, and Makoto Ando, "Application of RF signal (60 GHz) generated by optical beat frequency to photonic array-antennas," in *Proc. IEICE General Conf.*, C-14-23, Niigata, Japan, Mar. 2014.

[19] Takayoshi Hirasawa, Kyo Minoguchi, Masayuki Oishi, Shigeyuki Akiba, Jiro Hirokawa, and Makoto Ando, "Beam steering experiments for 40 GHz photonic array-antenna by using integrated photodiodes," in *Proc. IEICE Society Conf.*, C-14-6, Tokushima, Japan, Sep. 2014.

[20] Kyo Minoguchi, Masayuki Oishi, Shigeyuki Akiba, Jiro Hirokawa, and Makoto Ando, "Experiments for beam steering of 60 GHz-band photonic array-antennas by combining SMF and DSF," in *Proc. IEICE Society Conf.*, C-14-7, Tokushima, Japan, Sep. 2014.

[21] Abdelmoula Bekkali, Masayuki Oishi, Kosuke Nishimura, and Keiji Tanaka, "Impact of intermediate frequency selection on millimeter-wave-RoF system performance," in *Proc. IEICE Society Conf.*, C-14-14, Tokushima, Japan, Sep.

2014.

[22] Kyo Minoguchi, Takayoshi Hirasawa, Masayuki Oishi, Shigeyuki Akiba, Jiro Hirokawa, and Makoto Ando, “1 Gbit/s signal transmission in radio-over-fiber-based millimeter-wave antenna beam steering system,” in *Proc. IEICE General Conf.*, C-14-19, Kusatsu, Japan, Mar. 2015.

[23] Takayoshi Hirasawa, Kotoko Furuya, Masayuki Oishi, Shigeyuki Akiba, Jiro Hirokawa, and Makoto Ando, “Integrated photonic array-antenna for millimeter-wave-band antenna beam steering by radio-over-fiber,” in *Proc. IEICE Society Conf.*, C-14-9, Sendai, Japan, Sep. 2015.

[24] Kotoko Furuya, Takayoshi Hirasawa, Masayuki Oishi, Shigeyuki Akiba, Jiro Hirokawa, and Makoto Ando, “Estimation of handset position in 40 GHz-band array antenna beam control using radio-over-fiber,” in *Proc. IEICE Society Conf.*, C-14-10, Sendai, Japan, Sep. 2015.

[25] Takayoshi Hirasawa, Kotoko Furuya, Masayuki Oishi, Shotaro Maki, Shigeyuki Akiba, Jiro Hirokawa, and Makoto Ando, “3.5-Gbit/s QPSK radio-over-fiber signal transmission in beam forming of 60 GHz-band integrated photonic array-antenna,” in *Proc. IEICE General Conf.*, C-14-18, Fukuoka, Japan, Mar. 2016.

[26] Kotoko Furuya, Takayoshi Hirasawa, Masayuki Oishi, Shigeyuki Akiba, Jiro Hirokawa, and Makoto Ando, “Estimation of handset position in 60 GHz-band antenna beam steering system by radio-over-fiber,” in *Proc. IEICE General Conf.*, C-14-19, Fukuoka, Japan, Mar. 2016.

V. Domestic Technical Reports

[1] Masayuki Oishi, Kazuho Ohara, and Yukio Horiuchi, “Proposal of a rogue ONU isolation method with standardized multi-point control protocol messages,” *IEICE Technical Report*, vol. 110, no. 291, OCS2010-92, pp. 17-21, Nov. 2010.

[2] Masayuki Oishi, Yukio Horiuchi, and Kosuke Nishimura, “ONU tester

prototype for diagnosis of Ethernet passive optical networks using multi-point control protocol messages," *IEICE Technical Report*, vol. 111, no. 411, OCS2011-106, pp. 7-12, Jan. 2012.

[3] Masayuki Oishi, "Report on ECOC2012 －Optical access－," *IEICE Technical Report*, vol. 112, no. 258, OCS2012-49, pp. 47-50, Oct. 2012 [Invited].

[4] Masayuki Oishi, Takehiro Tsuritani, and Kosuke Nishimura, "Transmission experiments of upstream burst-mode repeaters for long-reach and high-split 10G/1G-EPON systems," *IEICE Technical Report*, vol. 112, no. 310, OCS2012-79, pp. 15-20, Nov. 2012.

[5] Masayuki Oishi, Naoyasu Kamiya, Takahide Murakami, Kosuke Nishimura, and Keiji Tanaka, "Highly resilient optical and radio seamless communication systems with agile deployment capability (2) －Optical link failure detection and switching technique－," *IEICE Technical Report*, vol. 113, no. 397, MWP2013-55, pp. 7-10, Jan. 2014.

(Co-author)

[6] Akira Agata, Masayuki Oishi, and Yukio Horiuchi, "Optical access network designing algorithm for suboptimal deployment of optical fiber cables," *IEICE Technical Report*, vol. 109, no. 302, OCS2009-93, pp. 61-66, Dec. 2009.

[7] Naoyasu Kamiya, Masayuki Oishi, Takahide Murakami, and Kosuke Nishimura, "Effectiveness evaluation of ONU registration scheme for TDMA-PON with ultra-high-split," *IEICE Technical Report*, vol. 112, no. 395, OCS2012-91, pp. 37-41, Jan. 2013.

[8] Yoshihiro Nishikawa, Masayuki Oishi, Shigeyuki Akiba, Jiro Hirokawa, and Makoto Ando, "2-dimensional beam steering of millimeter-wave band array-antenna by radio-over-fiber," *IEICE Technical Report*, vol. 113, no. 305, OCS2013-83, pp. 7-11, Nov. 2013.

[9] Kosuke Nishimura, Takahide Murakami, Masayuki Oishi, Naoyasu Kamiya, Yu Kawaguchi, Takehiro Tsuritani, and Keiji Tanaka, "Highly resilient optical and radio seamless communication systems with agile deployment capability (1) －Key Technologies－," *IEICE Technical Report*, vol. 113, no. 397,

MWP2013-54, pp. 1-5, Jan. 2014.

[10] Shintaro Hisatake, Tien-Dat Pham, and Masayuki Oishi, “Report on MWP2013,” *IEICE Technical Report*, vol. 113, no. 397, MWP2013-61, pp. 41-46, Jan. 2014 [invited].

[11] Kyo Minoguchi, Masayuki Oishi, Shigeyuki Akiba, Jiro Hirokawa, and Makoto Ando, “Photonic architecture for beam forming of RF phased array antenna,” *IEICE Technical Report*, vol. 114, no. 36, OCS2014-3, pp. 13-17, May 2014.

[12] Kosuke Nishimura, Masayuki Oishi, Naoyasu Kamiya, Abdelmoula Bekkali, and Keiji Tanaka, “W-band seamless optical and radio transmission system －Aiming for application to disaster recovery－,” *IEICE Technical Report*, vol. 114, no. 287, MWP2014-43, pp. 7-12, Nov. 2014.

[13] Akira Agata, Shinobu Nanba, Masayuki Oishi, Keiji Tanaka, Akihiro Maruta, and Ken-ichi Kitayama, “A study on the baseband signal compression and transmission technologies for enhancing transfer efficiency in C-RAN fronthaul link,” *IEICE Technical Report*, vol. 114, no. 300, OCS2014-86, pp. 19-24, Nov. 2014.

[14] Kyo Minoguchi, Masayuki Oishi, Takayoshi Hirasawa, Shigeyuki Akiba, Jiro Hirokawa, and Makoto Ando, “Beam steering of 60 GHz-band array-antenna utilizing radio-over-fiber technique,” *IEICE Technical Report*, vol. 114, no. 431, OPE2014-161, pp. 53-56, Jan. 2015.

[15] Abdelmoula Bekkali, Naoyasu Kamiya, Masayuki Oishi, Kosuke Nishimura, and Keiji Tanaka, “Study on signal modulation scheme for millimeter-wave band RoF transmission systems with optical signal re-modulation,” *IEICE Technical Report*, vol. 114, no. 434, MWP2014-77, pp. 193-198, Jan. 2015.

[16] Takayoshi Hirasawa, Kotoko Furuya, Masayuki Oishi, Shigeyuki Akiba, Jiro Hirokawa, and Makoto Ando, “Beam steering of 60 GHz-band integrated photonic array-antenna utilizing radio-over-fiber,” *IEICE Technical Report*, vol. 115, no. 407, OCS2015-96, pp. 47-50, Jan. 2016.

VI. Awards

[1] Masayuki Oishi, “The 10th International Conference on Optical Internet (COIN) Young Engineer Award,” received on May 2012.

[2] Masayuki Oishi, “The Institute of Electronics, Information and Communication Engineers (IEICE) Young Researcher’s Award,” received on Mar. 2014.

[3] Masayuki Oishi, Naoyasu Kamiya, Abdelmoula Bekkali, Kosuke Nishimura, and Keiji Tanaka, “The Institute of Electronics, Information and Communication Engineers (IEICE) Best Paper Award,” received on June 2016.

[4] Kotoko Furuya, Takayoshi Hirasawa, Masayuki Oishi, Shigeyuki Akiba, Jiro Hirokawa, and Makoto Ando, “The 21st Opto-Electronics and Communications Conference (OECC) Best Paper Award,” received on July 2016.